This is Chapter 10 "Stiff block next to excavation (3D): Validation case" from my PhD thesis

Kluckner, A. 2023. Tunnelling at greater depths: Study on the ground and system behaviour when passing a stiff rock block in a weak zone. PhD thesis. Graz University of Technology, Graz, Austria.

The full thesis can be downloaded from the TU Graz repository: LINK

If you have any questions or remarks, you can contact me on

ResearchGate: LINK

or on

LinkedIn: LINK.

Enjoy reading.

Best regards, Alexander Kluckner



Dipl.-Ing. Alexander Kluckner, BSc

Tunnelling at greater depths: Study on the ground and system behaviour when passing a stiff rock block in a weak zone

DOCTORAL THESIS

to achieve the university degree of Doktor der technischen Wissenschaften

submitted to

Graz University of Technology

Reviewers

Em.Univ.-Prof. Dipl.-Ing. Dr.mont. Wulf Schubert Faculty of Civil Engineering Sciences Graz University of Technology, Graz, Austria

Univ.-Prof. Dr. Nobuharu Isago Faculty of Urban Environmental Sciences Tokyo Metropolitan University, Tokyo, Japan

Contents

Li	st of	Figures	xxi
Li	st of	Tables	xxix
Li	st of	Acronyms, Symbols, and Notations	xxxv
1	Intr	roduction	1
	1.1	Research motivation	. 1
	1.2	Research questions	. 4
	1.3	Methodology	. 5
	1.4	Thesis structure and objectives	. 6
	1.5	Research limitations	. 7
2	Abo	out fault zones and block-in-matrix rocks	9
	2.1	Brittle fault zones	. 12
	2.2	Block-in-matrix rocks	. 14
3	Son	ne properties of rocks and rock masses	19
	3.1	Geometric properties of bimrock blocks	. 19
		3.1.1 Block shape	. 19
		3.1.2 Block location and orientation	. 21
		3.1.3 Block size	. 21
	3.2	Mechanical properties of rocks and rock masses	. 22
		3.2.1 Shear strength of the matrix material	. 22
		3.2.2 Uniaxial compressive strength of the matrix material	. 28
		3.2.3 Shear strength of the block material	. 28
		3.2.4 Uniaxial compressive strength of the block material $\ \ldots \ \ldots \ \ldots$. 28
		3.2.5 Tensile strength	. 30
		3.2.6 Dilation angle	. 32
		3.2.7 Poisson's ratio	. 33
		3.2.8 Density	. 36
		3.2.9 Young's modulus	. 36
		3.2.10 Block-matrix contacts	. 40
4	Son	ne characteristics of shotcrete	45
	4.1	Hardening of concrete	. 47
	4.2	Origin of strength and stiffness growth	. 47
	4.3	A note on the behaviour under pressure	. 48
	4.4	About strain in shotcreted tunnel linings	. 49
	15	Postroints	50

CONTENTS

	4.6	Strain	n components	51
		4.6.1	Elastic (instantaneous) strain	52
		4.6.2	Thermal elastic (instantaneous) strain	52
		4.6.3	Shrinkage (delayed) strain	54
		4.6.4	Creep (delayed) strain	57
		4.6.5	Plastic (instantaneous) strain	60
		4.6.6	Irrecoverable strain due to ageing	62
	4.7	Peak	strain	62
	4.8	Shotc	rete strength	63
	4.9	Shotc	rete deformability	66
		4.9.1	Poisson's ratio	67
		4.9.2	Empirical approximation	67
5	The	rmo-cl	nemo-mechanical shotcrete model	69
	5.1	Displa	acement and strain field	70
	5.2	Shote	rete model	71
		5.2.1	Chemo-thermal coupling	73
		5.2.2	Thermo-mechanical coupling	74
		5.2.3	Chemo-mechanical coupling	74
6	Stiff	f block	next to excavation (2D): Parametric study	81
	6.1		erical model setup	82
		6.1.1	Modelling of system features	82
		6.1.2	Modelling of material behaviour	84
		6.1.3	Mesh	86
		6.1.4	Model size	87
		6.1.5	Boundary conditions and initial state	87
		6.1.6	Solve criterion and damping	87
		6.1.7	Excavation method	88
	6.2	Nume	erical input parameters	89
		6.2.1	Tunnel shape and size	90
		6.2.2	Primary stress state	90
		6.2.3	Block shape	90
		6.2.4	Block location and orientation	90
		6.2.5	Distance of the block from the tunnel and block size	94
		6.2.6	Internal angle of friction of the matrix material	94
		6.2.7	Internal angle of friction of the block material	94
		6.2.8	Cohesion of the matrix material	95
		6.2.9	Uniaxial compressive strength of the matrix material	96
		6.2.10	Uniaxial compressive strength of the block material	97
		6.2.11	Cohesion of the block material	98
		6.2.12	Tensile strength	98
		6.2.13	Dilation angle	100
		6.2.14	Poisson's ratio	100
		6.2.15	Density	100
		6.2.16	Young's modulus	100
		6 2 17	Interface properties	101

CONTENTS xv

	6.3	Evalu	ation approach	103
		6.3.1	Angular deviation of in-plane tunnel displacement vectors	105
		6.3.2	Total in-plane tunnel displacements	107
		6.3.3	Shear strain increment along tunnel periphery	108
		6.3.4	Maximum in-plane block-matrix interface slip, and other interface related	
			variables	109
		6.3.5	Block bending	109
		6.3.6	Horizontal evaluation plane	
		6.3.7	Path of highest secondary in-plane major principal stresses	
		6.3.8	Parameter development with ongoing relaxation	
		6.3.9	Zone-by-zone comparison of different cases	
			Orientation of stresses along block periphery	
			Spalling limit and damage threshold	
			Work	
	6.4		ts: Summary	
	0.1	6.4.1	In-plane block-matrix interface slip	
		6.4.2	Shear strain increment	
		6.4.3	Block deformation	
		6.4.4	Block displacement	
		6.4.5	Path of the highest secondary in-plane major principal stresses	
		6.4.6	Shear strain increment along tunnel periphery	
		6.4.7	Displacement of the tunnel periphery	
		6.4.8	Yielded zones	
		6.4.9	Block failure	
			In-plane stresses	
			Orientation of in-plane stresses	
			Elastic work	
	6.5		pretation and discussion	
	0.0	6.5.1	The block-matrix interface rules	
		0.0.1		
		6.5.2	•	
		6.5.3	Small block distance: hazardous	
		6.5.4	Identification on site? It depends	
		6.5.5	Underestimation of the situation	
		6.5.6	About installing support	157
		6.5.7	On dynamic effects	
		6.5.8	Most probable scenario	158
7	Stiff	f block	next to excavation (3D): Supplementary study	159
	7.1		erical model setup	159
		7.1.1	Modelling of system features	159
		7.1.2	Mesh	160
		7.1.3	Model size	160
		7.1.4	Boundary conditions and initial state	
		7.1.5	Construction sequence and excavation method	
	7.2		erical input parameters	161
		7.2.1	Block shape	161
		7.2.2	Block location	
		_		

CONTENTS xvi

		7.2.3 Block distance from the tunnel	61
	7.3	Evaluation approach	61
	7.4	Results	62
	7.5	Interpretation and discussion	67
8	Fibi	re optic monitoring section: Data evaluation 1	69
	8.1	Distributed fibre optic sensing	
	8.2	Geological and hydrogeological conditions	
	8.3	Rock mass types	
	8.4	Primary stress state	
	0.1	8.4.1 General	
		8.4.2 Primary stress at the analysed section	
	8.5	Tunnelling method	
	0.0	8.5.1 Excavation sequence	
		8.5.2 Support	
		8.5.3 Work steps	
	0.6	•	
	8.6	Position of monitoring devices	
	8.7	Observed system behaviour: Geodetic measurements	
		8.7.1 Time-dependent displacements	
		8.7.2 Out-of-plane displacements	
		8.7.3 In-plane displacements	
	8.8	Observed system behaviour: DFOS	
		8.8.1 Strain in the circumferential and longitudinal direction	
		8.8.2 Evolution of strain with time	
		8.8.3 Strain rate	
	8.9	Observed system behaviour: Temperature	96
9	Fib	re optic monitoring section: Calibration case (3D)	01
	9.1	Limitations	02
		9.1.1 Time-dependent rock deformation	02
		9.1.2 Swelling	02
		9.1.3 Porewater pressure	02
	9.2	DFOS section: Strain components utilising a micromechanical model 2	03
		9.2.1 Neglecting thermal strain	04
		9.2.2 Neglecting shrinkage strain	05
	9.3	Burgers model	05
		9.3.1 Basic rheological models	207
		9.3.2 Combined rheological models	207
	9.4	•	10
		9.4.1 Modelling of system features	12
		9.4.2 Modelling of material behaviour	
		~	14
			15
			15
			15
		r o	16
		9.4.8 Creep time step	

CONTENTS xvii

	9.5	Numerical input parameters	20
		9.5.1 Tunnel shape and size	20
		9.5.2 Primary stress state	20
		9.5.3 Rock mass	20
		9.5.4 Backfill	25
		9.5.5 Shotcrete lining	25
		9.5.6 Rock bolts	33
	9.6	Evaluation approach	36
	9.7	Results	36
	9.8	Interpretation and discussion	40
10		,	43
	10.1	Limitations	
	10.2	Geological and hydrogeological conditions	
	10.3	Rock mass types	
	10.4	Primary stress state	
		10.4.1 General	
		10.4.2 Primary stress at the analysed section	
	10.5	Tunnelling method	
	10.6	Position of monitoring devices	
	10.7	Observed system behaviour: Geodetic measurements	
	10.8	Numerical model setup	
		10.8.1 Modelling of system features	
		10.8.2 Modelling of material behaviour	
		10.8.3 Mesh	
		10.8.4 Model size	
		10.8.5 Boundary conditions and initial state	
		10.8.6 Construction sequence	
	10.9	Numerical input parameters	
		10.9.1 Tunnel shape and size	
		v	60
			61
		9	67
			68
		**	68
			69
	10.12	Interpretation and discussion	71
11	Disc	ussion 2'	77
	11.1		77
	11.2	·	78
	11.3		79
	11.4		79
	11.5		81
	11.6		81
			81
		11.6.2 Tunnel support	
		* *	

CONTENTS xviii

	11.6.3 Tunnelling sequence	284
12 Con	clusion	285
Bibliog	raphy	287
Appen	dix A: Equations	317
A.1	Stress invariants	317
A.2	Strain invariants	317
A.3	Mohr-Coulomb failure criterion	318
A.4	Size of the yield zone in a homogeneous, isotropic rock mass	318
A.5	Elastic secondary tangential in-plane stresses around a circular opening in a	
	homogenous, isotropic medium	319
A.6	Elastic secondary tangential in-plane stresses around an elliptic opening in a	
	homogenous, isotropic medium	320
Appen	dix B: Some mechanical properties of rocks	321
B.1	Tensile strength	321
	B.1.1 Johnston (1985)	
	B.1.2 Kluckner (2012)	
	B.1.3 Rostami et al. (2016)	
B.2	Dilation angle	
	B.2.1 Terminology	
	B.2.2 Kluckner (2012)	
B.3	Poisson's ratio	326
B.4	Young's modulus	326
A	dia C. Stiff black mark to accounting (2D). Dominator at also	220
C.1	dix C: Stiff block next to excavation (2D): Parametric study Numerical model setup	329
0.1	C.1.1 Evaluation of constitutive model for matrix material	
	C.1.2 Evaluation of minimum in-plane model size	
	C.1.3 Evaluation of solve limit	337
	C.1.4 Evaluation of excavation method	342
C.2	Numerical input parameters	343
0.2	C.2.1 Mechanical properties of model features	343
	C.2.2 Evaluation of interface stiffnesses	350
C.3	Results: Details	355
	C.3.1 In-plane block-matrix interface slip	355
	C.3.2 Shear strain increment	370
	C.3.3 Block deformation: Bending	385
	C.3.4 Block deformation: Change in the block height	391
	C.3.5 Block deformation: Change in the block width	393
	C.3.6 Block displacement	396
	C.3.7 Path of the largest secondary in-plane major principal stresses	400
	C.3.8 Shear strain increment along tunnel periphery	405
	C.3.9 Displacement of the tunnel periphery	411
	C.3.10 Yielded zones	425
	C.3.11 Block failure	438

CONTENTS	xix
C.3.12 In-plane stresses	457
C.3.13 Orientation of in-plane stresses	472

C.3.14 Elastic work	485
Appendix D: Fibre optic monitoring section: Data evaluation	497

Chapter 10

Stiff block next to excavation (3D): Validation case

The final study is to show at a real case some features of the ground and system behaviour when a tunnel drive approaches and passes a stiff block embedded in a weak material. By comparison with the conclusions from the theoretical studies (cf. Chapter 6 on p. 81 and Chapter 7 on p. 159), the validity of the latter shall be proven. Further, the study shall demonstrate possibilities to discover the stiff block prior to excavating it by analysing the system behaviour.

This validation case refers to a tunnel section of the access tunnel Göstritz. The tunnel is part of the construction lot SBT 1.1 of the Semmering Base Tunnel project. It is the same construction lot the calibration case is from (cf. Chapter 9 on p. 201). The tunnel section analysed here was excavated in summer 2016.

The study analyses the site observations, performs a three-dimensional simulation of the tunnel drive through the selected tunnel section, and evaluates the simulation results. The simulation uses the settings for the shotcrete material from the calibration case (cf. Chapter 9).

Captions of some figures and tables in this chapter cite the abbreviation $Validation\ case$ referring to the simulation of the heading; it is $SBT1.1 \mid G\"{o}stritz$ if the figure or table refers to site conditions and observations.

Section 10.1 lists the main limitations of the numerical simulation. The geological and hydrogeological conditions of the analysed section are briefly described in Section 10.2. Relevant rock mass types are cited in Section 10.3 (p. 246). A summary of the primary stress state (Section 10.4 on p. 247) and of the tunnelling method applied (Section 10.5 on p. 248) follows. Section 10.6 (p. 248) describes the equipment of monitoring cross sections along the analysed tunnel section. The site system behaviour observed is discussed in Section 10.7 (p. 248). Section 10.8 (p. 256) and Section 10.9 (p. 260) outline the model setup and the input parameters, respectively, required to simulate the tunnel construction in this section. The approach to evaluate the numerical results is given in Section 10.10 (p. 268); the results are summarised in the section following (Section 10.11 on p. 269). Section 10.12 (p. 271) interprets the results and discusses the conclusions from this study.

10.1 Limitations

Two of the limitations in the calibration case (cf. Section 9.1 on p. 202) apply also here: it is any time-dependency of the rock mass deformation and swelling. According [61, p. 77ff], in the rock masses analysed here, sulphate rocks are predominantly massive but limited in size. They are present as shear bodies only. Further, they assume that most anhydrites already have altered to gypsum reducing the potential for swelling significantly. Since the maximum swelling pressure of 0.7 MPa is not to be considered before one to two years after excavation which is far beyond the scope of the simulation here, swelling is neglected.

The tunnel drive is simulated without performing coupled fluid-flow calculations. This is no simplification since the rock mass in the analysed tunnel section can be considered dry (cf. next section).

10.2 Geological and hydrogeological conditions

The tunnel section from chainage 235 m to chainage 335 m this study deals with is in the fault system Grassberg-Schlagl. It's a left-lateral strike-slip fault system accompanying the major Mur-Mürztal-Semmering-Wiener Becken fault system ([407, p. 150]). Related fault zones relevant for this study feature a W-E to WSW-ENE strike ([343, p. 138]). Faults predominantly strike from W to E and dip steeply to S ([407, p. 249]). The overburden increases from approx. 59 m to approx. 86 m. Along this section, tectonic events have stressed most parts of the rock mass considerably leading to a heterogeneous rock mass. Fig. 10.1 shows the rock mass structure of a 60 m long part of the section. The rocks are heavily fractured or even cataclastic. Its sericite phyllites and sericite schists that alternate with varying quality (incl. cataclasites) and proportion, often separated into finite zones by shear bands. Sometimes, one rock type transitions into the other. The sericite schists are present only approx. up to chainage 298 m. From approx. chainage 264 m, strongly fractured zones of thin layers of calcareous slates and of limestones pass through the analysed tunnel section up to its end. Shear bands border these zones. Around chainage 275 m, a 5 m thick shear body of dolomite and gypsum breccia crosses the excavation area from the right. It is massive and strong. Fine-grained cataclasites of sericite phyllites intercalated by quartizitic and dolomite beds or lenses (< 10 cm) accompany the shear body and the zones of slates and limestones. Within 30 m on both sides of the carbonate shear body, the total share of cataclasites ranges approx. from 40% to 70%. Fig. 3.7 (p. 29) shows the sketch of the tunnel face at chainage 282.3 m comprising the block and the weak material surrounding it. From chainage 302 m, the rock mass also comprises alternating layers of tectonically strongly compacted and folded cataclasites of sericite phyllites cemented with gypsum, strongly fractured slates (along shear bands), and more competent shear bodies of dolomite and gypsum breccia. [151, 152]

The zoning of the analysed tunnel section into Zone A to Zone E was done considering apparent boundaries of geological features visible in Fig. 10.1 and distinct changes in the evaluated rock mass characteristics mapped by the geologists (e.g., rock strength, dominant spacing of discontinuities).

All rocks are fresh and unweathered. The sericite phyllites are soft or loosened and folded, and bear quartzitic gravels or sheared beds. Foliation planes feature a spacing of < 0.6 to 6 cm. The rocks are moderately anisotropic. Less stressed parts feature a mapped rock strength category of 5–25 MPa, and 1–5 MPa for related cataclasites. For most parts, the sericite schists are more competent than the sericite phyllites and comprise quartzitic layers and joint fillings. The foliation spacing ranges from 0.6 to 6 cm. The rocks are moderately to highly anisotropic. Their strength has been assigned to the same categories as the phyllites. The slates are soft and

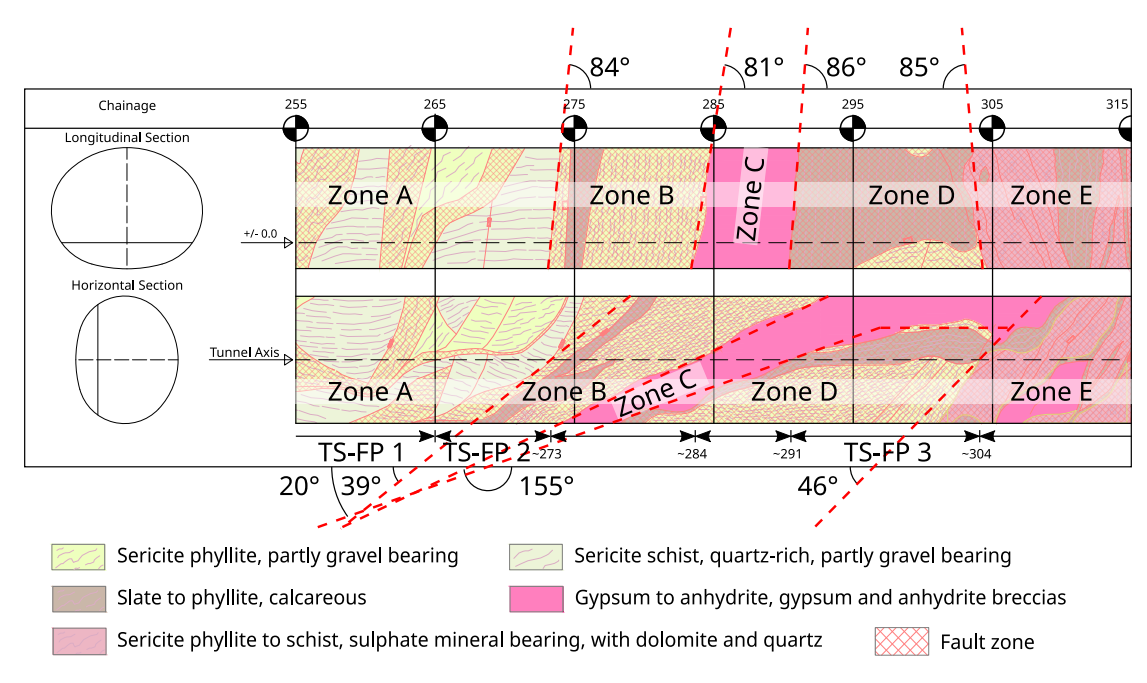


Figure 10.1: SBT1.1 | Göstritz: Longitudinal section (top) and horizontal section (bottom) from chainage 255 m to chainage 315 m (rock mass structure from [151]). For the subdivision of the tunnel into sections regarding the mean orientation of the foliation planes (TS-FP), refer to Tab. 10.8 (p. 261).

the limestones are strong (50–100 MPa; 25–50 MPa after chainage 275 m; related cataclasites: 5–25 MPa), both predominantly featuring a foliation spacing of 2 to 6 cm. The fine-grained cataclasites are weak (predominantly < 5 MPa) and do not show a dominant structure. The main carbonate shear body is isotropic to slightly anisotropic, and its strength was estimated with 50–100 MPa. The shear bodies encountered farther behind are smaller, have been stressed more, and are less competent (25–50 MPa) and partly foliated. The cemented cataclasite is cohesive and relatively strong (5–25 MPa), features a foliation spacing of < 0.6 to 6 cm, and is moderately anisotropic. [151, 152]

All mapped discontinuities (i.e., foliation planes, joints, faults, slickensides) are planar or undulated, and predominantly smooth. The walls of the foliation planes are sericitic. Many of the faults feature clayey to silty fillings. Some of them are shear bands. Fault planes are mostly at least 60 cm apart from each other. [152]

Approx. up to chainage 273 m, the azimuth of the foliation planes varies from NW to NE. They dip at a moderate to high angle (from 35° to 74°) and are mechanically effective (often tectonically overprinted to slickensides). In the next 30 m of rock mass, the azimuth varies from NW to N and the planes dip steeply (from 61° to 86°). After approx. chainage 302 m, because of the cementation with gypsum and the compaction, most discontinuities are mechanically insignificant. The remaining significant ones steeply dip to NW or SE. The dip angle of all faults mapped in the analysed section varies between 60° and 90°. The structural conditions along the analysed tunnel section partly deviate from the ones on a larger scale because of offsetting and folding during tectonic events ([343, p. 138]). [151, 152]

Considering the direction of the tunnel drive of 100° from north, all foliation planes mapped between chainage 255 m and chainage 298 m dip to the left, some in the direction of the drive (DOD) and some against it (cf. Fig. 10.2a) with a strike parallel to sub-parallel to the tunnel axis (i.e., $\leq 30^{\circ}$). Note that from chainage 298 m to chainage 316.1 m, no foliation planes have been mapped; probably because of their mechanical insignificance (cf. text above).

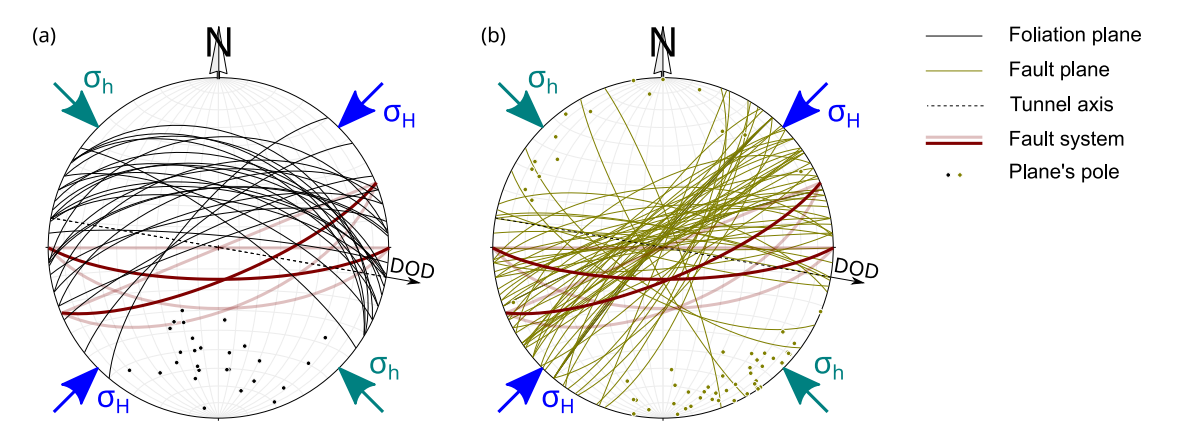


Figure 10.2: SBT1.1 | Göstritz: Schmidt net (equal area) plot of orientations of discontinuities mapped from chainage 255 m to chainage 316.1 m (data from [152]), and of the fault system the analysed tunnel section passes through. (a) Foliation planes; (b) fault planes. The light red great circles highlight the variation in the dip angle of the fault system. The plots also include the direction of the tunnel drive, and the approximate orientation of the minimum primary horizontal stress, σ_h , and of the maximum primary horizontal stress, σ_H . Graphs created with the free software Stereonet ([12, 13, 65]).

Fig. 10.2b plots the great circles of some mapped fault planes. From chainage 255 m to chainage 298 m, the strike of the faults deviates from the tunnel axis by 0° to 65° (mean value: 32°). Most faults dip against the DOD and to the left (NW). In the rock mass following, up to chainage 316.1 m, it is 0° to 80° (mean value: 49°). Here, most faults either dip in the DOD and to the right (SE) or against the DOD and to the left (NW).

Because of unfavourable intersections of discontinuities, shear bands, and the tunnel surface, along the entire tunnel section, small- to medium-sized rock bodies were prone to fall or slide into the opening during tunnelling. [151, 152]

In the excavation area, the rock mass is dry or features an inherent moisture. The maximum amount of water ingress was 0.002 l/s. Water trickling down from drillings and rock bolts could be observed. More water ingress was observed after the heading passed chainage 420 m where the rock mass comprises rauhwacke. Thus, for the simulation it is assumed that the rock mass close to the stiff block is dry locally featuring some joint water. [152]

Now the block this analyses is interested in, is this main carbonate shear body (hereinafter termed the *stiff block*) crossing the tunnel approx. from chainage 275 m to chainage 310 m. It is massive, strong, and lacks of many weakness planes, and weak to very weak material surrounds it. The mapped strength of the slates and limestones encountered before reaching this massive block is as high as of the block. The rock mass zone comprising the slates and limestones is strongly fractured resulting in a far lower strength compared to the block.

10.3 Rock mass types

The rock masses encountered in the tunnel section have been assigned to the rock mass type (RMT) 5f-1, 5f-2, 8c, or 8f.

RMT 5f comprises sulphate rocks like gypsum or anhydrite. RMT 5f-1 is the less competent one with layers of sericite phyllite or schist overall featuring a low to moderate strength. RMT 5f-2 refers to massive sulphate to sulphate-rich carbonate rocks with a high to very high strength. [380, p. 24f]

For RMT 8c and RMT 8f, refer to Section 8.3 (p. 172). Tab. 10.1 lists the shares of the RMT for each top/bench-heading tunnel face mapped.

Table 10.1: SBT1.1 | Göstritz: Areal share of the top/bench-heading tunnel face by the rock mass types (RMT) in the tunnel section from chainage 255 m to chainage 316.1 m (information from [152]). Note that the distribution is similar at the mapped tunnel faces of the invert heading (not listed).

Areal share of the top/bench-heading tunnel face in percent										
Chainage [m]	255	257.6	260.2	264.1	266.7	269.3	271.9	274.5		
RMT 5f-1	-	-	-	-	-	-	-	-		
RMT $5f-2$	-	-	-	-	-	-	-	-		
RMT 8c	100	100	100	100	100	100	74	52		
RMT 8f	-	-	-	-	-	-	26	48		
Chainage [m]	277.1	279.7	282.3	284.9	287.5	292.7	297.9	299.2		
RMT 5f-1	-	-	-	-	-	-	-	-		
RMT $5f-2$	15	22	33	29	39	33	33	31		
RMT 8c	48	35	23	19	-	-	-	-		
RMT 8f	37	43	45	52	60	67	67	69		
Chainage [m]	303.1	305.7	308.3	314.8	316.1					
RMT 5f-1	-	39	32	68	87					
RMT $5f-2$	30	-	-	-	-					
RMT 8c	-	-	-	-	-					
RMT 8f	69	60	67	32	14					

10.4 Primary stress state

The first of the two following subsections describes the primary stress state assumed to exist in the rock mass the underground constructions of the construction lot SBT 1.1 have to cope with. The second subsection draws conclusions about the primary stress state close to the tunnel section analysed here.

10.4.1 General

For the primary stress state conditions across the project area of the construction lot SBT 1.1, refer to Section 8.4.1 (p. 174).

10.4.2 Primary stress at the analysed section

The section of interest is part of a strike-slip fault system. The system's orientation relative to the estimated orientation of the horizontal principal stresses is like the one at the DFOS section (cf. Fig. 10.2 and Fig. 8.2 on p. 171). Thus, the same conclusions can be drawn (cf. Section 8.4.2 on p. 174): $\sigma_v \geq \sigma_H > \sigma_h$.

In contrast, for the fault system considered here, [61, p. 86] report extensional movements (i.e., dip-slip faulting), in particular around chainage 260 m. This extension may cause reduced horizontal stresses in zones nearby ([61, p. 85ff]). Because the rock mass here comprises also competent zones, which may be capable of preserving stress differences (cf. [61, p. 85ff]), this study sets $k_{0,H} = 0.75$ and $k_{0,h} = 0.5$.

Considering that the overburden varies from 59 m to 86 m, the resulting primary principal stresses at the tunnel level are (for the purpose of illustration here, $\gamma = 0.025 \text{ MN/m}^3$):

- $\sigma_v = -1.48... 2.15 \text{ MPa}$
- $\sigma_h = k_{0,h} \cdot \sigma_v = 0.5 \cdot (-1.48 \dots 2.15) = -0.74 \dots 1.08 \text{ MPa}$
- $\sigma_H = k_{0.H} \cdot \sigma_v = 0.75 \cdot (-1.48 \dots 2.15) = -1.11 \dots 1.61 \text{ MPa}$

The azimuth of the DOD is 100° from N and the direction of σ_H deviates from it by 55° (cf. Fig. 10.2).

10.5 Tunnelling method

The tunnel section has been excavated with an excavator. From chainage 273.2 m, because of the competent sulphate and carbonate rock blocks, cuttings or loosening blastings were required. The tunnel drive was separated into two headings: (1) the top/bench heading (tbh), and (2) the invert heading (ih). The round length of the top/bench heading is 1.3 m, of the invert heading it is 4.4 m. The distance between the top/bench heading and the invert heading ranged between 4 m and 10 m.

Up to chainage 275.8 m, the top/bench-heading round was excavated in two steps (i.e., partial face excavation). After that, it was a full-face excavation. The invert heading was done full-face entirely.

Tab. 10.2 and Tab. 10.3 list the installed support at the top/bench heading and invert heading from chainage 235 m to chainage 335 m. Refer to Fig. 8.7 (p. 182) for a schematic cross section of the shotcrete lining.

The tunnelling sequence for a standard top/bench-heading round is similar to the one close to the DFOS section (cf. left column in Tab. 8.5 on p. 179). At the tunnel section analysed here, up to chainage 321.3 m, spiles and radial rock bolts were installed before the second layer of shotcrete. Rock bolts ahead of the tunnel face were installed every 6th round. The tunnelling sequence for a standard invert-heading round is the same as close to the DFOS section (cf. left column in Tab. 8.6 on p. 179).

10.6 Position of monitoring devices

The monitoring cross sections of the top/bench heading are equipped with five bi-reflex targets for standard monitoring of the tunnel displacements with geodetic total stations. The monitoring targets (MT) are next to the crown, at the shoulders, and at the side walls. The positioning of the MT is like at the DFOS section (cf. Fig. 8.5 on p. 180). The only difference here is that MT1 is to the right of the crown. At its top, Tab. 10.4 lists the chainages of relevant monitoring cross sections.

10.7 Observed system behaviour: Geodetic measurements

Zone A highlighted in Fig. 10.1 (p. 245) extends from chainage 225 m up to chainage 273 m. There, the foliation planes strike sub-parallel to the tunnel axis and dip to the left side wall at a moderate to high angle. According to [92], when the planes strike parallel to the tunnel axis or if they deviate from it by 45° dipping against the DOD, and if the dip angle is 45° (moderate

Table 10.2: SBT1.1 | Göstritz: Specifications of the support of the top/bench heading from chainage 235 m to chainage 335 m. Information from [345].

Primary suppo	ort of the side walls and the crown								
Shotcrete	Shotcrete SpC 30/37/J2/XAT-C3A-free ([289, p. 26ff, 63]: minimum characteristic compressive strength $f_{ck,min}=40$ MPa for cores with $h/d=1$, early strength class J2, XAT-C3A-free resistant to sulphate), thickness $t=25$ cm								
Wire mesh	AQ 50 (in both directions: cross-sectional area $A = 1.96 \text{ cm}^2/\text{m}$), one layer of wire mesh in each shotcrete layer								
Lattice girder Bolts	3 bar type 95/20/30 (distance between upper and lower bar [mm]/diameter of lower bar [mm]/diameter of upper bar [mm]), cross-sectional area $A=13.35~{\rm cm^2/m}$, section modulus $S_x=66~{\rm cm^3}$ and area moment of inertia $I_x=485~{\rm cm^4}$ with x in the direction of the tunnel drive $14-15x$ grouted rock bolts (C3A-free) installed radially, length $L=4~{\rm m}$, maximum tensile force $F_{t,max}=250~{\rm kN}$								
Temporary fac									
Shotcrete	same as for side walls (see above), $0-50\%$ of face area with thickness $t=10$ cm and wire mesh, $100-50\%$ of face area with thickness $t=5$ cm and unreinforced								
Wire mesh Bolts	AQ 50 (in both directions: cross-sectional area $A=1.96~\rm cm^2/m$), one layer up to chainage 329.1 m 4–6x grouted IBO self-drilling rock bolts with hollow bars installed ahead of the tunnel face and up to chainage 321.3 m interlocked with the tunnel face by load distribution plates, length $L=12~\rm m$, maximum tensile force $F_{t,max}=350~\rm kN$								
Primary suppo	ort ahead of the tunnel face								
Spiles	14–33 spiles, up to chain age 300.5 m driven spiles and from chainage 301.8 m up to chain age 321.3 m non-grouted tube spiles, outer diameter $OD=30$ mm, length L=4 m, circumferential spacing $e<30$ cm								

angle), the left side wall displaces radially more than the right side wall (cf. Fig. 53 on p. 61 and Fig. 59 on p. 66 in the reference; in the latter, imagine the situation graphed there mirrored). It is similar here (cf. the categorisation of the horizontal and vertical displacements at the top of Tab. 10.4). However, when observing the graphs given in [92], it becomes clear that the resulting displacements and behaviour patterns (e.g., ratio between the horizontal displacement of the side walls) can change significantly depending on the dip angle (cf. also the comments at the end of Section 8.7.2 on p. 183).

Similarly, the longitudinal displacements also depend on the orientation of mechanically significant discontinuities. At the beginning of Zone A, all MT displace against the DOD. At some monitoring cross sections, the left side wall displaces a little more than the right side wall;

Table 10.3: SBT1.1 | Göstritz: Specifications of the support of the invert heading from chainage 235 m to chainage 335 m. Information from [345].

Support of the invert									
Shotcrete	SpC 30/37/J2/XAT-C3A-free ([289, p. 26ff, 63]: minimum characteristic compressive strength $f_{ck,min} = 40$ MPa for cores with $h/d = 1$, early strength class J2, resistant to sulphate), thickness $t = 25$ cm								
Wire mesh									

Table 10.4: SBT1.1 | Göstritz: Evaluation and categorisation (CAT) of monitored displacements between chainage 255 m and chainage 340 m.

Displacements at monitoring cross sections												
Chainage [m]	225	235	246	254	266	274	286	297	310	319	329	340
CAT of horiz. disp.*	2	2	2	2	2	2	2	2	3	3	1	1
CAT of vert. disp.*	2	1	2	2	2	2	2	1	1	3	1	1
CAT of long. disp.*, **	2	3	1	3	2	2	2	1	3	3	1	1
max. rad. disp. [mm]	56	47	40	45	45	34	38	19	10	14	16	23
mean rad. disp. [mm]	40	32	31	34	28	21	21	14	8	10	11	17
	1	R>L		2	L>R		3	L≈R		R righ	nt tunnel	side
										L left	tunnel s	ide

* Qualitative categorisation (CAT) considering the monitoring targets at the side walls and at the shoulders

(quantitative evaluation; cell colouring by value; colouring cut-off at x = 2) Disp. relations: $|V_{MT1}/max(H_{MT4}; |H_{MT5}|)|$ 0.8 1.0 0.9 1.5 0.4 0.5 0.7 0.8 0.7 0.5 1.4 0.8 $V_{MT1}/max(V_{MT4}; V_{MT5})$ 0.7 1.1 1.1 1.0 1.0 0.7 0.5 1.5 1.2 2.8 1.4 |H_{MT4}/H_{MT5}| 1.3 1.3 1.4 2.1 3.9 5.2 3.3 2.2 1.6 8.0 0.6 1.0

> V ... vertical displacements H ... horizontal displacements

MT1: monitoring target at the crown
MT4: monitoring target at the left side wall
MT5: monitoring target at the right side wall

at others it is the opposite. The former matches with the behaviour reported in [92, Fig. 53, p. 61] for the case with foliation planes striking parallel to the tunnel axis and dipping at a moderate to high angle. The latter refers to the case with the strike deviating from the tunnel axis and a high-angle dip (cf. [92, Fig. 59, p. 66]).

As the heading approaches the zones ahead of chainage 273 m that comprise more competent layers and blocks, the displacement level decreases (cf. maximum and mean radial displacement values in Tab. 10.4), and the MT at the crown and at the right tunnel half displace less against the DOD or even displace in the DOD (not shown). The latter complies with [382] showing that the longitudinal displacements deviate towards the DOD in case a stiffer zone is ahead (cf., e.g., Fig. 35 on p. 58 in the reference). Accordingly, here, the longitudinal displacements are categorised with 2 (cf. third row in Tab. 10.4). Because the stiff zones pass through the cross section from the right to the left (cf. bottom graph in Fig. 10.1 on p. 245), the right tunnel half displaces in-plane less horizontally resulting in an increase in the ratio of the horizontal displacement of the left side wall to the one of the right side wall (cf. last row in Tab. 10.4). Fig. 10.3 plots the recorded displacements at the monitoring cross section at chainage 266.2 m. Note here the strong anisotropy in all displacement components between the left and right tunnel half.

From chainage 286 m, the MT displace more or less in-plane only; mostly, the longitudinal displacements are below 5 mm. Note that the in-plane and out-of-plane displacement pattern not only depends on the orientation of discontinuities and zones but also on the primary stresses, the excavation geometry, and the heterogeneity of the rock mass (i.e., alternation of weak and strong zones). It is assumed that the latter is responsible for the variation in the displacement ratios involving the vertical displacement in Tab. 10.4.

Regarding the categorisation of the in-plane displacements, consider that the stiff block exits

^{**} Categorisation of the displacements against the direction of the drive (DOD)

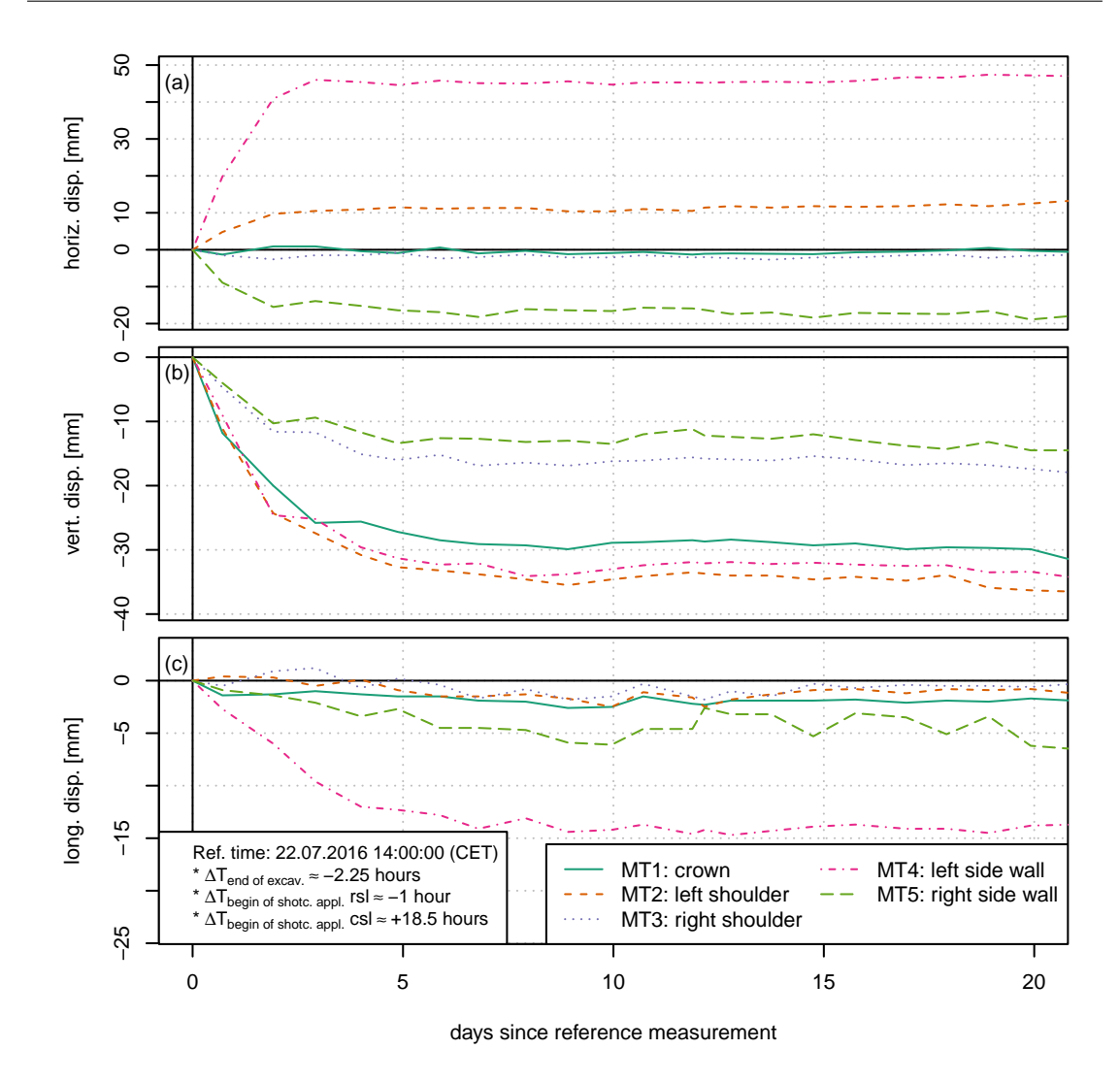


Figure 10.3: SBT1.1 | Göstritz | top/bench heading: Development of the tunnel displacements monitored with five geodetic targets (cf. Section 10.6 on p. 248). (a) horizontal displacements (displacement to the left: negative value); (b) vertical displacements (displacement downwards: negative value); (c) longitudinal displacements (displacement against the direction of the drive: negative value). Note the different scaling of the ordinate axes. csl...cavity-side layer, rsl...rock-side layer, MT...monitoring target.

the excavation section beginning approx. with chainage 293 m (cf. Fig. 10.1). It then accompanies the left tunnel side for a considerable part and may do so also outside the excavation area behind chainage 310 m. Anyway, now that the stiff block has changed the sides, the displacement pattern switched accordingly: from category 2 to 3, and then to 1 (cf. first two rows in Tab. 10.4). Note also the change in the horizontal displacement ratio (cf. last row in Tab. 10.4). That a weaker rock mass zone crosses into the excavation from the right from chainage 322 m (not shown) contributes to the change in the displacement pattern. Note here the increase in the radial displacements in Tab. 10.4.

Has the stiff block been discoverable?

The construction site provides the vertical displacement, V, horizontal displacement, H, and longitudinal displacement, L, of monitoring targets. Lots of ways exist to analyse the data, e.g.: individual displacement component separately (e.g., V of the target at the crown), displacement

differences (e.g., H of the target at the left side wall minus H of the target at the right side wall), displacement ratios (e.g., L/V of the target at the crown). For the analysis, either actual or absolute values can be used. Ratios can be of linear dimension, or of angular dimension by calculating the arc tangent. The evaluation quantity can be compared with the time passed since the reference measurement to get the temporal development. Or it is compared with the distance of the current tunnel face to the monitoring cross section. Many of the standard approaches are described in [291] and in the references it cites. [108] introduces thoughts on some new approaches.

In the case analysed here, a steeply dipping stiff zone crosses the tunnel from the right to the left at an acute angle. According to [218], for this scenario where the drive approaches a stiffer zone, the changes in the displacements listed in Tab. 10.5 are expected. The changes occur from monitoring cross sections farther away from the transition to monitoring cross sections close to the transition. The magnitude of changes depend on the stiffness and the strength contrast of the adjacent rock mass zones (cf., e.g., Fig. 14 in [139, p. 14]). The lower the contrast, the smaller are the changes. But also the size of the zones in the DOD (i.e., thickness) determines the characteristics of the changes. If, for example, the drive needs to go through a stiff-soft-stiff rock mass setup, then changes in the displacements showing the soft zone ahead are rather small and short-lived if the soft zone is thin (cf., e.g., Fig. 16 in [139, p. 17]). They get altered quickly because of the effect of the stiff zone following. Note that the trends given, for example, in [218] and [139] refer to setups where the individual rock mass zones are homogeneous, isotropic, and extend to infinity to all sides perpendicular to the tunnel axis. None of those conditions apply to the validation case.

Table 10.5: Trends of displacement evaluation quantities according to [218, Structure type 3.7 in Tab. 6, p. 49] for a tunnel approaching a stiff zone with a vertical dip striking the tunnel axis at an angle of 45° from the right to the left.

Evaluation quantity	Crown (MT1)	Left side wall (MT4)	Right side wall (MT5)
$V \\ H$	abs. amount decreases more to the right	no change no change	abs. amount decreases more to the right
L/V H/V L/H	more towards the DOD more to the right	no change no change	more towards the DOD more towards the DOD
$V_{ m MT4}/V_{ m MT5} \ H_{ m MT4}/H_{ m MT5} \ V_{ m MT4}/V_{ m MT1} \ V_{ m MT5}/V_{ m MT1}$	dec	creases (i.e., $ V_{\rm MT5} $ decreases (i.e., $ H_{\rm MT5} $ decreases on change creases (i.e., $ V_{\rm MT5} $ decreases (i.e., $ V_{\rm MT5} $	eases)

Assumptions for the statements made here (cf. Fig. 8.8 on p. 182): all targets displace downwards and displacement values are negative; the left side wall displaces to the right and the displacement value is positive; the right side wall displaces to the left and the displacement value is negative.

Fig. 10.4 plots the displacement vectors of the three monitoring cross sections before the stiff block (MS 246, MS 254, MS 266), and of the one at chainage 274 m where the block is already part of the tunnel face. The rock mass conditions at the first three monitoring cross sections is similar (cf. Fig. 10.1 on p. 245 for the rock mass structure from chainage 255 m). Note that the vertical displacements at MS 254 are larger because of the sub-vertical weak shear band. The situation is not that bad at MS 266. Thus, the displacement level is lower. Anyway, the difference

in the displacements between MS 254 and MS 266 is largest at the right tunnel half being close to the stiff block. In-plane, only MT3 at MS 266 rotates a little to the right. Out-of-plane, it is MT1 and MT3 that displace more towards the direction of the drive (DOD). Surprisingly, MT5 does not change its in-plane displacement direction and even displaces out-of-plane more against the DOD. At MS 274, the displacement level at the right tunnel half is lowest.

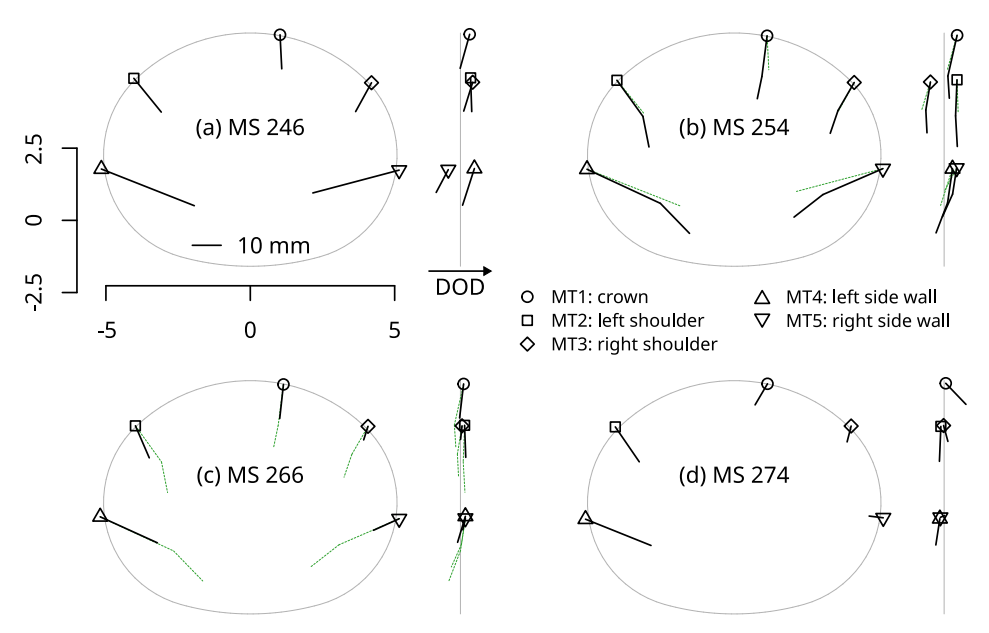


Figure 10.4: SBT1.1 | Göstritz: Displacement vector plots in the cross and longitudinal section view for the monitoring cross sections (MS) at chainage 246 m, 254 m, 266 m, and 274 m. Displacement vectors are scaled up by a factor of 100. At MS 266, the last follow-up measurement before the top heading encounters the stiff block was 46 hours after the reference measurement. Thus, for the purpose of identifying differences, all graphs only plot the displacements that have developed within 46 hours. To ease interpretation, graph (b) and (c) show the vectors of the monitoring cross section behind the one plotted in the graph with dashed green lines. Graph (d) is just for comparison as it shows displacements that have developed when the tunnel drive already hit the block.

Fig. 10.5 shows trend lines for selected displacement quantities. They "are created by connecting values from the" state lines "at a constant distance behind the face" ([291, p. 55]). Here it is 5 m and 10 m. For the concept of state lines, refer to Section 7.3 (p. 161).

For the evaluation Fig. 10.5, consider that around chainage 35 m quartzite zones with a rock strength over 100 MPa were encountered. Weak material also surrounds those stiff zones and similar displacement patterns are expected to have developed. There it is an alternating sequence of stiff and soft zones (not shown) in contrast to the one block of the validation case here. Note also that approx. from chainage 110 m up to chainage 268 m the rock mass conditions are similar. The overburden continuously increases from the portal of the tunnel to the analysed section (cf. Section 10.2 on p. 244).

Graph (a) in Fig. 10.5 plots the horizontal displacement of the right side wall. At the end, the trends point upwards but the levels of the trends differ little from those around chainage 110 m. In addition, the variation of the trend lines is large reflecting the rock mass heterogeneity and one could assume that they point downwards soon again. Thus, the evidence for a stiff block ahead is not clear. It is similar for the graphs (b) and (c) that plot the vertical and longitudinal displacement of the right side wall, respectively. The level of longitudinal displacement is low. Thus, some of the variation in the trends must be ascribed to measurement inaccuracy. The trends in graph (c), and in other graphs too, would be probably more distinct if the block is

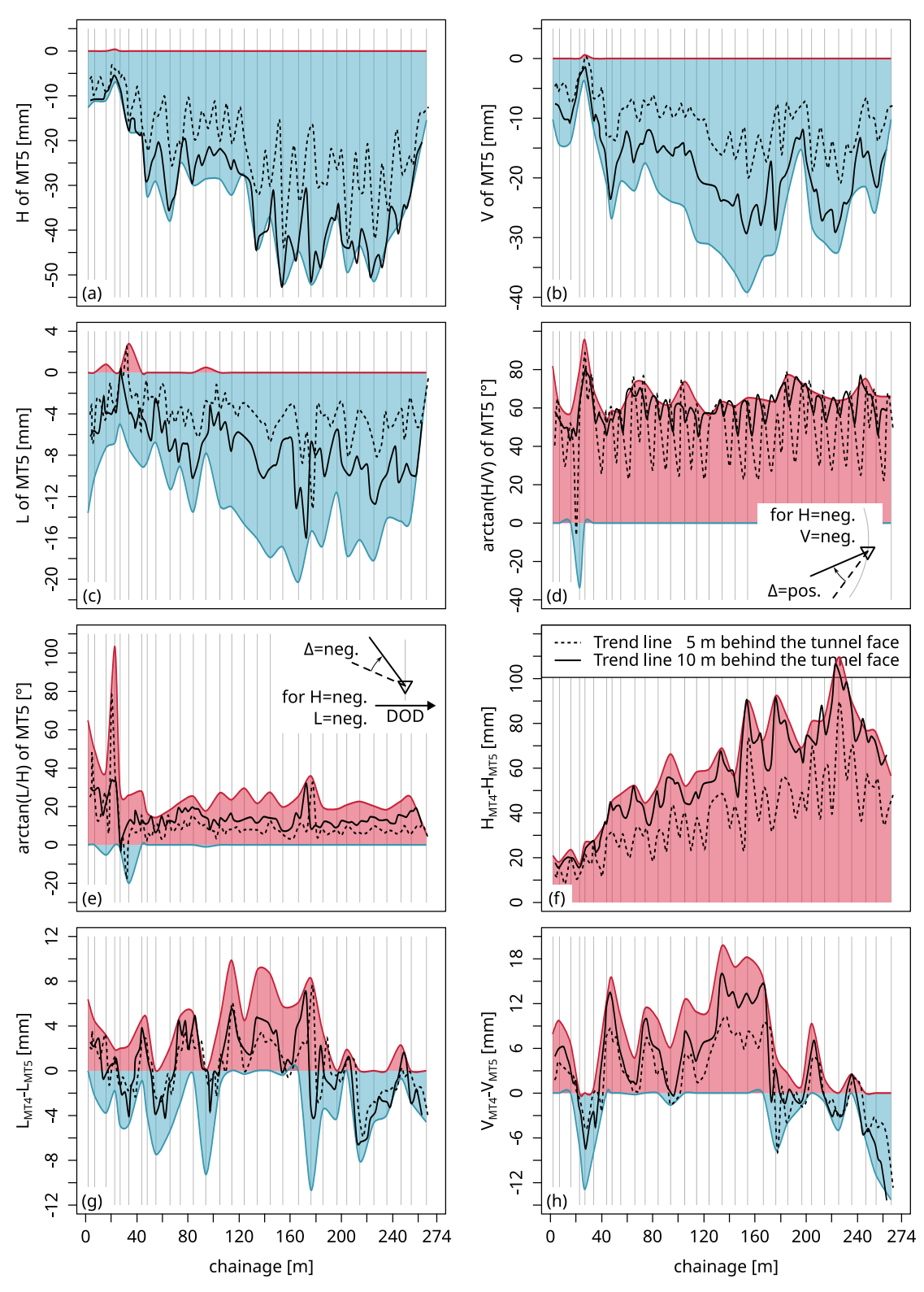


Figure 10.5: SBT1.1 | Göstritz: Trend lines of selected displacement evaluation quantities. The graphs end on 24:00 of July 24th, 2016, when the tunnel drive is at chainage 273.2 m right before arriving at the stiff block. The red and blue lines are the envelopes of the state lines on the positive or negative side of the ordinate axis, respectively. Note the different scaling of the ordinate axes. Evaluated displacement quantities: (a) $H_{\rm MT5}$, (b) $V_{\rm MT5}$, (c) $L_{\rm MT5}$, (d) arctan $(H_{\rm MT5}/V_{\rm MT5})$, (e) arctan $(L_{\rm MT5}/H_{\rm MT5})$, (f) $H_{\rm MT4}-H_{\rm MT5}$, (g) $L_{\rm MT4}-L_{\rm MT5}$, (h) $V_{\rm MT4}-V_{\rm MT5}$. H ... horizontal displacements, V ... vertical displacements, L ... longitudinal displacements, MT4 ... left side wall, MT5 ... right side wall. The vertical grey lines highlight the location of the monitoring cross sections.

larger in the DOD. Knowing of the block and considering the displacement development, one could conclude the small size of the block. As was already observed at the vector plots (cf. Fig. 10.4c), in-plane, the displacement vector does not change its orientation (cf. Fig. 10.5d). Thus, concentrated shearing along the surface of the foremost block part assumed to be almost vertical is not pronounced or is still too far away to affect the tunnel displacements significantly.

The displacements of MT1 at the crown (not shown) do not feature any signs for the block. In contrast to what is listed in Tab. 10.5 (p. 252), the vertical displacements even show an increasing trend.

According to Tab. 10.5, the out-of-plane vector L/H should change its orientation pointing more towards the DOD. It does in the case here (cf. graph (e)) but only to a minor extent considering the variability of the trend lines (it is similar at the $\arctan(L_{\rm MT5}/V_{\rm MT5})$ plot; not shown). The trends may be still explained to be within the normal range because of the heterogeneity of the project's rock masses. The evaluation of graph (f) is problematic. If the value gets higher, either the displacements of MT4 are larger or those of MT4, or both increase, or the increase in one component outweighs the decrease in the other. So, which one is the case here? It is impossible to tell without considering other graphs. Note that the horizontal displacements of the left side wall are positive, whereas those of the right side wall are negative. Anyway, the graph shows that the level of displacement increases from the tunnel portal up to the analysed section. This complies with the overburden increasing steadily. There is a decreasing trend at the end. However, it is still within the usual range of variation.

Graph (g) does not feature that problem because usually both the longitudinal displacements of the left side wall and right side wall are negative pointing against the DOD (cf. graph (c) and Fig. 10.4). Thus, if MT5 displaces less, then the value in the graph gets lower (i.e., less positive, or more negative). Close to the block, the trend shows this decrease but is too less pronounced compared to the large variation from approx. chainage 170 m. Now in graph (h), clear signs for the block exist. Both the vertical displacements of the left side wall and right side wall are negative pointing downwards. If MT5 displaces less, then the value gets lower (i.e., less positive, or more negative). The latter is the case here, and the change is much larger as it has been observed between chainage 20 m and chainage 40 m comprising the strong quartzite zones. The trend is significant and extends for over 30 m. From all graphs, in graph (h), close to the block, the envelope of the state lines exceeds the envelope of the maxima or minima at tunnel sections before for the first time.

In the case here, the last monitoring cross section is too close to the stiff block. Otherwise, data from more follow-up measurements would be available before the heading hits the block. Anyway, if the monitoring cross section is farther away, changes because of the block will be less significant. Considering the global orientation of the rock mass structure, larger zones not encountered yet may (!) cross into the tunnel from the right. Thus, it is likely that plots comparing the left and right tunnel half will show the largest changes. The heterogeneity of the rock mass makes a prognosis difficult. Some zones may fail under the loading, others may not. Some metres ahead, because the overburden increases, more zones may fail. Without investigation drillings ahead of the face, or sound investigation campaigns in the design phase and a continuous update of the geological model during construction, in the case here, only Fig. 10.5h clearly indicates the block being ahead. The engineers and geologists at the site following the construction from the beginning on may see more clear signs that something is coming.

 $^{^1\}mathrm{One}$ could overcome this problem by evaluating the displacement ratio (e.g., $H_{\mathrm{MT4}}/H_{\mathrm{MT5}})$ rather than the displacement difference.

10.8 Numerical model setup

This study simulates the tunnel drive from chainage 235 m to chainage 335 m using the program FLAC3D ([178]). Regarding the rock mass conditions only the tunnel section visible in Fig. 10.1 (p. 245) is evaluated. It is assumed that the influence of the rock mass conditions farther away on the system behaviour close to the stiff block in the centre of the numerical model is negligibly small. The rock mass of interest is modelled with five homogeneous zones (cf. Section 10.2 on p. 244 and Fig. 10.1): Zone A, B, C, D, and E. The dip angles cited in the top graph in Fig. 10.1 are the apparent ones. The actual dip angles are 86°, 86°, 89°, and 86°, respectively.

The numerical model is set up in the same way as it is done for the calibration case (cf. Section 9.4 on p. 210). Thus, this section only cites relevant differences and specifics of this study.

Fig. 10.6 and Fig. 10.7 show the numerical model from different points of view. The bottom graph in Fig. 10.7 shows the moment before step 1 (cf. Tab. 9.1 on p. 217) of the top/bench-heading round from y = 33.8 m to y = 35.1 m. The initial state is illustrated in the two other graphs. The following subsections introduce the features visible in the graphs and some model and calculation settings. System related parameters (i.e., rock mass, tunnel, support) and the selected primary stress state are cited in the next section, Section 10.9 (p. 260). For a more general overview of the site conditions, refer to the sections above.

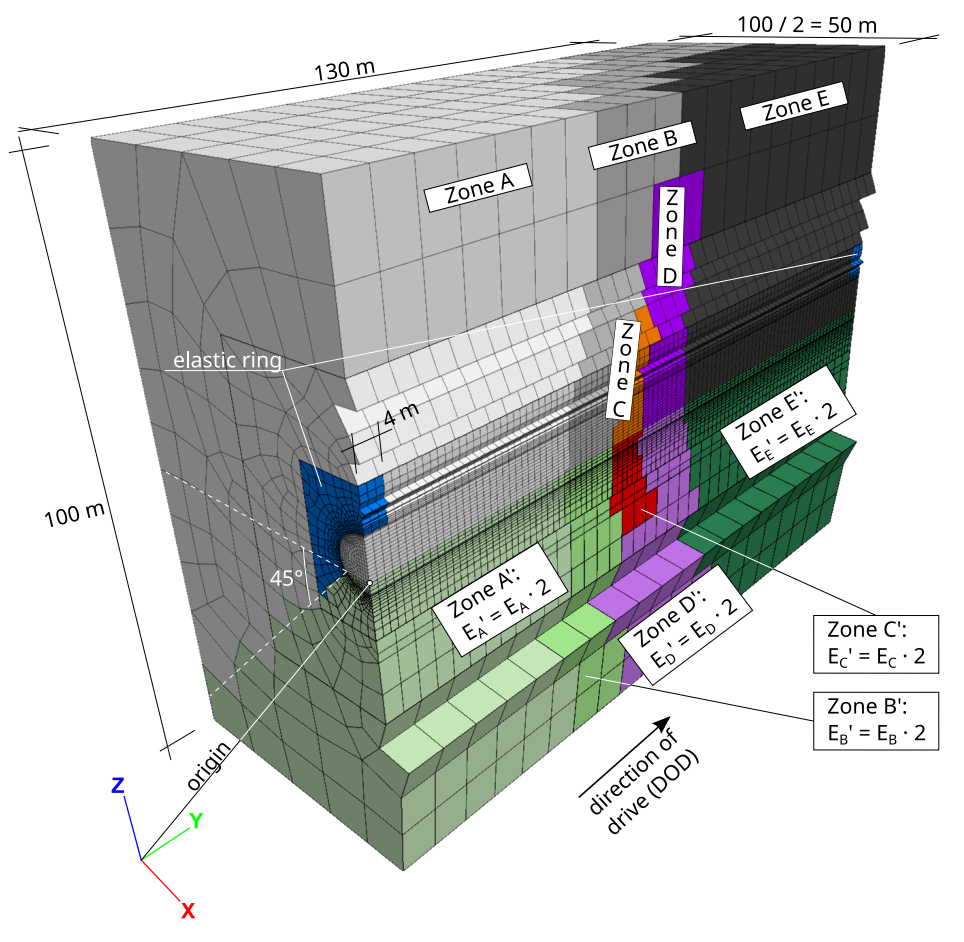


Figure 10.6: Validation case: Perspective view of the numerical model (initial state). The graph only shows the left model half.

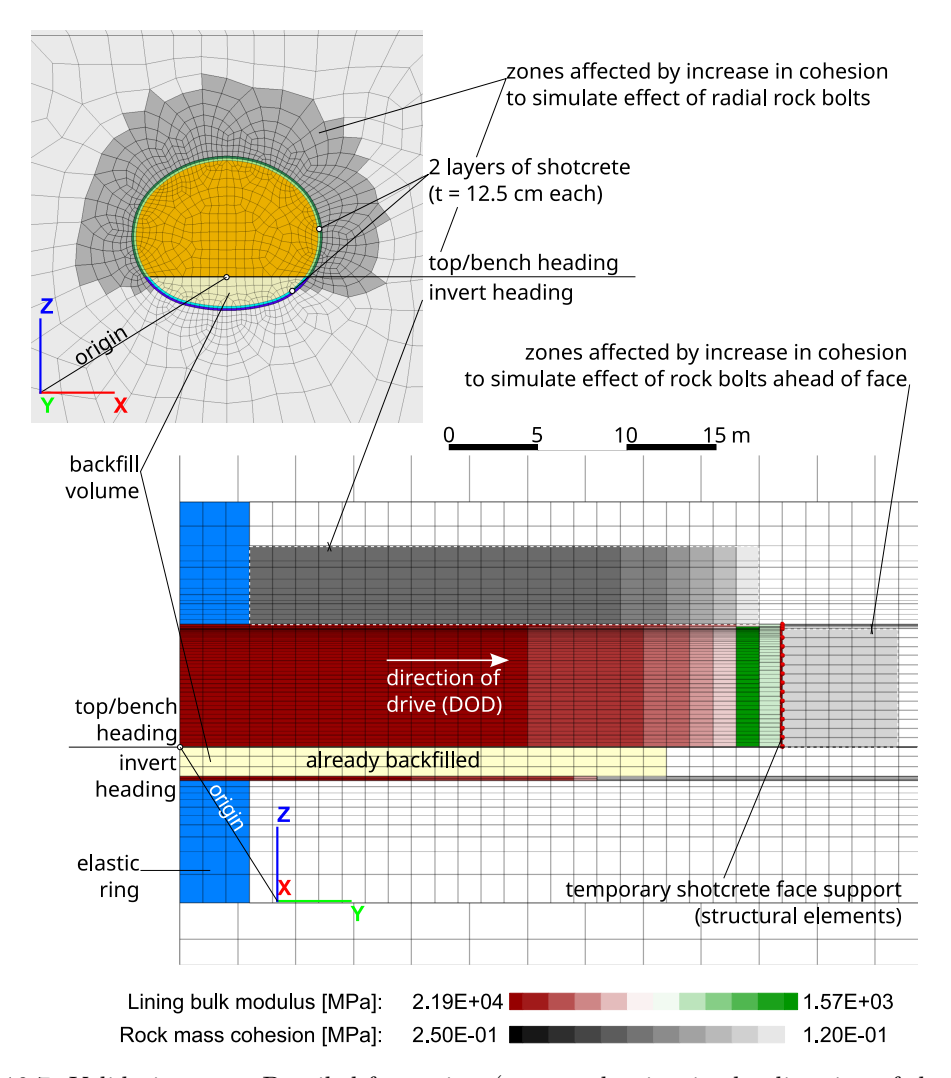


Figure 10.7: Validation case: Detailed front view (top graph; view in the direction of the tunnel drive) and detailed side view (bottom graph; view onto the left model half). The top and bottom graph do not share colours. The colour bars refer to the bottom graph only.

10.8.1 Modelling of system features

Like for the calibration case, the model was subdivided into rock mass zones by assigning different properties to the mesh elements that fall within the zone boundaries. The mesh was obtained using the extrusion option in FLAC3D and, thus, is in-plane all the same in the longitudinal direction. The zone boundaries are then not planar but characterised by the faces of the mesh elements oriented differently resulting in a zigzag shape (cf. Fig. 10.8). Consequently, the same applies also to the walls of the stiff block and to the interface separating the block from the surrounding weaker material.

In the vertical direction, the interfaces only range from 10 m below the tunnel to 10 m above the tunnel. And no interfaces are installed at the outermost block walls parallel to the tunnel axis. This made the simulation a little more stable. Since the block is large compared to the tunnel, and because the strong block limits the volume of influence of the tunnel excavation, the simplifications are valid.

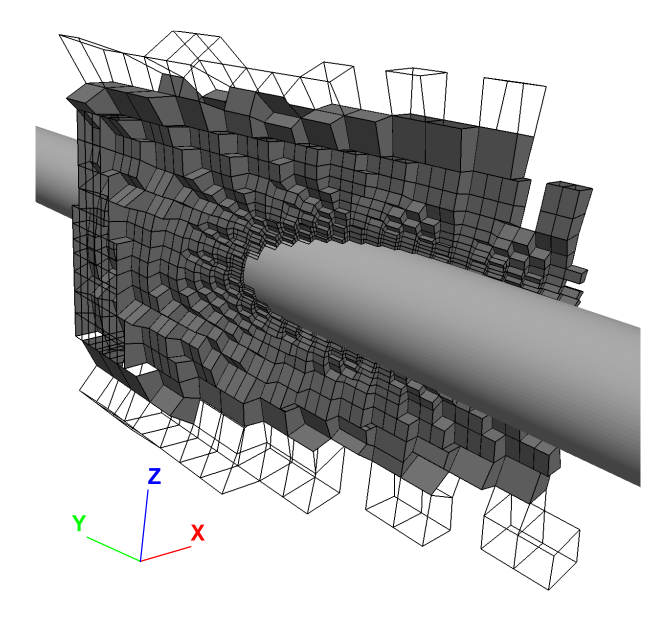


Figure 10.8: Validation case: Side view of the block-matrix interface (dark grey). The mesh grid outlines the stiff block (Zone C and Zone C*). The rock mass-lining interface is highlighted in light grey.

10.8.2 Modelling of material behaviour

The study uses the Ubiquitous Joint model and the Mohr-Coulomb (MC) model to simulate the behaviour of the rock mass zones. Zone B, D, and E share RMT 8f (cf. Fig. 10.1 on p. 245 and Tab. 10.1 on p. 247) for which the design documents report stress-dependent stiffnesses suitable for, e.g., the Plastic Hardening model. However, other RMT accompany RMT 8f. Because the RMT 8f layers are not modelled explicitly but are part of the homogenised zones, MC parameters are used for averaging considering the RMT shares (cf. Section 10.9.3 on p. 261). The design documents report MC parameters for all RMT.

10.8.3 Mesh

Most volumes are eight-node brick elements, some are six-node wedge elements. In the direction of the tunnel drive (DOD), because of the round length of 1.3 m of the top/bench heading, the minimum element size is also 1.3 m. In contrast to the region close to the DFOS section in the calibration case, here, no densification is performed in the DOD close to the block.

The model features 150,420 zones.

10.8.4 Model size

The tunnel displacements in the case here (cf. Tab. 10.4 on p. 250) are of the same magnitude as in the calibration case (cf. Tab. 8.7 on p. 183). Thus, the model size selected for the calibration case (cf. Section 9.4.4 on p. 215) is assumed to be suitable here too.

Because the extrusion option in FLAC3D is used to create the model, the top/bench-heading round length is 1.3 m, and FLAC3D [178]² suggests using numbers for the segmentation (or densification) "that are directly multiples of each other" (e.g., 1, 2, 4), in the DOD, a model size of 130 m is selected (cf. Fig. 10.6). Anyway, the tunnel drive in the simulation proceeds only until model chainage 100 m. For convenience, Zone B and Zone E are simply extended up to model chainage 130 m.

 $^{^2 \}dots / \texttt{doc/flac3d/zone/doc/manual/zone_manual/zone_commands/cmd_zone.densify.html}$

The model starts at tunnel chainage 235 m and ends at chainage 365 m. Thus, in the model, the stiff block crosses the excavation the first time approx. at chainage 39.5 m (= tunnel chainage 274.5 m).

10.8.5 Boundary conditions and initial state

With an overburden of \geq 59 m, the tunnel section is considered deep. Thus, the ground surface is not modelled explicitly.

In this study, the large-strain mode (cf. Footnote 7 on p. 87) remains turned off for the simulation of the excavation. Turning it on resulted in a few numerical incompatibilities where the rock mass-lining interface crosses the block-matrix interface. Note that according to [410, p. 52], the small-strain mode suffices for a shear band analysis.

10.8.6 Construction sequence

The following subsections list information on the site and simulation tunnelling sequences for the top/bench heading and the invert heading. The simulation comprises 78 top/bench-heading rounds and 24 invert-heading rounds. Those 102 rounds are processed by 760 simulation steps. The creep calculations cover 3,708,900 seconds. That are 42.9 days. The information on the site actions is from [341].

At the site, the top/bench-heading round length is 1.3 m and the invert-heading round length is 4.4 m. Because of the approach selected to create the mesh (cf. Section 10.8.4), in the simulation, the invert-heading round lengths must be a multiple of the top/bench-heading round length. The invert-heading round lengths were selected in a way that the error is smallest. It is 3.9 m or 5.2 m.

The standard site sequences for a top/bench-heading round and for a invert-heading round at the access tunnel *Göstritz* (analysed here) are similar to the ones for a top-heading round and for a bench/invert-heading round, respectively, at the tunnel *Gloggnitz* (calibration case; cf. Chapter 9 on p. 201). For the latter, Tab. 9.1 (p. 217) and Tab. 9.3 (p. 219) give simplified descriptions about the site actions and on how the sequences are implemented in the numerical simulation. The following subsections list the differences in the site actions and the implementations.

Top/bench heading

The sequence listed in Tab. 9.1 (p. 217) applies here from chainage 321.3 m. From chainage 235 m up to chainage 321.3 m, the rock bolts got installed before the installation of the 2nd shotcrete layer.

Tab. 10.6 lists all versions of simulation tunnelling sequences for the top/bench heading in this study.

Invert heading

The sequence listed in Tab. 9.3 (p. 219) does not apply here but is the basis for the tunnelling sequence that applies to all invert-heading rounds simulated in this study (cf. Tab. 10.7).

Table 10.6: Validation case: Variations of the simulated tunnelling sequence of top/bench-heading (tbh) rounds. For the simulation actions, refer to Tab. 9.1 (p. 217).

#	1	2	3	4	5	6	7	8
v0.1	tbh_excav = Standard		tbh_shot_1 equence for t	tbh_pass_2 he top/bench	tbh_bolt heading up to cha	tbh_pass_3 ainage 321.3 m	tbh_shot_2	tbh_pass_4
v0.2	tbh_excav = Standard			tbh_pass_2 he top/bench	tbh_shot_2 heading from cha	tbh_pass_3 inage 321.3 m	tbh_bolt	tbh_pass_4
v1	addition to simulating	on sequence for tbh_pass_3 b installation o	or a top/bence ut before cree f face bolts w	ep calculation hen top/bend	nd at which face b , set flag in partic	ular zones ahead c	tbh_shot_2 every 6th round); tbh_f f tunnel face for increaser ahead; at other scenar	se of cohesion
v2	otherwise, cohesion in	lation sequence one of the ot rock mass zo	ce scenario for her sequence nes around ex	r a top/bench s); tbh_bolt_c ccavation at re	louble: in addition	fore switch to invent to tbh_bolt but nstallation of radia	tbh_shot_2_ext ert heading (executed or before creep calculation al bolts at round i; tbh_ at round i	n, increase of
v3	otherwise, of but before of	ulation seque one of the oth creep calculat	nce scenario ner sequences ion, set flag in	for a top/ber); tbh_shot_2, a particular zo	.ext: cf. v2; tbh_b	olt_double_face: in el face for increase	tbh_bolt_double_face invert heading (execut addition to tbh_bolt_d of cohesion simulating	ed only once; ouble (cf. v2)
v4			- /	h-heading rou	and after switch from	om invert heading	to top/bench heading (executed only

Table 10.7: Validation case: Simulated tunnelling sequence of invert-heading (ih) rounds. For the simulation actions, refer to Tab. 9.3 (p. 219).

#	1	2	3	4	5	6
v0	= Standa	rd simulation	n sequence f	for the inver	t heading; il	ih_pass_3_ext n_pass_3_ext: in
	but befor		culation, ba	ckfill of exc	avated inve	. 9.3 on p. 219) rt section, and kfill

10.9 Numerical input parameters

The following subsections list site-specific conditions, geometries, and material parameters. Some input parameters are selected in the same way as in the calibration case (cf. Section 9.5 on p. 220) and, thus, are not cited here (e.g., stiffness cone, backfill, shotcrete strength and stiffness).

10.9.1 Tunnel shape and size

The tunnel cross section is mouth-shaped and circumscribes an area of approx. 66 m^2 . The cross-sectional area of the top/bench heading is approx. 56 m^2 (max. width = 10.2 m, max. height = 6.5 m), and it is approx. 10 m^2 (max. width = 8.6 m, max. height = 1.6 m) of the invert heading.

10.9.2 Primary stress state

The stress values cited in Section 10.4.2 (p. 247) match with the stresses at the model origin in the numerical simulation. For the calculation of the overburden stress using the specific weight, Zone C is not considered since it features a limited size (cf. Section 10.9.3).

10.9.3 Rock mass

Refer to Section 10.2 (p. 244) for a description of the geological and hydrogeological conditions and to Section 10.3 (p. 246) for the relevant design rock mass types (RMT).

Upon the rock mass description by the site geologists and the section views given in Fig. 10.1 (p. 245), the numerical model is split into the zones A-E. Along the tunnel axis, from model chainage 0 m up to model chainage 38 m, it is Zone A. Everything after model chainage 69 m is Zone E. It is assumed that what is before tunnel chainage 235 m or what comes after tunnel chainage 315 m has negligible effect on the system behaviour close to the foremost part of the block, which is of interest in this study. Except for Zone C, all other zones extend up to the model boundaries. This is an assumption as the rock mass structure outside the excavation area is unknown. The latter applies also for Zone C. Anyway, it seems unlikely that the stiff block extends that far considering its shape. The site head geologist confirmed that the extension outside the excavation area is probably limited ([170]). Often the extent is unknown, but drillings occasionally showed an extension of such blocks of maximum 1.5 times the equivalent tunnel diameter. For convenience, this value is used in the numerical simulation to limit the extension of the block to all sides. Horizontally, the boundaries of Zone C intersect within the defined thresholds at an acute angle (cf. lower graph in Fig. 10.1). It is assumed that such sharp edges break and, thus, in the simulation, the block is cut off at x = -11.5 m and at x = 6.5 m. The resulting height of the block in the model is approx. 28 m. Its in-plane width is 18 m. The vertical distance between the block top and the crown is approx. 9.5 m.

Tab. 10.8 lists the orientation of the foliation planes mapped at the tunnel faces from chainage 255 m to chainage 297.9 m. Three characteristic sections can be recognised, TS-FP 1–3. They relate to the model rock mass zones A and D (cf. Fig. 10.1). Since no planes have been mapped in the zones B, C, and E, it is assumed that in those zones the foliation is mechanically insignificant or non-present.

Table 10.8: Validation case: Orientation of foliation planes mapped at the top/bench-heading tunnel faces in the tunnel section from chainage 255 m to chainage 297.9 m (information from [152]).

Zone	Chainage [m]	DD/dip [°]				Mean DD/dip [°]	TS-FP			
	255	340/60	009/62	010/67						
	257.6	010/60	025/70	020/55		000/69	1			
	260.2	020/61	355/61			008/62	1			
Α	264.1	016/46	(310/71)	351/74	(030/35)					
	266.7	355/35	025/40							
	269.3	031/42	031/46			011/46	2			
	271.9	010/50	354/52			011/40	2			
	274.5	345/50	013/52							
	No foliation	on planes map	oped at cha	inage 277.	1 m, 279.7	m, and 282.3 m				
	284.9	005/84								
D	287.5	345/70	036/78			348/76	3			
D	292.7	335/80	340/86	322/75		340/10	3			
	297.9	356/61								
	No foliation planes mapped at chainage 299.2 m, 303.1 m, 305.7 m,									

308.3 m, 314.8 m, and 316.1 m

DD ... dip direction, dip ... dip angle

TS-FP ... Tunnel section regarding the orientation of the foliation planes

() ... Values in parentheses are not used for the arithmetic averaging

At the site, the rock masses encountered have been assigned to RMT 5f-1, 5f-2, 8c, or 8f. Part I of Tab. 10.9 gives the design values for each RMT. The following subsections³ outline the decisions on the rock mass parameters for the model zones A–E. For estimates of the tunnel displacements, the site utilisations of the lining are used (cf. Tab. 10.10). Tab. 10.11 lists the rock strengths mapped at the tunnel faces. In combination with the discontinuity spacings (not shown), they allow to assess the rock mass quality to some extent.

Table 10.9: Validation case: Rock mass parameters of the rock mass types (RMT) 5f-1, 5f-2, 8c, and 8f (from [61, 103]), and of the model zones A–E.

	$\gamma m [kN/m^3]$	ν [-]	E_n [GPa]	E_p [GPa]	φ_n [°]	$arphi_p$ [°]	c_n [MPa]	c_p [MPa]		
Ι	Design values ([61, Appendix 1, p. 1, 3], [103, p. 21])									
I.a	Representative calculation values									
RMT 5f-1	26	0.2	0.2 25 33					2		
RMT $5f-2$	28	0.15	65		4	0		10		
RMT 8c	25	0.27	0.2(2)		2	4	0.5	0.12		
			0.45(5)	2(5)						
			0.85(11)							
			1.25(20) 2	2.5(20)						
RMT $8f$	24	0.3	$50 \cdot \sigma_1 + 0.$	015	2	4		0.12		
I.b				Value r	anges					
RMT 5f-1	26	0.150.25	1045		29	.38	0.74			
RMT $5f-2$	28	0.10.2	4585		36.	.44	5	15		
RMT 8c	25	0.250.3	0.40.9(5)	210	2330	2327	0.40.8	0.060.15		
			1.22(20)							
RMT 8f	24	0.250.35	$\{30\dots70\}\cdot \sigma_1 $	+0.015	2325		0.10.15			

 $_{\rm n}$...normal to weakness planes

^{() ...} Values in parentheses are the absolute values of the major principal stress, σ_1 , (in mega-pascal), for which the stiffnesses are valid

II	Selected for the numerical model								
Zone A	25	0.27	0.165	24	0.12				
Zone B	24.4^{a}	0.29	0.132	24	0.12				
Zone C	28	0.15	65	40	10				
Zone C^*	26	0.2	25	33	2				
Zone D	24^{a}	0.25	0.140	25	0.15				
Zone E	25	0.25	1	25	0.2				

 $^{^{\}ast}$ From model chainage 70 m.

Zone A (from y = 0 m to y = 38 m)

Zone A entirely is of RMT 8c.⁴ The average overburden is approx. 63 m. With $\gamma=25$ kN/m³, the average overburden stress results to -1.58 MPa. According to the site documentation, the foliation planes are mechanically effective. Like it was done for the calibration case (cf. Section 9.5.3 on p. 220), the use of the Ubiquitous Joint model is intended and finding a valid rock mass parameter set for the simulation starts with the favourable values of the representative design rock mass parameters given in Tab. 10.9 (part I.a): $\nu=0.27$, $E=E_p=1886$ MPa, $\varphi=24^\circ$, $c=c_n=0.5$ MPa. With R=4.57 m, $k_0=0.75$, and a mean internal pressure of $p_i=0.4$ MPa (cf. Tab. 10.10), the analytical solution by [117] yields a mean radial displacement of 2.9 mm. The average of the mean radial displacements recorded at the monitoring cross sections from chainage 225 m to chainage 266 m (cf. Tab. 10.4 on p. 250) plus one-third to consider for the

 $_{\rm p}$. . . parallel to weakness planes

^a For convenience, all rock mass zones in the model except for Zone C feature a specific weight of 25 kN/m³.

³The chainages cited in the subsection headings refer to the tunnel axis (cf. Fig. 10.1 on p. 245).

⁴The share of RMT 8f in Tab. 10.1 (p. 247) from chainage 271.9 m relates to Zone B.

Table 10.10: Validation case: Shotcrete lining utilisations and values for the equivalent internal pressure, p_i , at monitoring cross sections between chainage 235 m and chainage 329 m (information on the utilisations from the software suite TUNNEL:Monitor). Estimates of p_i with Eq. 9.7 (p. 222) assume an equivalent tunnel radius of 4.57 m. For the shotcrete strength, refer to Section 10.9.4 (p. 267).

Chainage [m]	235	246	254	266	274	286	297	310	319	329
MT			Util	isation	after	1 day	in per	cent		
1	30	23	29	12	19	14	37	13	20	6
2	27	19	44	36	40	27	26	14	29	8
3	24	30	37	33	16	11	26	11	8	22
4	86	48	98	95	62	62	19	23	28	35
5	88	61	97	82	38	48	37	18	22	40
mean	51	36	61	51	35	32	29	15	21	22
p_i [MPa]	0.3	0.2	0.4	0.3	0.2	0.2	0.2	0.1	0.1	0.1
MT			Utili	sation	after	5 days	in per	rcent		
1	16	15	11	12	10	11	10	10	19	10
2	~ ~			~ -						4.0
<u> </u>	22	14	32	27	24	11	22	11	15	12
3	$\frac{22}{44}$	14 31	32 73	$\frac{27}{30}$	$\frac{24}{37}$	11 15	$\frac{22}{24}$	$\frac{11}{17}$	15 11	12 48
									-	
3	44	31	73	30	37	15	24	17	11	48
$\frac{3}{4}$	44 74	31 28	73 86	30 65	$\begin{array}{c} 37 \\ 45 \end{array}$	15 54	24 26	17 15	11 19	48 28
3 4 5	44 74 88	31 28 25	73 86 88	30 65 67	37 45 43	15 54 42	24 26 34	17 15 12	11 19 17	48 28 43

pre-displacements is 44 mm. Thus, the selected modelling parameters are too good. As noted in Section 8.3 (p. 172), RMT 8c is a rock mass with a moderate share of cataclasites (according to [61, p. 61]: 30...70%). The share of cataclasites from chainage 255 m to chainage 279.7 m ranges from 44% to 74% (not shown) and is higher at the end of Zone A. Note the low rock strengths mapped at the site (cf. Tab. 10.11). The material encountered is at the least favourable end of the definition of RMT 8c. Thus, for the numerical model, the least favourable values of the representative calculation parameters in Tab. 10.9 are used: $\nu = 0.27$, $E = E_n = 165$ MPa, $\varphi=24^{\circ},\,c=c_p=0.12$ MPa; cf. also part II in Tab. 10.9. The resulting mean radial displacement is 41 mm. Note that the analytical solution yields larger displacements at the crown than at the side walls. This is in contrast to the site observations (cf. Tab. 10.4) and shows the inability of the simple analytical approach to reproduce displacements of a non-circular tunnel in anisotropic heterogeneous rock masses excavated with two consecutive headings. Zone A of the calibration case also comprises RMT 8c and conditions are similar (cf. Section 9.5.3 from p. 222). There, the internal angle of friction derived for the numerical model is also 24°. Thus, the model here uses the same parameters for the weakness planes of the Ubiquitous Joint model: $\varphi = 20.7^{\circ}$, c=0.06 MPa, $\psi=0^{\circ}$, $\sigma_t=0.01$ MPa. Because the strength parameters of the weakness planes are close to those of the rock mass, the influence of the former on the overall displacement pattern will be probably minor. By arithmetic averaging, two sections with a reasonable mean orientation of the weakness planes can be identified, namely TS-FP 1 and TS-FP 2 (cf. Tab. 10.8). Note that in the model, the displacement level will decrease with the heading approaching the stiff block, like it was observed at the site (cf. Tab. 10.4).

Table 10.11: Validation case: Share of the rock strength mapped at the top/bench-heading tunnel faces in the tunnel section from chainage 255 m to chainage 314.8 m (information from [152]).

		Share of the rock strength mapped at the top/bench-heading tunnel face in percent									
Chainage [m]	255	257.6	260.2	264.1	266.7	269.3	271.9	274.5	277.1	279.7	
15 MPa 525 MPa	50 50	48 52	44 56	54 45	56 41	61 29	64 27	68 21	58 19	46 19	
2550 MPa 50100 MPa	-	- -	-	2	3	10	10	- 11	8 15	13 22	
Chainage [m]	282.3	284.9	287.5	292.7	297.9	299.2	303.1	305.7	308.3	314.8	
15 MPa 525 MPa 2550 MPa 50100 MPa	46 14 6 33	38 30 4 29	41 17 3 39	36 25 6 33	28 31 8 33	43 22 4 31	37 20 12 30	36 30 2 30	43 14 13 29	23 45 1 32	

Zone B (from y = 38 m to y = 49 m)

Zone B comprises RMT 8c and RMT 8f each with variable shares from 0% to 100%⁵. Overall, RMT 8f predominates in the zone. At the monitoring cross section at chainage 274 m, the mean radial displacement is 21 mm (cf. Tab. 10.4 on p. 250). Plus one-third for the pre-displacements, it is then 28 mm. The displacement level is only two-thirds of the one in Zone A. However, Zone B borders the stiff block which takes most of the loading. Without the block, the tunnel in Zone B would probably displace as much as in Zone A. The mapped rock strength of the slate is as high as of the gypsum block, but the slate is strongly fractured resulting in a low rock mass strength. The share of cataclasites in Zone B is a little larger than in Zone A, but the more competent slate makes up for some of the difference in the overall rock mass quality. Thus, the quality of the zones differs little. With 40% of RMT 8c (least favourable calculation parameters) and 60% of RMT 8f, an average overburden of approx. 69 m, and an average overburden stress of -1.73 MPa, the modelling parameters are (cf. Tab. 10.9): $\nu = 0.29$, E = 132 MPa, $\varphi = 24^{\circ}$, c = 0.12 MPa. The analytical solution yields 62 mm for the mean radial displacement considering $p_i = 0.4$ MPa. At MS 274, the mean internal support pressure is 0.3 MPa (cf. Tab. 10.10). But for the calculation, it is assumed as high as in Zone A where there is no block. The calculated displacements are quite large. Considering that in the DFOS calibration case modelling parameters resulting in matching displacement levels (i.e., analytical solution \approx site observation) eventually still yielded a too low displacement level in the numerical simulation, here, the determined modelling parameters are used even if they overestimate the displacement level. The foliation planes mapped from chainage 255 m up to chainage 274.5 m all relate to Zone A (cf. Tab. 10.8 on p. 261). From chainage 284.9 m up to chainage 292.7 m, they all relate to Zone D. Thus, no information of foliation planes in Zone B exist. According to the site documentation ([152]), the rock mass zones don't show an initial structure. Thus, the simulation assumes Zone B being isotropic and applies the Mohr-Coulomb model. The anisotropy of the tunnel displacements results because of the stiff block crossing into the tunnel drive.

⁵The percentages in Tab. 10.1 (p. 247) refer to the entire tunnel face without differentiating between the individual zones created for this study. The shares in the text, however, refer to the Zone B parts of the mapped tunnel faces.

Zone C (from y = 49 m to y = 56 m)

The moment the heading hit the stiff block at chainage 274.5 m, here marked as Zone C, the small portion of the tunnel face was assigned to RMT 8f (weak). However, the geologist noted its massive characteristics and high strength. In the report of the next mapped face at chainage 277.1 m, it is already RMT 5f-2 (very strong). From chainage 305.7 m, it is RMT 5f-1 (less strong than RMT 5f-2). It looks like that shearing between the block and the not-that-weak zone E affected the block quality at its rear part. Up to the model chainage 70 m (= tunnel chainage 305 m), the modelling parameters for Zone C are (cf. Tab. 10.9 on p. 262): $\nu = 0.15$, E = 65,000 MPa, $\varphi = 40^{\circ}$, c = 10 MPa; from model chainage 70 m, i.e., for Zone C*, they are: $\nu = 0.2$, E = 25,000 MPa, $\varphi = 33^{\circ}$, c = 2 MPa. Both RMT 5f-1 and RMT 5f-2 are considered isotropic since no foliation has been mapped (cf. Tab. 10.8 on p. 261).

Zone D (from y = 56 m to y = 69 m)

At the beginning, Zone D comprises RMT 8c and RMT 8f (cf. Tab. 10.1 on p. 247). Farther behind, it is only RMT 8f. The material is like the one before the block. However, overall, Zone D is a little more competent (cf. the shares of the first three strength categories in Tab. 10.11, e.g., at chainage 297.7 m vs at chainage 297.9 m). According to the site documentation, shear bodies of quartzite, dolomite, or limestone are slightly larger in Zone D (from < 10 cm to dm range) ([152]). In Zone D, also foliation planes have been mapped (cf. Tab. 10.8 on p. 261). More competent rock masses border the rather small Zone D on both sides. Thus, the displacements recorded at the site (cf. Tab. 10.4 on p. 250) are not representative for the zone material. Except for the first few metres, Zone D comprises only RMT 8f. Neglecting RMT 8c is assumed to have negligible effect on the displacements in Zone D since the affected rock mass parts are next to the block. As Zone D is more competent than Zone B, considering an average overburden of approx. 74 m and an average overburden stress of -1.78 MPa, the upper bound values (i.e., more favourable) for RMT 8f are (cf. part I.b in Tab. 10.9): $\nu = 0.25$, E = 140 MPa, $\varphi = 25^{\circ}$, c = 0.15 MPa. With the data in Tab. 9.9 (p. 224) for $\varphi \leq 24^{\circ}$ and with two additional test results⁶ from [199] where $24^{\circ} < \varphi \le 25^{\circ}$, the mean values of the joint strength parameters relevant for the Ubiquitous Joint model applied to Zone D are: $\psi = 6.1^{\circ}$, $\varphi = 21.7^{\circ}$, c = 0.05 MPa. In contrast to Zone A where all mapped foliation planes are smooth, in Zone D some are also rough and, thus, the dilation angle is not set 0 but the value from the averaging is used. The tensile strength is set to 0.01 MPa. Tab. 10.8 lists the mean orientation of the foliation planes used in the model.

Zone E (from y = 69 m to y = 130 m)

Zone E comprises RMT 8f and RMT 5f-1 (not the stiff block but other shear bodies). The phyllites are cemented with gypsum and more competent than in preceding sections. Considering the size of the shear body behind chainage 304 m sketched in Fig. 10.1 (p. 245), the rock mass may be considered as block-in-matrix rock. However, this shear body is the only one reported explicitly in the site documentation. The parameter finding starts with the upper bound values for RMT 8f (cf. part I.b in Tab. 10.9). It then continuously increases stiffness and strength (approaching those of RMT 5f-1) to consider for the cementation and the shear bodies until a combination is found with which the analytical solution yields a mean radial displacement that matches with the site recordings. Considering MS 310, MS 319, and MS 329 in Tab. 10.4,

⁶⁽¹⁾ CNS test on phyllite: sampling depth = 709 m, shear area = 106 cm², $\psi = 6.4^{\circ}$, $\varphi = 24.6^{\circ}$, c = 0.05 MPa, $\varphi_r = 24.1^{\circ}$, $c_r = 0$, $\tau_{max} = 0.49$ MPa, $s_{max} = 4.14$ mm. (2) CNS test on schist: sampling depth = 611 m, shear area = 102 cm², $\psi = 5.5^{\circ}$, $\varphi = 25^{\circ}$, c = 0.05 MPa, $\varphi_r = 25.7^{\circ}$, $c_r = 0$, $\tau_{max} = 0.38$ MPa, $s_{max} = 7.99$ mm.

the mean radial displacement plus one-third for the pre-displacement is 13 mm. The average internal pressure is considered with 0.2 MPa (cf. Tab. 10.10 on p. 263). The average overburden from chainage 304 m to chainage 315 m is approx. 78 m. With $\gamma=25$ kN/m³, this results in an average overburden stress of -1.95 MPa. A suitable parameter combination is: $\nu=0.25$, E=1,000 MPa, $\varphi=25^{\circ}$, c=0.2 MPa. The analytical solution yields 14 mm. The lower displacement level at chainage 310 m compared to at chainage 319 m (cf. Tab. 10.4 on p. 250) will result because of the stiff block taking some of the loading. No foliation planes have been mapped in Zone E (cf. Tab. 10.8). The simulation considers it isotropic and applies the Mohr-Coulomb model. The meshing approach required the enlargement of the model in the DOD from 100 m to 130 m (cf. Section 10.8.4 on p. 258). Thus, Zone E extends up to y=130 m.

For convenience, the dilation angle of all rock masses in the model is considered being 0° complying with a suggestion by [61, p. 95].⁷ And following the conclusions for the parametric study (cf. Section 6.2.12 on p. 98), the tensile strength of the rock mass is considered being one-tenth of the uniaxial compressive strength. This also applies to all model zones. The flag-brittle option (cf. p. 86) is set to false for all zones. Instead of setting the option to true for Zone C and Zone C*, which would imply an instantaneous softening to zero tensile strength upon tensile failure, a routine is coded that reduces the tensile strength to 25% of the initial value. This was done for numerical stability.

Block-matrix interface

The site documentation (cf. [152]) reports that from chainage 305.7 m, soft layers of cataclasites from sericite phyllites and slates cross the block. The material surrounding the block is of phyllite cataclasites being partly cohesive because of fine grains, or of strongly fractured limestones and slates where the walls of foliation planes are frequently graphitic. All mapped discontinuities that border the block are faults. From chainage 303.1 m, those faults are declared as shear bands. The surfaces of the faults are usually undulated, either rough or smooth, and coated with clayey to silty fillings.

This study assumes that fillings mainly comprise crushed fractions of the weaker matrix material (i.e., the material surrounding the stiff block). It further assumes that, by average, the internal angle of friction of the filling material differs little from the one of the parent material. Thus, it is reasonable to use the same value for the interface friction angle (cf. part II in Tab. 10.9 on p. 262): 24...25°. The parametric study followed the same approach (cf. Section 6.2.17 on p. 101).

Similar as for the foliation planes in Zone D (cf. p. 265), taking results from shear tests on discontinuities in relevant material with $\varphi \leq 25^{\circ}$, the average parameters are: $\psi = 6.1^{\circ}$, $\varphi = 23.4^{\circ}$, c = 0.05 MPa, $\varphi_r = 19.6^{\circ}$, $c_r = 0.01$ MPa. To account for the favourable hard rock characteristics of the stiff block to some extent, the parameters of the weak material are averaged with results from a shear test on a joint in gypsum⁸: $\psi = 7.8^{\circ}$, $\varphi = 29.4^{\circ}$, c = 0.19 MPa, $\varphi_r = 27.2^{\circ}$, $c_r = 0.01$ MPa. The simulation uses a dilation angle of 10° considering that the block surfaces are probably more undulated than those tested. The value is then identical to the one in the parametric study. For numerical stability, the tensile strength is set to: $\sigma_t = 0.05$ MPa and $\sigma_{t,r} = 0.01$ MPa.

⁷Data analysed in [199] show that the dilation angles obtained with shear tests on intact samples (not on discontinuities) varies from 0° up to 11°. The range was observed at soft material (like phyllite cataclasites), but also at stiffer material (like carbonate breccias). Thus, setting the angle to 0° is valid.

⁸CNS test: sampling depth = 200 m, shear area = 208 cm², $\psi = 9.5^{\circ}$, $\varphi = 37.0^{\circ}$, c = 0.32 MPa, $\varphi_r = 35.0^{\circ}$, $c_r = 0$, $\tau_{max} = 4.28$ MPa, $s_{max} = 3.72$ mm.

Eq. 6.7 (p. 102) is applied to determine suitable interface stiffnesses. K and G required are of the softer material from those the interface separates. Here, it is Zone B, Zone D, and Zone E. With $\Delta z_{min} \approx 0.2$ m, the equation yields the apparent normal zone stiffness, $k_{n,rm}$ (in mega-pascal per metre): 865 (Zone B), 840 (Zone D), 6000 (Zone E). Thus, the simulation uses $k_{n,if} = k_{s,if} = 1\text{E}+03$ MPa/m for Zone B and Zone D, and $k_{n,if} = k_{s,if} = 5\text{E}+03$ MPa/m for Zone E. The bonded-slip option is turned on.

10.9.4 Shotcrete lining

In the tunnel section analysed for the calibration (cf. Chapter 9), a C20/25/J2 shotcrete was installed (cf. Section 8.5.2 on p. 176). The tunnel section analysed here is supported by a C30/37/J2 shotcrete.

Within the first hours after the shotcrete application, at some chainages, the lining is almost fully utilised (cf. Tab. 10.10 on p. 263). As the deformation rate of the rock mass decreases and the lining hardens, the utilisation usually decreases too. In some sections, the utilisation remains constant (at a relatively low level) or even increases (starting from a relatively low level) because of late stress redistributions and related deformations. Anyway, because of lack of information, it is assumed that both shotcrete types feature approximately the same strength at early ages. Later, when the strength of the shotcrete of higher quality exceeds the strength of the shotcrete of lower quality, the difference is irrelevant because of the utilisation being far from 100%. It is also assumed that the stiffness development is similar; at least in the first days when the increase in deformation is largest. Then, the settings for the shotcrete material selected for the calibration case (cf. Section 9.5.5 on p. 225) can be applied also here.

The following subsections only address the tensile strength of the shotcrete lining and the rock mass-lining interface parameters since all other settings for the shotcrete lining are the same as in the calibration case.

Tensile strength

In the calibration case, all lining layers comprise the same wire mesh (i.e., one layer of type AQ 60; cf. Tab. 8.3 on p. 178 and Tab. 8.4 on p. 178). Here, the wire mesh in the top/bench-heading lining layers and in the rock-side lining layer of the invert heading is of the same type (i.e., one layer of type AQ 50; cf. Tab. 10.2 and Tab. 10.3, both on p. 249). The equivalent increase in the tensile strength is 0.86 MPa. However, the cavity-side lining layer of the invert heading comprises two layers of type AQ 60 and the equivalent increase in the tensile strength then is 2.49 MPa.

Interface

The rock mass parameters of the weaker zones (i.e., Zone A, B, D, and E) are close to those of the rock masses in the calibration case. Regarding the rock mass-lining interface strength, the same approach (cf. Section 9.5.5 from p. 232) is used here. The value ranges then are: $\varphi_{if} = 24 \dots 25^{\circ}$, $c_{if} = 0.12 \dots 0.2$ MPa, $\psi_{if} = 25^{\circ}$, $\varphi_{if,r} = 21 \dots 22^{\circ}$, $c_{if,r} = 0.006 \dots 0.01$ MPa, $\sigma_{t,if} = 0.074 \dots 0.126$ MPa, $\sigma_{t,if,r} = 0.004 \dots 0.006$ MPa.

In Zone C, not the rock mass is the weaker part but the shotcrete lining, at least at the early stages of the hardening process. For shotcrete applied to limestone, [205] (cited in [388, Fig. 2.8, p. 27]) reports a bond strength of $\{c \approx 3.7 \text{ MPa}; \varphi \approx 21^{\circ}\}$. Considering the internal angle of friction of the rock mass of Zone C of 40° (cf. part II in Tab. 10.9 on p. 262), the reported interface friction angle seems too low to be applied here. Thus, the simulation applies the average,

i.e., $\varphi_{if} = (40+21)/2 = 31^{\circ}$, to both Zone C and Zone C*. The value is in the range for the internal angle of friction of shotcrete cited in Section 9.5.5 (p. 228). It complies also with the lowest value of the range for the joint friction angle of RMT 5f-1 and RMT 5f-2 given in [380, p. 24f]. The reported cohesion of 3.7 MPa (cf. text above) is close to the value of 3.19 MPa for the cohesion of the shotcrete after one day of hardening (cf. Section 9.5.5 on p. 229). Because of lack in information, for Zone C, the cohesion is set to $c_{if} = 3$ MPa. This is approx. one-third of the cohesion of the rock mass (cf. Tab. 10.9). And for Zone C*, $c_{if} = 2/3 \approx 0.7$ MPa. Using the approach from the calibration case, the residual values and tensile strengths then are: $\varphi_{if,r} = 28^{\circ}$, $c_{if,r} = \{0.15; 0.035\}$ (in mega-pascal), $\sigma_{t,if} = \{2.06; 0.5\}$ (in mega-pascal), $\sigma_{t,if,r} = \{0.1; 0.023\}$ (in mega-pascal). The dilation angle is set to $\psi_{if} = 25^{\circ}$.

To determine suitable rock mass-lining interface stiffnesses, also the approach from the calibration case is used. With $\Delta z_{min} \approx 0.2$ m, the resulting values for ten times the apparent zone normal stiffness, $k_{n,rm}$, are approx. (in mega-pascal per metre): 1E+04 (Zone A), 9E+03 (Zone B), 3E+06 (Zone C), 1E+06 (Zone C from model chainage 70 m), 8E+03 (Zone D), 6E+04 (Zone E). For Zone A, Zone B, and Zone D, the model applies $k_{n,if} = k_{s,if} = 1E+04$ MPa/m; for Zone E, it is $k_{n,if} = k_{s,if} = 5E+04$ MPa/m. The approach described in Section 9.5.5 requires the stiffness of the softer material of those the interface delimits. Where the shotcrete is sprayed onto the rock mass of Zone C, the softer material is not the rock mass but the shotcrete. There, with $\Delta z_{min} \approx 0.125$ m, the values are approx. (in mega-pascal per metre): 2E+05 (shotcrete at t=1 hour), 3E+06 (shotcrete at t=28 days).

10.9.5 Rock bolts

The mean effective area of one radial rock bolt is 2.42 m². The equivalent increase in the cohesive strength, Δc_p , at t=28 d then is (in mega-pascal): 0.08 (Zone A, B, D, and E), 0.11 (Zone C), 0.10 (Zone C*). In the case here, the radial rock bolts are only 4 m long. Thus, the volume affected by the installation of 14 rock bolts at the top/bench heading is smaller than in the calibration case (cf. Fig. 10.7 on p. 257).

Of the 6 rock bolts installed ahead of the tunnel face of the top/bench heading, the mean effective area of one rock bolt is approx. 9.61 m². Then, at t=28 d, Δc_p is (in mega-pascal): 0.03 (Zone A, B, C*, D, and E), 0.04 (Zone C). The face rock bolts are installed at every 6th top/bench-heading round (e.g., at chainage 238.1 m = model chainage 3.1 m). They are overcored for two round lengths (i.e., 2.6 m). The bottom graph in Fig. 10.7 highlights the volume ahead of the tunnel face affected by the increase in cohesion due to the face rock bolts.

10.10 Evaluation approach

Like for the numerical studies detailed in previous chapters, the evaluations here focus on the secondary principal stresses, failure thresholds, and shear strain increments. The evaluation approaches are the same (e.g., parameter developments as the headings proceed, contour plots, zone-by-zone plots).

Tunnel displacements developing in the simulation are compared with site recordings to evaluate the validity of the numerical simulation settings. Since here the simulation for the first time considers a stiff block and a tunnel lining, it monitors the loading of selected lining sections.

The simulation is run twice, once with the stiff block (= with-block case) and once without it where it is substituted by a matrix block (= matrix-only case). Of both cases the displacement of the rock mass zones is analysed to observe the effect the block has on the ground behaviour.

10.11 Results

Fig. 10.9 plots the tunnel displacements at model chainage 31.2 m (= tunnel chainage 266.2 m). Qualitatively, they fit well with the site recordings (cf. Fig. 10.3 on p. 251). Both in the model and at the site, the left tunnel side displaces horizontally and vertically more than the right tunnel side (cf. graphs (a) and graphs (b)). In the model in the longitudinal direction, the displacement of the left side wall is ok whereas of the other monitoring points it is too large (cf. graphs (c)). Note that in the matrix-only case, those other monitoring points displace less against the DOD (not shown) and match better with the site observations. Thus, the block may be less competent than simulated. Overall, like it was for the calibration case (cf. Chapter 9 on p. 201), the displacement magnitude in the model is too small and the pre-displacements are relatively large.

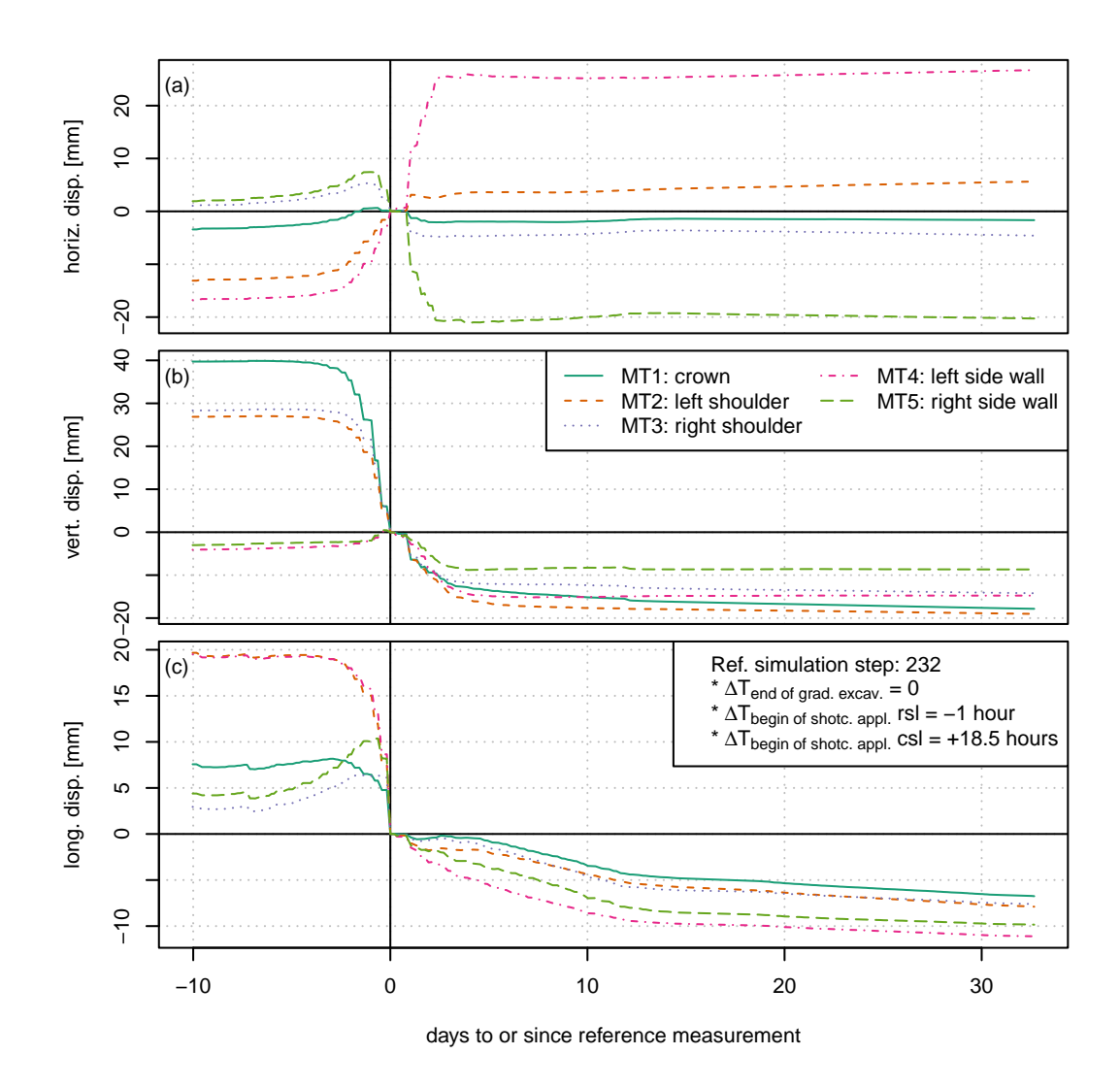


Figure 10.9: Validation case: Development of the tunnel displacements monitored at five grid points at the inner surface of the cavity-side shotcrete layer at model chainage 31.2 m. (a) horizontal displacements (displacement to the left: negative value); (b) vertical displacements (displacement downwards: negative value); (c) longitudinal displacements (displacement against the direction of the drive: negative value). Note the different scaling of the ordinate axes. csl...cavity-side layer, rsl...rock-side layer, MT...monitoring target.

The graphs in Fig. 10.10 show the development of some stress related evaluation parameters within the block (Zone C only; excluding Zone C*) as the tunnel drive approaches, crosses, and heads beyond the block. Note that the block enters the excavation section approx. at chainage 39.5 m (= tunnel chainage 274.5 m) and exits it approx. at chainage 73.5 m (= tunnel chainage 308.5 m; cf. Fig. 10.1 on p. 245). The tunnel drive affects the block approx. 10 m before it reaches the block. The secondary major principal stress, σ_1 , and the share of failed block zones increases steadily (cf. Fig. 10.10a-c). The influence continues until the drive is approx. 10 m behind the block. The largest increase in σ_1 occurs in the block regions closest to the tunnel (cf. Fig. 10.13ba on p. 274 and Fig. 10.15ba on p. 275). In graph (c), the share of approx. 14% refers to zones of which almost all have failed in tension. Theoretically, damage initiates before the drive reaches the block (cf. graph (b)). Up to when the heading is approx. at model chainage 56 m, the mean value of the strength-stress ratio, SSR, of all considered block zones increases. Note the simultaneous increase in the mean value of the secondary minor principal stress, σ_3 , (cf. graph (a)). In the case analysed here, the horizontal primary stresses are lower than the vertical primary stress (cf. Section 10.4.2 on p. 247). It is similar for the $k_0=0.5$ cases of the parametric study (cf. Chapter 6 on p. 81). There it was identified that because of the directed stresses zones next to the side walls but farther away and outside the yield zone⁹ are pushed away from the tunnel (cf. Section C.3.6 on p. 396). The same can be observed here: consider the light blue zone ahead of the tunnel face in Fig. 10.11ab/bb (p. 273). In the with-block case, with its stiffness the block acts like a shield preventing displacements at some locations (e.g., less positive x-displacement of zones farther ahead of the tunnel face in Fig. 10.11ba) and forcing some displacements to accumulate at other locations (e.g., more positive x-displacement of zones to the left of the block at the chainage of the tunnel face in Fig. 10.11ba). Anyway, this pushing results in an increase in the lateral support of the block or of its preservation (cf. Fig. 10.13bb and Fig. 10.15bb). Because of the same reason, almost no slip along the block-matrix interface takes place. At the final state when both the top/bench heading and the invert heading are at model chainage 100 m, the mean value of the total interface shear displacement at the block front of interface elements within 2 m around the tunnel is approx. 1.5 mm. Note here also the fact that the zones farther ahead of the tunnel face displace little in the vertical direction and that they displace upwards rather than downwards (cf. Fig. 10.11bc). The uplift of the upper model half ahead of the tunnel face is less pronounced if the block is not present (cf. Fig. 10.11ac). 10 Further, because of all that no distinct shear bands crossing from the block towards the tunnel could be observed (cf. Fig. 10.13bc and Fig. 10.15bc).

When the top/bench heading has passed the block for most of its part, more load is redistributed to the block (cf. increase of σ_1 in Fig. 10.10a). Simultaneously, σ_3 decreases (i.e., less compression or more tension), SSR decreases, and lots of zones fail (cf. Fig. 10.10a/c/d).

Not shown here is the development of the stress ratio σ_1/σ_3 being a measure for spalling. Because of the primary stresses, the setup of the numerical model, and the stiffness contrast between the block and matrix material, already at the initial state many of the block zones experience little compression or even tension in the minor principal stress direction. ¹¹ Accordingly, first zones fail in tension. During the simulation of the heading, the mean value of σ_1/σ_3 of zones with $\sigma_3 < 0$ is always above the spalling threshold of 10.

 $^{^9}$ For the moment plotted in Fig. 10.13ba/bb/bc (p. 274), the yield zone extends approx. four rounds ahead of the top/bench-heading face (not shown).

¹⁰Some of the uplift may relate to the overestimation of the zone deformation at unloading by the Mohr-Coulomb model

¹¹This may or may be not true in reality.

Fig. 10.12 graphs the development of two measures for the loading of four top/bench-heading lining sections. The sections in front of the block are loaded more: higher mean stress, p, in graph (a) and lower strength-stress ratio, SSR, in graph (b) (except for the peaks¹²). Comparing the with-block case with the matrix-only case shows that the sections in front of the block experience almost the same loading, at least for the most part. When the top/bench-heading drive is at model chainage 56 m, in the with-block case the loading is higher and still increases even though the lining segment is > 25 m behind. Further, the lining sections at the block back experience less loading than in the matrix-only case.

The decrease in p and the increase in SSR as soon as the heading is outside the volume of influence relates to relaxation of the shotcrete. Regarding SSR consider that the ratio depends on the strength which increases with time. Further, note that in the matrix-only case p features an increasing trend at the lining sections farther behind even when the top/bench heading is at the model chainage 100 m. This shows that there the displacements related to the heading (top/bench, or invert) are not finished yet.

Anyway, the increasing trend of SSR at a low rate in Fig. 10.12b matches well with the decrease of the utilisation of the lining at the site plotted in Fig. 10.14 (p. 274). Neglecting the up and downs, there, the utilisation also decreases at a low rate.

10.12Interpretation and discussion

Although the stiffness contrast between the block and the matrix material of over 460 is enormous, the negative effects of the block on the ground and system behaviour are little. In contrast to the fictitious with-block scenarios in this thesis, the block here is simply too big. The scenario here lacks of the possibility that redistributed stresses accumulate at the block top and bottom and later when significant interface slip occurs to introduce pronounced shear bands in front of the block. Even though first signs of shear band formation can be observed here as some interface slip occurs (not shown), the favourable stress situation¹³ prevents the shear bands to further develop. In addition, the yield zone surrounding the excavated tunnel is rather small.¹⁴ As already mentioned for the fictitious studies, shear bands are well pronounced only when they can develop predominantly within the yield zone. If the stress situation is less favourable (e.g., k₀=1) or if the yield zone ahead of the tunnel face is larger reaching the block much earlier than the heading, then in the case here the shear bands would be more pronounced.

The rock mass and stress settings in this case also promote early block failure. Already at the beginning, the lateral support of many of the block zones is low. Soon the first zones fail in tension. At any time, stresses in most block zones exceed the spalling limit. And with the block entering the excavation volume, considerable block failure occurs. At that moment the site engineers already know about the block (cf. also Subsection 'Has the stiff block been discoverable?' on p. 251) and can set appropriate measures. ¹⁵ Here the block fails gradually rather than abruptly. And its existence is known to the engineers prior to reaching it by interpreting the monitoring displacement data. However, the simulation results show an increase in the loading

 $^{^{12}}$ The peaks Fig. 10.12b relate to when the cavity-side lining layer is installed which experiences almost no loading at the beginning resulting in a very high SSR.

¹³It is always the combination of the orientation of the stresses and the orientation of the block surfaces that matters.

¹⁴Before the block at model chainage 30 m, the vertical distance between the yield front and the tunnel crown

is approx. 3 m (not shown).

15 The site engineers were aware of the tunnelling problems that heterogeneous rock masses with high stiffness contrasts can bring along and checked the lining for cracks in more detail the moment they encountered the stiff block (cf. [344, p. 41])

of the lining section in front of the block even if the heading is far ahead (cf. Fig. 10.12a). In the matrix-only case, the increase stagnates when the top/bench heading is approx. 18 m ahead. In the with-block case the increase continues up to when the heading is approx. 30 m ahead. The repetitive increases in the lining utilisation at the site also show that rock mass deformations and stress redistributions continue for a long time (cf. MS266 in Fig. 10.14). Anyway, such variation can be observed also in rock mass sections without such a stiff block (or at least its existence is unknown; e.g., in the case detailed in Chapter 8 on p. 169; note that there the variation is not described or graphed).

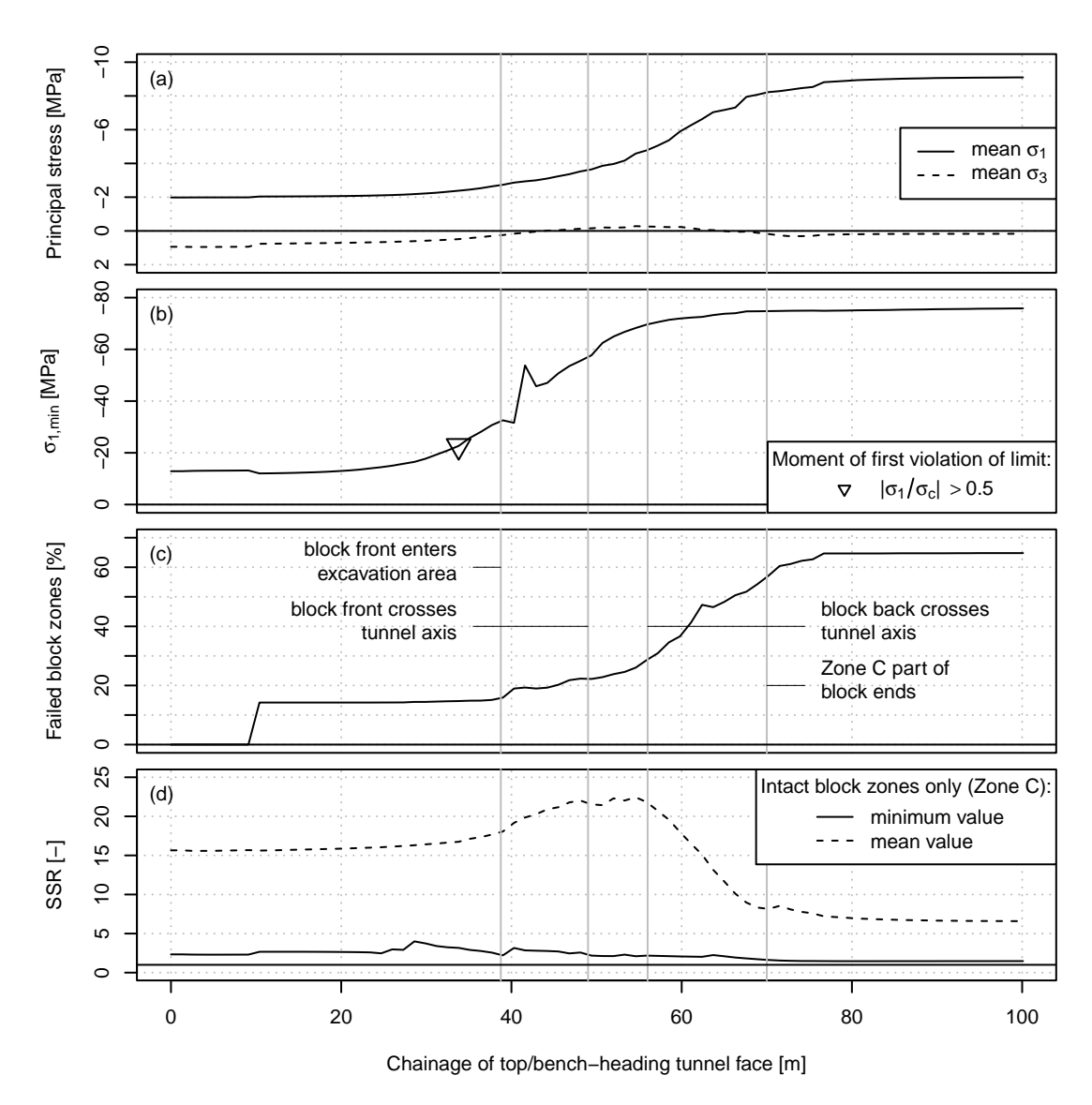


Figure 10.10: Validation case: Development of some block evaluation parameters. Analysed is only Zone C but not Zone C*. (a) mean values of the secondary principal stresses, σ_1 and σ_3 ; (b) minimum value of σ_1 ; (c) ratio of the number of failed block zones to the total number of non-excavated block zones (the latter changes as the heading proceeds); (d) mean and minimum value of the strength-stress ratio, SSR. Note for graph (b) that the marker for the moment of first violation of limit refers to yet intact zones; some zones have failed already before. For the grey vertical solid lines consider the annotations in graph (c) and compare with Fig. 10.1 (p. 245).

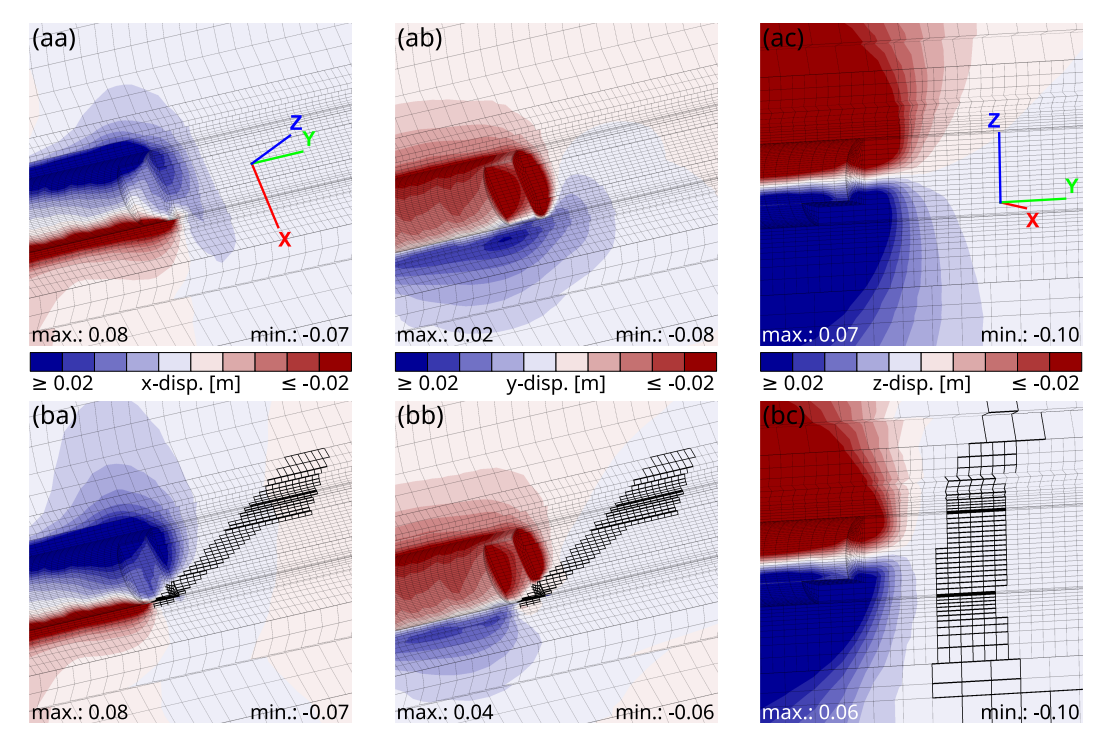


Figure 10.11: Validation case: Contour plot of the in-plane horizontal displacement (i.e., in the x-direction) (aa/ba), the out-of-plane horizontal displacement (i.e., in the y-direction; longitudinal displacement) (ab/bb), and the vertical displacement (i.e., in the z-direction) (ac/bc) in the matrix-only case (top graphs) and with-block case (bottom graphs). The graphs show the moment when the top/bench heading is at model chainage 41.6 m (= tunnel chainage 276.6 m) and the invert heading is at model chainage 36.4 m (= tunnel chainage 271.4 m). (aa/ab/ba/bb) perspective top view: lower model half; (ac/bc) perspective side view: left model half. The black solid lines in the bottom graphs outline the block zones. The graphs only show non-excavated rock mass material (i.e., no lining or backfill zones).

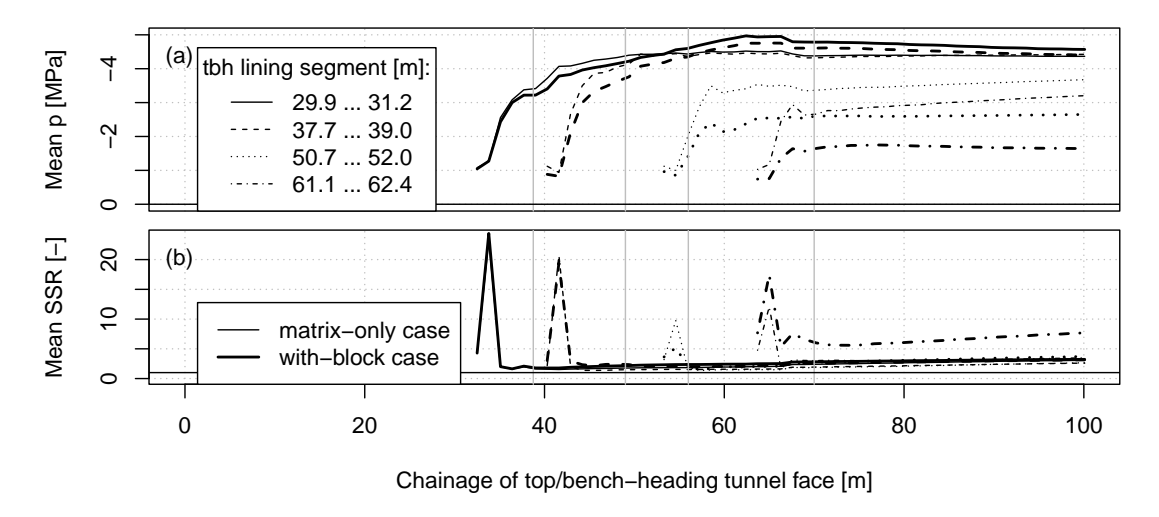


Figure 10.12: Validation case: Development of the mean value of the mean stress, p, (cf. Eq. A.1 on p. 317 in the appendix) (a) and of the strength-stress ratio, SSR, (b) in the zones of the top/bench-heading (tbh) lining segments of four different rounds. The rounds match with chainages at the site where monitoring cross sections have been installed (cf. Fig. 10.1 on p. 245 and Fig. 10.14): 266 m, 274 m, 286 m, and 297 m. For the grey vertical solid lines, refer to the caption of Fig. 10.10.

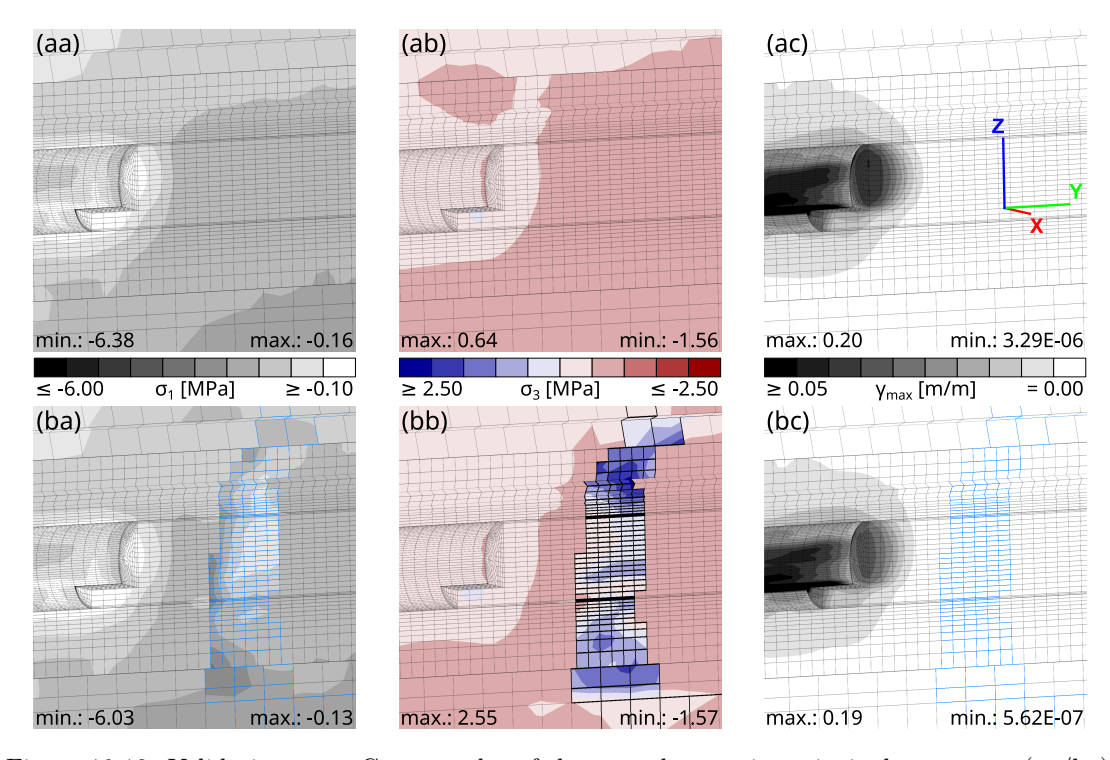


Figure 10.13: Validation case: Contour plot of the secondary major principal stress, σ_1 , (aa/ba), the secondary minor principal stress, σ_3 , (ab/bb), and the maximum shear strain increment, $\gamma_{max} = \varepsilon_3 - \varepsilon_1$, (ac/bc) in the matrix-only case (top graphs) and with-block case (bottom graphs). The graphs show the moment when the top/bench heading is at model chainage 41.6 m (= tunnel chainage 276.6 m) and the invert heading is at model chainage 36.4 m (= tunnel chainage 271.4 m). Perspective side view: left model half. The black or blue solid lines in the bottom graphs outline the block zones. The graphs only show non-excavated rock mass material (i.e., no lining or backfill zones).

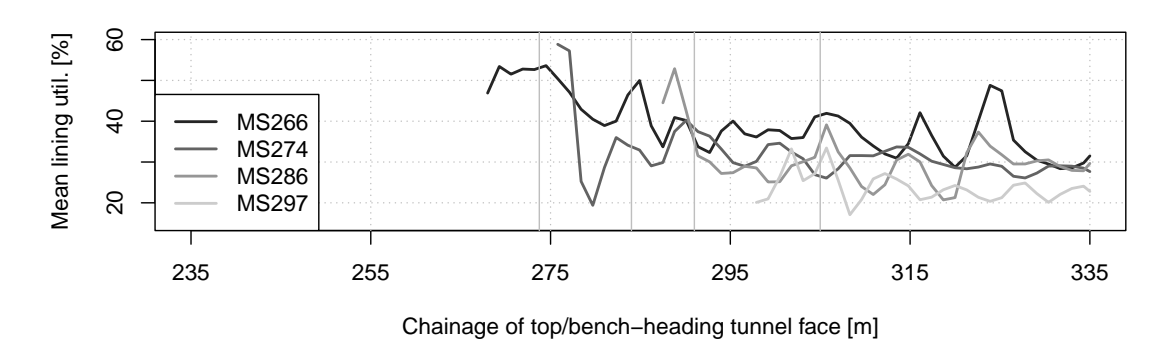


Figure 10.14: SBT1.1 | Göstritz: Development of the mean value of the utilisation of the top/bench-heading lining at monitoring cross sections (MS) at following site chainages (cf. Fig. 10.1 on p. 245): 266 m, 274 m, 286 m, and 297 m. For the grey vertical solid lines, refer to the caption of Fig. 10.10. Utilisation data from the software suite TUNNEL:Monitor ([142]) installed at the site.

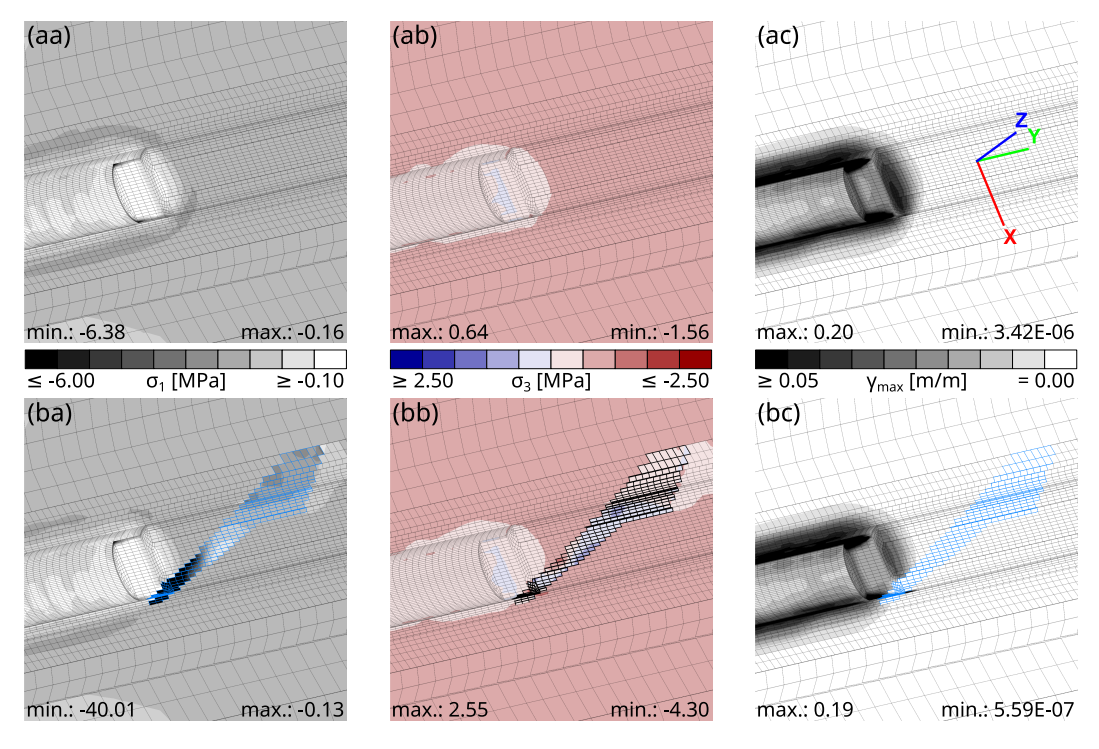


Figure 10.15: Validation case: Contour plot of the secondary major principal stress, σ_1 , (aa/ba), the secondary minor principal stress, σ_3 , (ab/bb), and the maximum shear strain increment, $\gamma_{max} = \varepsilon_3 - \varepsilon_1$, (ac/bc) in the matrix-only case (top graphs) and with-block case (bottom graphs). The graphs show the moment when the top/bench heading is at model chainage 41.6 m (= tunnel chainage 276.6 m) and the invert heading is at model chainage 36.4 m (= tunnel chainage 271.4 m). Perspective top view: lower model half. The black or blue solid lines in the bottom graphs outline the block zones. The graphs only show non-excavated rock mass material (i.e., no lining or backfill zones).

Bibliography

- [1] Abler, P. Einflüsse auf das Verformungsverhalten von jungem Spritzbeton im Tunnelbau. Diploma thesis, University of Innsbruck, Innsbruck, Austria, 1992.
- [2] ACI. ACI Manual of Concrete Practice. Technical report, American Concrete Institute (ACI), 1978.
- [3] ACI Committee 209. 209R-92. Prediction of Creep, Shrinkage, and Temperature Effects in Concrete Structures. Technical report, American Concrete Institute (ACI), March 1992. Reapproved 1997.
- [4] ACI Committee 209. 209.1R-05. Report on Factors Affecting Shrinkage and Creep of Hardened Concrete. Technical report, American Concrete Institute (ACI), July 2005.
- [5] ACI Committee 209. 209.2R-08. Guide for Modeling and Calculating Shrinkage and Creep in Hardened Concrete. Technical report, American Concrete Institute (ACI), May 2008.
- [6] Acker, P. Comportement mécanique du béton: Apports de l'approche physico-chimique (Mechanical behavior of concrete: A physico-chemical approach). PhD thesis, Ecole Nationale des Ponts et Chaussées, Paris, France, 1988.
- [7] Acker, P. Micromechanical Analysis of Creep and Shrinkage Mechanisms. In Ulm, F.-J., Bažant, Z. P., and Wittmann, F. H., editors, Creep, Shrinkage and Durability Mechanics of Concrete and other Quasi-brittle Materials. Proceedings of the 6th International Conference CONCREEP@MIT, pages 15–26, Cambridge, USA, August 2001. Elsevier: Amsterdam.
- [8] Adhikary, D. P. Shortcomings in the standard continuum based implicit joint model of layered rocks. *Journal of Geology and Mining Research*, 2(2):23–28, May 2010.
- [9] Alber, M. and Kahraman, S. Predicting the uniaxial compressive strength and elastic modulus of a fault breccia from texture coefficient. *Rock Mechanics and Rock Engineering*, 42(1):117–127, January 2009.
- [10] Aldrian, W. Beitrag zum Materialverhalten von früh belastetem Spritzbeton. PhD thesis, Montanuniversität Leoben, Leoben, Austria, May 1991.
- [11] Allaby, M., editor. A Dictionary of Geology and Earth Sciences. Oxford University Press, 4th edition, January 2013.
- [12] Allmendinger, R. W. Stereonet, September 2020. URL https://www.rickallmendinger.net/stereonet. Last access: 26.09.2020.
- [13] Allmendinger, R. W., Cardozo, N., and Fisher, D. M. Structural Geology Algorithms: Vectors and Tensors. Cambridge University Press, December 2011.

BIBLIOGRAPHY 288 of 498

[14] ASTM. D5607-02. Standard Test Method for Performing Laboratory Direct Shear Strength Tests of Rock Specimens Under Constant Normal Force. Standard, 2002.

- [15] ASTM. D7012-10. Test Methods for Compressive Strength and Elastic Moduli of Intact Rock Core Specimens under Varying States of Stress and Temperatures. Standard, 2010.
- [16] Atkins, P., Jones, L., and Laverman, L. Chemical principles. W. H. Freeman and Company, 6th edition, 2013.
- [17] Atzl, G., Brandtner, M., Selan, V., and Moritz, B. Numerical analyses of deep tunnels driven through massive faults. In Schubert, W. and Kluckner, A., editors, *Proceedings of the ISRM Regional Symposium EUROCK 2015 & 64th Geomechanics Colloquium–Future Development of Rock Mechanics*, pages 877–882, Salzburg, Austria, October 2015. Austrian Society for Geomechanics.
- [18] Austin, S. A. and Robins, P. J., editors. Sprayed Concrete: Properties, Design and Application. Whittles Publishing, 1995.
- [19] Austrian Standards Institute. ÖNORM EN 14487-1-1:2006. Spritzbeton: Teil 1: Begriffe, Festlegungen und Konformität. Standard, May 2006.
- [20] Austrian Standards Institute. ÖNORM EN 1992-1-1:2015. Eurocode 2: Bemessung und Konstruktion von Stahlbeton- und Spannbetontragwerken Teil 1-1: Allgemeine Bemessungsregeln und Regeln für den Hochbau (konsolidierte Fassung). Standard, February 2015.
- [21] Aydan, O., Sezaki, M., and Kawamoto, T. Mechanical and numerical modelling of shotcrete. In Pande, G. N. and Pietruszczak, S., editors, Proceedings of the Fourth International Symposium on Numerical Models in Geomechanics (NUMOG IV), pages 757–764, Swansea, Wales, August 1992. Taylor & Francis, London.
- [22] Bandis, S. C., Lumsden, A. C., and Barton, N. R. Fundamentals of rock joint deformation. International Journal of Rock Mechanics and Mining Sciences & Geomechanics Abstracts, 20(6):249–268, December 1983.
- [23] Barbero, M., Bonini, M., and Borri-Brunetto, M. Numerical modelling of the mechanical behaviour of bimrock. In Ribeiro e Sousa, L., Olalla, C., and Grossmann, N., editors, Proceedings of the 11th Congress of the International Society for Rock Mechanics—The Second Half Century of Rock Mechanics, volume 1 & 2, pages 377–380, Lisbon, Portugal, July 2007. Taylor & Francis Group, London.
- [24] Barbero, M., Bonini, M., and Borri-Brunetto, M. Three-Dimensional Finite Element Simulations of Compression Tests on Bimrock. In Proceedings of the 12th International Conference of International Association for Computer Methods and Advances in Geomechanics (IACMAG), pages 631–637, Goa, India, October 2008.
- [25] Bažant, Z. P., editor. Mathematical Modelling of Creep and Shrinkage in Concrete. Wiley & Sons Ltd, New York, 1988.
- [26] Bažant, Z. P. Creep and thermal effects in concrete structures: a conceptus of some new developments. In Mang, H. A., Bicanic, N., and de Borst, R., editors, *Proceedings of the* Int. Conf. EURO-C "Computational Modelling of Concrete Structures", pages 461–480, Swansea, Wales, 1994. Pineridge Press.

BIBLIOGRAPHY 289 of 498

[27] Bažant, Z. P. Materials Science of Concrete IV, chapter Creep and Damage in Concrete, pages 335–389. American Ceramic Society, Westerville, USA, 1995.

- [28] Bažant, Z. P. and Panula, L. Practical prediction of time-dependent deformations of concrete. *Matériaux et Constructions*, 11(5):317–328, September 1978.
- [29] Bažant, Z. P. and Prasannan, S. Solidification Theory for Concrete Creep. I: Formulation. Journal of Engineering Mechanics, 115(8):1691–1703, 1989.
- [30] Bažant, Z. P. and Wittmann, F. H., editors. *Creep and Shrinkage in Concrete Structures*. John Wiley & Sons Ltd, Chichester, 1982.
- [31] Bažant, Z. P., Hauggaard, A. B., and Baweja, S. Microprestress solidification theory for concrete creep. II: Algorithm and verification. *Journal of Engineering Mechanics*, 123(11): 1195–1201, November 1997.
- [32] Bažant, Z. P., Hauggaard, A. B., Baweja, S., and Ulm, F.-J. Microprestress solidification theory for concrete creep. I: Aging and drying effects. *Journal of Engineering Mechanics*, 123(11):1188–1194, 1997.
- [33] Bell, F. G. Engineering Properties of Soils and Rocks. Butterworth-Heinemann Ltd: Oxford, 3rd edition, 1992.
- [34] Benz, T., Vermeer, P. A., and Schwab, R. A small-strain overlay model. International Journal for Numerical and Analytical Methods in Geomechanics, 33(1):25–44, January 2009.
- [35] Benz, T. Small-strain stiffness of soils and its numerical consequences. PhD thesis, University of Stuttgart, 2007.
- [36] Bergmair, M., Harer, G., Riedmüller, G., and Stadlmann, T. Die Baugeologie des Galgenbergtunnels. Felsbau, 14(1):15–21, 1996.
- [37] Biscoping, M. and Kampen, R. Zusammensetzung von Normalbeton Mischungsberechnung, February 2017. URL https://mitglieder.vdz-online.de/fileadmin/gruppen/vdz/3LiteraturRecherche/Zementmerkblaetter/ZM_B20_2017_2.pdf. Zement-Merkblatt Betontechnik B 20; last access: December 16th, 2022.
- [38] Bjureland, W., Johansson, F., Sjölander, A., Spross, J., and Larsson, S. Probability distributions of shotcrete parameters for reliability-based analyses of rock tunnel support. *Tunnelling and Underground Space Technology*, 87:15–26, May 2019.
- [39] Bjurström, S. Shear strength of hard rock joints reinforced by grouted untensioned bolts. In Proceedings of the 3rd Congress of the International Society for Rock Mechanics (ISRM), pages 1194–1199, Denver, Colorado, USA, September 1974.
- [40] Blair, T. C. and McPherson, J. G. Grain-size and textural classification of coarse sedimentary particles. *Journal of Sedimentary Research*, 69(1):6–19, January 1999.
- [41] Blümel, M. Personal communication, November 2020.
- [42] Boos, P. and Dietermann, M. Wet Shotcrete Performance—Laboratory Test Methods and influencing Factors in Practice. *Tunnel*, 29(6):31–41, 2010.

BIBLIOGRAPHY 290 of 498

[43] Bossart, P., Meier, P. M., Moeri, A., Trick, T., and Mayor, J.-C. Geological and hydraulic characterisation of the excavation disturbed zone in the Opalinus Clay of the Mont Terri Rock Laboratory. *Engineering Geology*, 66(1–2):19–38, October 2002.

- [44] Boumiz, A., Vernet, C., and Tenoudji, F. C. Mechanical properties of cement pastes and mortars at early ages. *Advanced Cement Based Materials*, 3(3-4):94–106, April 1996.
- [45] Brady, B. H. G. and Brown, E. T. Rock Mechanics for underground mining. Springer Netherlands, 3rd edition, 2004.
- [46] Brandtner, M. Numerical Analysis of Fault Zones—Coming Closer to a Solution. In Schubert, W., Kluckner, A., and Pilgerstorfer, T., editors, *Proceedings of the Workshop "Characterization of Fault Zones" as part of the 62nd Geomechanics Colloquium*, pages 60–63, Salzburg, Austria, October 2013. Austrian Society for Geomechanics.
- [47] Brandtner, M. Personal communication, June 2020.
- [48] Brandtner, M. Personal communication, April 2022.
- [49] Brandtner, M. Personal communication, May 2022.
- [50] Brandtner, M. and Lenz, G. Checking the system behaviour using a numerical model. Geomechanics and Tunnelling, 10(4):353–365, August 2017.
- [51] Bray, J. W. Unpublished note. 1977.
- [52] BRITE-EURAM. BRE-CT92-0231. new Materials, Design and Construction Techniques for Underground Structures in Soft Rock and Clay Media. Technical report, Mott MacDonald Ltd (project coordinator), 1998. Research project funded by EU (programme: FP3-BRITE/EURAM 2).
- [53] Brodie, K., Fettes, D., Harte, B., and Schmid, R. Towards a unified nomenclature of metamorphic petrology: 5. structural terms including fault rock terms. PDF, November 2004. URL https://www.ugr.es/~agcasco/personal/IUGS/pdf-IUGS/scmr_struc2_structuraltermsincludingfaultrockterms.pdf. Recommendations by the IUGS Subcommission on the Systematics of Metamorphic Rocks. Last access: 07.01.2023.
- [54] Brosch, F.-J. and Pischinger, G. Small- to meso-scale brittle rock structures and the estimation of "paleostress" axes—A case study from the Koralm region (Styria/Carinthia). Austrian Journal of Earth Sciences, 107(2):37–59, 2014.
- [55] Brown, E. T. and Gonano, L. P. Improved compression test technique for soft rock. *Journal of the Geotechnical Engineering Division*, 100(2):196–199, 1974.
- [56] Brugg Kabel AG. Datasheet: BRUsens strain V3 (LLK-BSST V3 7.2 mm). Version: 2012/09/12 Rev. 02 TH. Technical report, Brugg, Switzerland, 2012.
- [57] Bryne, L. E. Time Dependent Material Properties of Shotcrete for Hard Rock Tunnelling. PhD thesis, KTH Royal Institute of Technology, Stockholm, Sweden, May 2014.
- [58] Buchmayer, F., Monsberger, C. M., and Lienhart, W. Advantages of tunnel monitoring using distributed fibre optic sensing. *Journal of Applied Geodesy*, 15(1):1–12, December 2020.

BIBLIOGRAPHY 291 of 498

[59] Budil, A. Längsverschiebungen beim Tunnelvortrieb. PhD thesis, Graz University of Technology, Graz, Austria, May 1996.

- [60] Bürgi, C. Cataclastic fault rocks in underground excavations A geological characterisation. Phd thesis, École Polytechnique Fédérale de Lausanne, Lausanne, Switzerland, 1999.
- [61] Burgstaller, M., Goricki, A., and Vanek, R. Semmering Base Tunnel new—Tender documents: Report on the geotechnical ground characterisation. Project document (in german), Austrian Federal Railways, April 2014.
- [62] Button, E. A. A Contribution to the Characterization of Phyllitic and Schistose Rock Masses for Tunnelling. PhD thesis, Graz University of Technology, Graz, Austria, 2004.
- [63] Byfors, J. Plain concrete at early ages. Technical report, Swedish Cement and Concrete Research Institute, Stockholm, Sweden, 1980.
- [64] Candappa, D. C., Sanjayan, J. G., and Setunge, S. Complete Triaxial Stress-Strain Curves of High-Strength Concrete. *Journal of Materials in Civil Engineering*, 13(3):209–215, June 2001.
- [65] Cardozo, N. and Allmendinger, R. W. Spherical projections with OSXStereonet. Computers & Geosciences, 51:193–205, February 2013.
- [66] Çengel, Y. A., Boles, M. A., and Kanoğlu, M. Thermodynamics: an engineering approach. McGraw-Hill Education, New York, USA, 9th edition, 2019.
- [67] CEB. International System of Unified Standard Codes of Practice for Structures—Volume 2: CEB-FIP Model Code for Concrete Structures. In CEB Bulletins d'information, number 124. Comité Euro-International du Béton (CEB), 1978.
- [68] CEB. CEB-FIP Model Code 90: Design Code. Technical report, Comité Euro-International du Béton (CEB), 1993.
- [69] Cervera, M., Oliver, J., and Prato, T. Thermo-Chemo-Mechanical Model for Concrete. I: Hydration and Aging. *Journal of Engineering Mechanics*, 125(9):1018–1027, September 1999.
- [70] Cervera, M., Oliver, J., and Prato, T. Thermo-Chemo-Mechanical Model for Concrete. II: Damage and Creep. Journal of Engineering Mechanics, 125(9):1028–1039, September 1999.
- [71] Chang, Y. Tunnel support with shotcrete in weak rock—a rock mechanics study. PhD thesis, KTH Royal Institute of Technology, Stockholm, Sweden, 1994.
- [72] Chen, A. C. T. and Chen, W.-F. Constitutive Relations for Concrete. *Journal of the Engineering Mechanics Division*, 101(4):465–481, August 1975.
- [73] Chen, G., Kemeny, J. M., and Harpalani, S. Fracture propagation and coalescence in marble plates with pre-cut notches under compression. In Myer, L. R., Cook, N. G. W., Goodman, R. E., and Tsang, S. F., editors, *Proceedings of the International Symposium on Fractured and Jointed Rock Masses*, pages 443–448, Lake Tahoe, California, USA, June 1992. A.A. Balkema.
- [74] Chen, W.-F. Plasticity in Reinforced Concrete. McGraw-Hill, New York, 1982.

BIBLIOGRAPHY 292 of 498

[75] Cheng, C. Influence of discontinuities on post-peak behavior of rock in uniaxial compressive test by numerical study. In Farag, A. A., editor, *Proceedings of the 2nd International Conference on Multimedia Technology (ICMT 2011)*, pages 6406–6409, Hangzhou, China, July 2011. Institute of Electrical and Electronics Engineers.

- [76] Cheng, Z. and Detournay, C. Plastic hardening model I: Implementation in FLAC3D. In Gómez, P., Detournay, C., Hart, R., and Nelson, M., editors, *Proceedings of the 4th Itasca Symposium on Applied Numerical Modeling*, pages 267–276, Lima, Perú, March 2016. Itasca International Inc., Minneapolis.
- [77] Cheng, Z. and Lucarelli, A. Plastic hardening model II: Calibration and validation. In Gómez, P., Detournay, C., Hart, R., and Nelson, M., editors, *Proceedings of the 4th Itasca Symposium on Applied Numerical Modeling*, pages 393–402, Lima, Perú, March 2016. Itasca International Inc., Minneapolis.
- [78] Codegone, G., Festa, A., and Dilek, Y. Formation of Taconic mélanges and broken formations in the Hamburg Klippe, Central Appalachian Orogenic Belt, Eastern Pennsylvania. Tectonophysics, 568-569:215–229, September 2012.
- [79] Coli, N., Berry, P., and Boldini, D. Analysis of the block-size distribution in the Shale-Limestone Chaotic Complex (Tuscany, Italy). In Wilson, S., Ewy, R., and Tutuncu, A., editors, Proceedings of the 42nd US Rock Mechanics Symposium and 2nd U.S.-Canada Rock Mechanics Symposium, pages 1–7, San Francisco, California, 29 June–2 July, 2008. American Rock Mechanics Association (ARMA): Alexandria. ARMA 08-233.
- [80] Coli, N., Boldini, D., and Bandini, A. Modeling of complex geological rock mixtures under triaxial testing conditions. In *Proceedings of the 2012 Regional Symposium of the International Society for Rock Mechanics (EUROCK 2012)—Rock Engineering and Technology for Sustainable Underground Construction*, pages 1–12, Stockholm, Sweden, May 2012.
- [81] Cook, N. G. W. The application of seismic techniques to problems in rock mechanics. International Journal of Rock Mechanics and Mining Sciences & Geomechanics Abstracts, 1(2):169–179, March 1964.
- [82] Cook, N. G. W. An experiment proving that dilatancy is a pervasive volumetric property of brittle rock loaded to failure. *Rock Mechanics*, 2(4):181–188, December 1970.
- [83] Cook, N. G. W., Hoek, E., Pretorius, J. P. G., Ortlepp, W. D., and Salamon, M. D. G. Rock mechanics applied to the study of rockbursts. *Journal of the South African Institute* of Mining and Metallurgy, 66:436–528, 1966.
- [84] Cordes, T., Weifner, T., Unteregger, D., and Bergmeister, K. Interaction between deep tunnel drives and an existing tunnel in fault zones-Modelling against reality. *Geomechanics* and Tunnelling, 12(6):641-650, December 2019.
- [85] Cornejo-Malm, G. Schwinden von Spritzbeton. Research report, ETH Zurich, 1995.
- [86] Coussy, O. Mechanics of Porous Continua. Wiley: Chichester, United Kingdom, 1995.
- [87] Coussy, O. Mechanics and physics of porous solids. John Wiley & Sons, Ltd: Chichester, United Kingdom, 1st edition, 2010.

BIBLIOGRAPHY 293 of 498

[88] Cowan, D. S. Structural styles in Mesozoic and Cenozoic mélanges in the western Cordillera of North America. *GSA Bulletin*, 96(4):451–462, April 1985.

- [89] Cudny, M. and Truty, A. Refinement of the Hardening Soil model within the small strain range. *Acta Geotechnica*, 15(8):2031–2051, March 2020.
- [90] Daller, J., Atzl, G., and Blümel, M. Festschrift zum 60. Geburtstag von Wulf Schubert, chapter Bestimmung von Gesteinskennwerten an Störungsmaterial, pages 50–58. Institute of Rock Mechanics and Tunnelling, Graz University of Technology, Graz, Austria, 2010.
- [91] Dassault Systèmes Simulia Corp. Abaqus/CAE 2017 documentation.
- [92] Davila Mendez, J. M. Displacements Analysis in Layered Rock Masses. PhD thesis, Graz University of Technology, Graz, Austria, January 2016.
- [93] Deere, D. U. Rock Mechanics in Engineering Practice, chapter Geological considerations, pages 1–20. Wiley, New York, 1968. Chapter 1.
- [94] Deere, D. U. and Miller, R. P. Engineering classification and index properties for intact rock. Technical report AFWL-TR-65-116, Air Force Weapons Laboratory, Kirtland Air Force Base, New Mexico, USA, December 1966.
- [95] Deutsche Gesellschaft für Geotechnik e.V. (DGGT). Empfehlungen des Arbeitskreises "Numerik in der Geotechnik"–EANG. Wilhelm Ernst & Sohn, Verlag für Architektur und technische Wissenschaften GmbH & Co. KG, Berlin, Germany, February 2014.
- [96] Dickmann, T. Personal communication, July 2021.
- [97] Diederichs, M. S., Carvalho, J. L., and Carter, T. G. A Modified Approach For Prediction of Strength And Post Yield Behaviour For High GSI Rockmasses In Strong, Brittle Ground. In Eberhardt, E., Stead, D., and Morrison, T., editors, Proceedings of the 1st Canada-US Rock Mechanics Symposium: Rock Mechanics: Meeting Society's Challenges and Demands, pages 249–257, Vancouver, Canada, April 2007. ARMA-07-031.
- [98] Ding, Y. Technologische Eigenschaften von jungem Stahlfaserbeton und Stahlfaserspritzbeton. PhD thesis, University of Innsbruck, Innsbruck, Austria, 1998.
- [99] Dorfmann, E. M. Zugkriechen von Beton in Abhängigkeit der Spannungsgeschichte. Master's thesis, Graz University of Technology, Graz, Austria, June 2017.
- [100] Eberhardt, E. Numerical modelling of three-dimension stress rotation ahead of an advancing tunnel face. *International Journal of Rock Mechanics and Mining Sciences*, 38(4):499–518, June 2001.
- [101] Eberly, D. Approximating an Ellipse by Circular Arcs, April 2016. URL https://www.geometrictools.com/Documentation/ApproximateEllipse.pdf. Last access: 26.09.2020.
- [102] Egger, P. Einfluss des Post-Failure Verhaltens von Fels auf den Tunnelausbau unter besonderer Berücksichtigung des Ankerausbaus. PhD thesis, Universität Karlsruhe, Karlsruhe, Germany, 1973.
- [103] Ekici, Z. Semmering Base Tunnel, construction lot SBT 1.1, tunnel Gloggnitz—Tender documents: Calculation values. Project document (in german), Austrian Federal Railways, 2014.

BIBLIOGRAPHY 294 of 498

[104] Engels, S., Wieselthaler, F., Pischinger, G., and Holzer, R. Semmering Base Tunnel, construction lot SBT 1.1, tunnel Gloggnitz, track 1—Engineering geological documentation. Project document (in german), Austrian Federal Railways, 2016.

- [105] Engels, S., Wieselthaler, F., and Holzer, R. Semmering Base Tunnel, construction lot SBT 1.1, tunnel Gloggnitz, track 1—Geotechnical horizontal and longitudinal section. Project document (in german), Austrian Federal Railways, 2017.
- [106] Engl, D. A., Fellin, W., and Zangerl, C. Scherfestigkeiten von Scherzonengesteinen—Ein Beitrag zur geotechnischen Bewertung von tektonischen Störungszonen und Gleitzonen von Massenbewegungen. Bulletin für Angewandte Geologie, 13(2):63–81, 2008.
- [107] England, G. L. and Illston, J. M. Methods of computing stress in concrete from a history of measured strain. *Civil Engineering and Public Works Review*, 60(1–3):513–517, 692–694, 846–847, April, May, June 1965.
- [108] Entfellner, M. Prediction of Displacements and Shotcrete Lining Utilization—Decision strategy for a timely application of ductile support systems in conventional tunnelling. Master's thesis, Graz University of Technology, Graz, Austria, August 2017.
- [109] Entfellner, M., Schubert, W., and Moritz, B. A. Early warning of overbreaks in tunnels. In Proceedings of the 2022 Regional Symposium of the International Society for Rock Mechanics (EUROCK 2022)–Rock and Fracture Mechanics in Rock Engineering and Mining, pages 1–8, Espoo, Finland, September 2022.
- [110] European Committee for Standardization. EN 1992-1-1:2004. Eurocode 2: Design of concrete structures - Part 1-1: General rules and rules for buildings. Standard, December 2004.
- [111] Fairhurst, C. E. and Hudson, J. Draft ISRM suggested method for the complete stress-strain curve for intact rock in uniaxial compression. *International Journal of Rock Mechanics* and Mining Sciences & Geomechanics Abstracts, 36:279–289, 1999.
- [112] Farmer, I. W. Stress distribution along a resin grouted rock anchor. *International Journal of Rock Mechanics and Mining Sciences & Geomechanics Abstracts*, 12(11):347–351, November 1975.
- [113] Farmer, I. W. Engineering Behaviour of Rocks. Springer Netherlands, 1st edition, 1983.
- [114] Fasching, F. and Vanek, R. Engineering geological characterisation of fault rocks and fault zones. *Geomechanics and Tunnelling*, 4(3):181–194, June 2011.
- [115] Faulkner, D. R., Lewis, A. C., and Rutter, E. H. On the internal structure and mechanics of large strike-slip fault zones: field observations of the Carboneras fault in southeastern Spain. *Tectonophysics*, 367(3-4):235–251, June 2003.
- [116] Faulkner, D. R., Jackson, C. A. L., Lunn, R. J., Schlische, R. W., Shipton, Z. K., Wibberley, C. A. J., and Withjack, M. O. A review of recent developments concerning the structure, mechanics and fluid flow properties of fault zones. *Journal of Structural Geology*, 32(11): 1557–1575, November 2010.
- [117] Feder, G. and Arwanitakis, M. Zur Gebirgsmechanik ausbruchsnaher Bereiche tiefliegender Hohlraumbauten (unter zentralsymmetrischer Belastung). Berg- und Hüttenmännische Monatshefte, 121(4):103–117, 1976.

BIBLIOGRAPHY 295 of 498

[118] Feenstra, P. H. and de Borst, R. Aspects of Robust Computational Models for Plain and Reinforced Concrete. *HERON*, 38(4):1–76, 1993.

- [119] Feynman, R. P., Leighton, R. B., and Sands, M. The Feynman Lectures on Physics, volume I: Mainly Mechanics, Radiation, and Heat. Basic Books, 2010.
- [120] fib. Structural Concrete: Textbook on Behaviour, Design and Performance: Updated knowledge of the CEB/FIP Model Code 1990. Technical report, fédération internationale du béton (fib), Lausanne, Switzerland, July 2000.
- [121] fib. CEB-FIP Model Code for Concrete Structures 2010. Technical report, fédération internationale du béton (fib), 2013.
- [122] Fischnaller, G. Untersuchungen zum Verformungsverhalten von jungem Spritzbeton im Tunnelbau—Grundlagen und Versuche. Master's thesis, University of Innsbruck, Innsbruck, Austria, 1992.
- [123] Fjellström, P. Measurement and Modelling of Young Concrete Properties. Licentiate thesis, Luleå University of Technology, Luleå, Sweden, 2013.
- [124] Forth, J. P. Predicting the tensile creep of concrete. Cement and Concrete Composites, 55: 70–80, January 2015.
- [125] Fossen, H. Structural Geology. Cambridge University Press, 2nd edition, 2016.
- [126] GEOKON. Instruction Manual: Model 4200 Series, Vibrating Wire Strain Gauges. Version: 11/08/2019 (revision DD). Technical report, Lebanon, New Hampshire, USA, 2019.
- [127] Glawe, U. and Upreti, B. N. Better Understanding the Strengths of Serpentinite Bimrock and Homogeneous Serpentinite. *Felsbau*, 22(5):53–60, 2004.
- [128] Golser, J., Schubert, P., and Rabensteiner, K. A new concept for evaluation of loading in shotcrete linings. In *Proceedings of the International Congress on Progress and Innovation* in *Tunnelling*, volume I, pages 79–85, Toronto, Canada, September 1989.
- [129] Golser, J., Rabensteiner, K., Sigl, O., Aldrian, W., Wedenig, H., Brandl, J., and Maier, C. Materialgesetz für Spritzbeton. Technical report, Bundesministerium für wirtschaftliche Angelegenheiten: Straßenforschung, 1990.
- [130] Goodman, R. E. Introduction to Rock Mechanics. John Wiley & Sons, 2nd edition, 1989.
- [131] Goodman, R. E. Engineering geology: rock in engineering construction. John Wiley & Sons, Inc., 1993.
- [132] Goricki, A. and Pimentel, E. Triaxial Tests on Cataclasites. Rock Mechanics and Rock Engineering, 48(5):2167–2171, November 2014.
- [133] Granet, I., Alvarado, J. L., and Bluestein, M. Thermodynamics and Heat Power. CRC Press, Boca Raton, USA, 9th edition, 2021.
- [134] Grassl, P. and Jirásek, M. Damage-plastic model for concrete failure. *International Journal of Solids and Structures*, 43(22-23):7166–7196, November 2006.
- [135] Graziani, A., Boldini, D., and Ribacchi, R. Practical Estimate of Deformations and Stress Relief Factors for Deep Tunnels Supported by Shotcrete. *Rock Mechanics and Rock Engineering*, 38(5):345–372, June 2005.

BIBLIOGRAPHY 296 of 498

[136] Green, S. J. and Swanson, S. R. Static constitutive relations for concrete. Technical report AFWL-TR-72-244, Air Force Weapons Laboratory, Kirtland Air Force Base, New Mexico, USA, April 1973.

- [137] Groshong, R. H. j. Low-temperature deformation mechanisms and their interpretation. Geological Society of America Bulletin, 100(9):1329–1360, September 1988.
- [138] Gross, D., Hauger, W., and Wriggers, P. Technische Mechanik 4: Hydromechanik, Elemente der Höheren Mechanik, Numerische Methoden. Springer Berlin Heidelberg, 7th edition, 2009.
- [139] Großauer, K. Tunnelling in Heterogeneous Ground—Numerical Investigation of Stresses and Displacements. Diploma thesis, Graz University of Technology, Graz, Austria, October 2001.
- [140] Großauer, K. Expert System Development for the Evaluation and Interpretation of Displacement Monitoring Data in Tunnelling. PhD thesis, Graz University of Technology, Graz, Austria, February 2009.
- [141] Grübl, P., Weigler, H., and Karl, S. Beton—Arten, Herstellung und Eigenschaften. Ernst & Sohn Verlag, Berlin, 2nd edition, 2001.
- [142] Gruppe TUNNEL:Monitor. TUNNEL:monitor (v2021.1.4). URL https://igt-engineering.com/de/forschung-und-entwicklung/tunnelmonitor/. Last access: 15.11.2022.
- [143] Gschwandtner, G. G. Analytische Berechnungsansätze zum Kennlinienverfahren. Master's thesis, Montanuniversität Leoben, Leoben, Austria, January 2010.
- [144] Gudmundsson, A., Simmenes, T. H., Larsen, B., and Philipp, S. L. Effects of internal structure and local stresses on fracture propagation, deflection, and arrest in fault zones. *Journal of Structural Geology*, 32(11):1643–1655, November 2010.
- [145] Guntli, P., Keller, F., Lucchini, R., and Rust, S. Gotthard-Basistunnel: Geologie, Geotechnik, Hydrologie zusammenfassender Schlussbericht. Technical report 7, Landesgeologie, 2016.
- [146] Guo, P. and Su, X. Shear strength, interparticle locking, and dilatancy of granular materials. Canadian Geotechnical Journal, 44(5):579–591, May 2007.
- [147] Harer, G., Prein, R., Schwab, P., and Wehr, H. Tunnelling in Poor Ground Conditions Case History Galgenbergtunnel. *Felsbau*, 14(2):82–86, 1996.
- [148] Hartog, A. H. An Introduction to Distributed Optical Fibre Sensors. CRC Press, May 2017.
- [149] Hauggaard-Nielsen, A. B. Mathematical Modelling and Experimental Analysis of Early Age Concrete. PhD thesis, Technical University of Denmark, Lyngby, Denmark, October 1997.
- [150] Havlásek, P., Šmilauer, V., Hájková, K., and Baquerizo, L. Thermo-mechanical simulations of early-age concrete cracking with durability predictions. In *IOP Conference Series:*Materials Science and Engineering, volume 236, pages 1–7. IOP Publishing, September 2017.
- [151] Heinisch, M., Mayr, B., Millen, B., and Holzer, R. Semmering Base Tunnel, construction lot SBT 1.1, access tunnel Göstritz—Geotechnical horizontal and longitudinal section. Project document (in german), 2016.

BIBLIOGRAPHY 297 of 498

[152] Heinisch, M., Mayr, B., Millen, B., and Holzer, R. Semmering Base Tunnel, construction lot SBT 1.1, access tunnel Göstritz—Engineering geological documentation. Project document (in german), Austrian Federal Railways, 2016.

- [153] Heinrich, P. J. Effiziente Erfassung viskoelastischer Eigenschaften bei der Spannungsermittlung von gezwängten Betonbauteilen. PhD thesis, Graz University of Technology, Graz, Austria, November 2018.
- [154] Hellmich, C. Shotcrete as part of the New Austrian Tunneling Method: From Thermochemomechanical Material Modeling to Structural Analysis and Safety Assessment of Tunnels. PhD thesis, Vienna University of Technology, Vienna, Austria, 1999.
- [155] Hellmich, C., Ulm, F.-J., and Mang, H. A. Multisurface Chemoplasticity. I: Material Model for Shotcrete. *Journal of Engineering Mechanics*, 125(6):692–701, 1999.
- [156] Hellmich, C., Ulm, F.-J., and Mang, H. A. Multisurface Chemoplasticity. II: Numerical Studies on NATM Tunneling. *Journal of Engineering Mechanics*, 125(6):702–713, 1999.
- [157] Hellmich, C., Sercombe, J., Ulm, F.-J., and Mang, H. A. Modeling of Early-Age Creep of Shotcrete. II: Application to Tunneling. *Journal of Engineering Mechanics*, 126(3):292–299, 2000.
- [158] Hellmich, C., Mang, H. A., and Ulm, F.-J. Hybrid method for quantification of stress states in shotcrete tunnel shells: combination of 3D in situ displacement measurements and thermochemoplastic material law. *Computers & Structures*, 79(22):2103–2115, 2001.
- [159] Henzinger, M. R., Schachinger, T., Lienhart, W., Buchmayer, F., Weilinger, W., Stefaner, R., Haberler-Weber, M., Haller, E.-M., Steiner, M., and Schubert, W. Fibre-optic supported measurement methods for monitoring rock pressure. *Geomechanics and Tunnelling*, 11(3): 251–263, June 2018.
- [160] Hettler, A. and Vardoulakis, I. Behaviour of dry sand tested in a large triaxial apparatus. Géotechnique, 34(2):183–197, June 1984.
- [161] Hill, R. The mathematical theory of plasticity. The Clarendon Press, Oxford, 1951.
- [162] Hodgson, K. and Cook, N. G. W. The effects of size and stress gradient on the strength of rock. In Proceedings of the 2nd Congress of the International Society for Rock Mechanics, volume 2, pages 31–34, Belgrade, Serbia, September 1970.
- [163] Hoek, E. and Brown, E. T. Practical estimates of rock mass strength. *International Journal of Rock Mechanics and Mining Sciences*, 34(8):1165–1186, December 1997.
- [164] Hoek, E. and Diederichs, M. S. Empirical estimation of rock mass modulus. *International Journal of Rock Mechanics and Mining Sciences*, 43(2):203–215, February 2006.
- [165] Hoek, E. Brittle failure of rock. Rock Mechanics in Engineering Practice. Wiley: New York, 1968.
- [166] Hoek, E. and Brown, E. T. *Underground Excavations in Rock*. CRC Press, 1st edition, 1980.
- [167] Hoek, E. and Brown, E. T. Empirical Strength Criterion for Rock Masses. *Journal of the Geotechnical Engineering Division*, 106(9):1013–1035, September 1980.

BIBLIOGRAPHY 298 of 498

[168] Holt, E. E. Early age autogeneous shrinkage of concrete. Vtt publications 446, Technical Research Centre of Finland, Espoo, Finland, 2001.

- [169] Holter, K. G. Properties of waterproof sprayed concrete tunnel linings: A study of EVAbased sprayed membranes for waterproofing of rail and road tunnels in hard rock and cold climate. PhD thesis, Norwegian University of Science and Technology, Trondheim, Norway, December 2015.
- [170] Holzer, R. Personal communication, September 2022.
- [171] Holzer, R., Prall, K., Wagner, O. K., and Gobiet, G. Semmering Base Tunnel Tunnelling in challenging geotechnical and geological conditions in major fault zones. *Geomechanics and Tunnelling*, 13(5):509–518, October 2020.
- [172] Hösthagen, A. Thermal Crack Risk Estimation and Material Properties of Young Concrete. Licentiate thesis, Luleå University of Technology, Luleå, Sweden, 2017.
- [173] Huber, H. Untersuchungen zum Verformungsverhalten von jungem Spritzbeton im Tunnelbau. Master's thesis, University of Innsbruck, Innsbruck, Austria, 1991.
- [174] Ikumi, T., Salvador, R. P., and Aguado, A. Mix proportioning of sprayed concrete: A systematic literature review. *Tunnelling and Underground Space Technology*, 124(104456): 12, June 2022.
- [175] Itasca Consultants S.A.S. Dynamic Analysis in FLAC3D. Electronical, 2020. URL https://www.itasca.fr/software/dynamic-analysis-in-flac3d. Last access: 23.12.2020.
- [176] Itasca Consulting Group, Inc. UDEC 5.0 documentation, 2011.
- [177] Itasca Consulting Group, Inc. FLAC3D 6.0 documentation, 2017.
- [178] Itasca Consulting Group, Inc. FLAC3D 7.0 documentation, 2019.
- [179] Itasca Consulting Group, Inc. Learning Itasca Educational Partnership. Electronical, 2023. URL https://www.itascainternational.com/learning/iep/iep-research-program. Last access: 05.01.2023.
- [180] Jaeger, J. C. and Cook, N. G. W. Fundamentals of Rock Mechanics. Chapman & Hall: London, 3rd edition, 1979.
- [181] Jaeger, J. C., Cook, N. G. W., and Zimmerman, R. W. Fundamentals of Rock Mechanics. Blackwell Publishing, 4th edition, 2007.
- [182] Johnson, R. B. and DeGraff, J. V. Principles of Engineering Geology. John Wiley & Sons, Inc., 1988.
- [183] Johnston, I. W. Strength of Intact Geomechanical Materials. Journal of Geotechnical Engineering, 111(6):730-749, June 1985.
- [184] Kahraman, S. and Alber, M. Estimating unconfined compressive strength and elastic modulus of a fault breccia mixture of weak blocks and strong matrix. *International Journal of Rock Mechanics and Mining Sciences*, 43(8):1277–1287, December 2006.

BIBLIOGRAPHY 299 of 498

[185] Kahraman, S., Alber, M., Fener, M., and Gunaydin, O. Evaluating the geomechanical properties of Misis fault breccia (Turkey). *International Journal of Rock Mechanics and Mining Sciences*, 45(8):1469–1479, December 2008.

- [186] Kahraman, S., Gunaydin, O., Alber, M., and Fener, M. Evaluating the strength and deformability properties of Misis fault breccia using artificial neural networks. *Expert Systems with Applications*, 36(3):6874–6878, April 2009.
- [187] Kainrath-Reumayer, S., Gschwandtner, G., Schuller, E., and Galler, R. Beitrag zur Anwendung des Kennlinienverfahrens. *Berg- und Hüttenmännische Monatshefte*, 155(2): 83–89, February 2010.
- [188] Kainrath-Reumayer, S., Neugebauer, E., Charette, F., Plouffe, M., and Galler, R. Ankerung im Untertagebau - Entwicklungen in Theorie und Praxis. Geomechanik und Tunnelbau, 1 (5):345–351, October 2008.
- [189] Kaiser, P. K. and Kim, B. H. Rock mechanics challenges of underground constructions and mining. In *Proceedings of the Korean Rock Mechanics Symposium*, pages 1–16, Seoul, South Korea, 2008. Korean Society for Rock Mechanics.
- [190] Kaiser, P. K. and Tannant, D. D. The Role of Shotcrete in Hard Rock Mines. In Hustrulid, W. A. and Bullock, R. L., editors, *Underground Mining Methods—Engineering Fundamentals* and International Case Studies, chapter 67, pages 579–592. Society for Mining, Metallurgy, and Exploration, Inc. (SME), 2001.
- [191] Kaiser, P. K., Diederichs, M. S., Martin, C. D., Sharp, J., and Steiner, W. Underground Works In Hard Rock Tunnelling And Mining. In *Proceedings of the International Conference on Geotechnical & Geological Engineering (GeoEng2000)*, ISRM International Symposium, pages 841–926, Melbourne, Australia, November 2000. Technomic Publishing Co.
- [192] Kaiser, P. K., Amann, F., and Steiner, W. How Highly Stressed Brittle Rock Failure Impacts Tunnel Design. In Proceedings of the 2010 Regional Symposium of the International Society for Rock Mechanics (EUROCK 2010), pages 1–12, Lausanne, Switzerland, June 2010. ISRM-EUROCK-2010-003.
- [193] Kalender, A., Sönmez, H., Medley, E. W., Tunusluoglu, C., and Kasapoglu, K. E. An approach to predicting the overall strengths of unwelded bimrocks and bimsoils. *Engineering Geology*, 183:65–79, December 2014.
- [194] Kastner, H. Statik des Tunnel- und Stollenbaues: auf der Grundlage geomechanischer Erkenntnisse. Springer Berlin Heidelberg, 1962.
- [195] Kettunen Linder, M. and Kilic, O. En studie av sprutbetongförstärkningen i Citybanan -Norrströmstunneln. Master's thesis, KTH Royal Insitute of Technology, Stockholm, Sweden, March 2011. Examensarbete 326.
- [196] Kim, Y.-S., Peacock, D. C. P., and Sanderson, D. J. Fault damage zones. *Journal of Structural Geology*, 26(3):503–517, March 2004.
- [197] Kirsch, G. Die Theorie der Elastizität und die Bedürfnisse der Festigkeitslehre. Zeitschrift des Vereines Deutscher Ingenieure, 42(29):797–807, 1898.

BIBLIOGRAPHY 300 of 498

[198] Klein, C. and Philpotts, A. R. Earth materials: introduction to mineralogy and petrology. Cambridge University Press, 1st edition, 2013.

- [199] Kluckner, A. Aspekte der Gebirgscharakterisierung im Tunnelbau. Master's thesis, Graz University of Technology, Graz, Austria, October 2012.
- [200] Kluckner, A. and Schubert, W. Study on the Anisotropic Displacement Pattern at a Conventional Tunnel Drive. In *Proceedings of the 5th ISRM Young Scholars' Symposium on Rock Mechanics and International Symposiumon Rock Engineering for Innovative Future (YSRM2019 & REIF2019)*, pages 1–6, Okinawa, Japan, December 2019.
- [201] Knipe, R. J. Deformation mechanism path diagrams for sediments undergoing lithification. Structural Fabric in Deep Sea Drilling Project Cores From Forearcs, Memoir 166:151–160, 1986.
- [202] Kovler, K. Why sealed concrete swells. ACI Materials Journal, 93(4):334-340, 1996.
- [203] Kropik, C. and Mang, H. A. Computational mechanics of the excavation of tunnels. Engineering Computations, 13(7):49–69, November 1996.
- [204] Kulhawy, F. H. Stress deformation properties of rock and rock discontinuities. *Engineering Geology*, 9(4):327–350, December 1975.
- [205] Kusterle, W. Qualitätsverbesserungen beim Spritzbeton durch technologische Massnahmen, durch den Einsatz neuer Materialien und auf Grund der Erfassung von Spritzbetoneigenschaften. Habilitation dissertation, University of Innsbruck, Innsbruck, Austria, 1992.
- [206] Kusterle, W. Comparison of shrinkage behaviour and creep properties under different compressive stress levels for wet-mix sprayed concrete from ten hours up to two weeks. Technical report, Morgan Tunnelling, 1999.
- [207] Kusterle, W. and Lukas, W. Spritzbeton hoher Güte für die einschalige Spritzbetonbauweise. In Tagungsband der 3. Internationalen Fachtagung Spritzbeton-Technologie, Innsbruck, Austria, pages 29–40, 1990.
- [208] Kusterle, W., Jäger, J., John, M., Neumann, C., and Röck, R. Spritzbeton im Tunnelbau. In Bergmeister, K., Fingerloos, F., and Wörner, J.-D., editors, Beton-Kalender 2014: Unterirdisches Bauen, Grundbau, Eurocode 7, chapter IX, pages 303–390. Ernst & Sohn GmbH & Co. KG., 2014.
- [209] Kuwajima, F. M. Early Age Properties of Shotcrete. In Celestino, T. B. and Parker, H. W., editors, Proceedings of the Eighth International Conference on Shotcrete for Underground Support, São Paulo, Brazil, April 1999. American Society of Civil Engineers.
- [210] Lackner, R. and Mang, H. A. Cracking in shotcrete tunnel shells. *Engineering Fracture Mechanics*, 70(7–8):1047–1068, May 2003.
- [211] Lackner, R., Hellmich, C., and Mang, H. A. Constitutive modeling of cementitious materials in the framework of chemoplasticity. *International Journal for Numerical Methods in Engineering*, 53(10):2357–2388, 2002.
- [212] Lackner, R., Macht, J., Hellmich, C., and Mang, H. A. Hybrid Method for Analysis of Segmented Shotcrete Tunnel Linings. *Journal of Geotechnical and Geoenvironmental Engineering*, 128(4):298–308, April 2002.

BIBLIOGRAPHY 301 of 498

[213] Lama, R. D. and Vutukuri, V. S. *Handbook on Mechanical Properties of Rocks*, volume 2 of *Series on Rock and Soil Mechanics*. Trans Tech Publications, Clausthal, Germany, 1978.

- [214] Laplante, P. Propriétés mécaniques des bétons durcissants: analyse comparée des bétons classiques et à très hautes performances [Mechanical properties of hardening concrete: a comparative analysis of classical and high strength concretes]. PhD thesis, Ecole Nationale des Ponts et Chaussées, Paris, France, 1993.
- [215] Laplante, P. and Boulay, C. Evolution du coefficient de dilatation thermique du béton en fonction de sa maturité aux tout premiers âges. *Materials and Structures*, 27(10):596–605, December 1994.
- [216] Leber, C. Einfluss der Primärspannungsorientierung auf die Verschiebungscharakteristik. Master's thesis, Graz University of Technology, Graz, Austria, March 2009.
- [217] Lebschy, D. Investigation of the influence of the tunnel lining on the displacement development. Master's thesis, Graz University of Technology, Graz, Austria, September 2014.
- [218] Lenz, G. Displacement monitoring data in tunnelling—Development of a semiautomatic evaluation system. Diploma thesis, Graz University of Technology, Graz, Austria, April 2007.
- [219] Lenz, G. Characterization of ground and system behaviour in water-bearing fault zones. PhD thesis, Graz University of Technology, Graz, Austria, July 2020.
- [220] Lenz, G. Personal communication, May 2022.
- [221] Lenz, G. Personal communication, July 2022.
- [222] Lenz, G. Personal communication, November 2022.
- [223] Lepique, M. Empfehlung Nr. 10 des Arbeitskreises 3.3 "Versuchstechnik Fels" der Deutschen Gesellschaft für Geotechnik e. V.: Indirekter Zugversuch an Gesteinsproben Spaltzugversuch. Bautechnik, 85(9):623–627, September 2008.
- [224] Lienhart, W., Schubert, W., Henzinger, M. R., Buchmayer, F., Weilinger, W., and Stefaner, R. Faseroptisch unterstützte Messmethoden zur Beobachtung von Gebirgsdruck. Research report, Federal Ministry Republic of Austria, Climate Action, Environment, Energy, Mobility, Innovation and Technology, Vienna, Austria, October 2018.
- [225] Lindlar, B., Jahn, M., and Schlumpf, J. Sika Sprayed Concrete Handbook. Sika AG, 2020. URL https://www.sika.com/content/dam/dms/corporate/n/glo-sprayed-concrete-handbook-2021.pdf. Last access: 14.01.2023.
- [226] Lindquist, E. S. and Goodman, R. E. Strength and deformation properties of a physical model melange. In Nelson, P. P. and Laubach, S. E., editors, Rock Mechanics - Models and Measurements - Challenges from Industry: Proceedings of the 1st North American Rock Mechanics Symposium (NARMS), pages 843–850. The University of Texas at Austin, A.A. Balkema: Rotterdam, June 1994.
- [227] Lindquist, E. S. The Strength and Deformation Properties of Melange. PhD thesis, University of California, Berkeley, California, USA, 1994.

BIBLIOGRAPHY 302 of 498

[228] Lockner, D. A. Rock Physics and Phase Relations: A Handbook of Physical Constants, volume 3 of AGU Reference Shelf, chapter Rock Failure, pages 127–147. American Geophysical Union, Washington, D.C., USA, 1st edition, January 1995.

- [229] Logan, J. M., Friedmann, M., Higgs, N., Dengo, C., and Shimamoto, T. Experimental studies of simulated gouge and their application to studies of natural fault zones. In Proceedings of Conference VIII—Analysis of Actual Fault Zones in Bedrock, pages 305—343, Menlo Park, California, USA, April 1979. United States Department of the Interior, Geological Survey, Office of Earthquake Studies. Open-file report 79-1239.
- [230] Lu, T. Autogenous shrinkage of early age cement paste and mortar. PhD thesis, Delft University of Technology, Delft, Netherlands, 2019.
- [231] Lucarelli, A. Personal communication, June 2022.
- [232] Luna Innovations Inc. Datasheet: Luna Optical Backscatter Reflectometer (OBR) Model 4600. Version: LTOBR4600 REV. 004 02/13/2014. Technical report, Blacksburg, Virginia, USA, 2014.
- [233] Luna Innovations Inc. Datasheet: Luna Optical Backscatter Reflectometer (OBR) Model 4600. Version: LTOBR4600 REV. 006 03/09/2018. Technical report, Blacksburg, Virginia, USA, 2018.
- [234] Lupini, J. F., Skinner, A. E., and Vaughan, P. R. The drained residual strength of cohesive soils. *Géotechnique*, 31(2):181–213, June 1981.
- [235] Ma, J. Faserfreier Ultrahochfester Beton—Entwicklung und Materialeigenschaften. PhD thesis, Leipzig University, Leipzig, Germany, 2010.
- [236] Macht, J. Hybrid Analysis of Shotcrete Tunnel Linings: Assessment and Online Monitoring of the Level of Loading. PhD thesis, Vienna University of Technology, Vienna, Austria, 2002.
- [237] Mair, K., Frye, K. M., and Marone, C. Influence of grain characteristics on the friction of granular shear zones. *Journal of Geophysical Research: Solid Earth*, 107(B10):ECV 4–1–ECV 4–9, October 2002.
- [238] Małkowski, P., Ostrowski, L., and Brodny, J. Analysis of Young's modulus for Carboniferous sedimentary rocks and its relationship with uniaxial compressive strength using different methods of modulus determination. *Journal of Sustainable Mining*, 17(3):145–157, 2018.
- [239] Mandl, G. Discontinuous fault zones. *Journal of Structural Geology*, 9(1):105–110, January 1987.
- [240] Mandl, G. Mechanics of Tectonic Faulting: Models and Basic Concepts. Developments in Structural Geology, 1. Elsevier Science Publishers B.V.: Amsterdam, 1988.
- [241] Mandl, G. Faulting in Brittle Rocks: An Introduction to the Mechanics of Tectonic Faults. Springer Berlin Heidelberg, 1st edition, 2000.
- [242] Mang, H. A. and Hofstetter, G. Festigkeitslehre. Springer Berlin Heidelberg, 5th edition, 2018.

BIBLIOGRAPHY 303 of 498

[243] Manton, N. and Mee, N. *The Physical World*. Oxford University Press, 1st edition, April 2017.

- [244] Marcher, T. Personal communication, January 2021.
- [245] Marinos, P. V. and Tsiambaos, G. Strength and Deformability of Specific Sedimentary and Ophiolithic Rocks. *Bulletin of the Geological Society of Greece*, 43(3):1259–1266, January 2010.
- [246] Marshak, S. Earth: portrait of a planet. New York: W.W. Norton & Company, 6th edition, 2019.
- [247] Martin, J. Back-analysis of rock mass parameters at the Semmering Base Tunnel based on the convergence confinement method. Master's thesis, Graz University of Technology, Graz, Austria, December 2022.
- [248] Medley, E. W. Using stereological methods to estimate the volumetric proportions of blocks in melanges and similar block-in-matrix rocks (bimrocks). In Oliveira, R., Rodrigues, L. F., Coelho, A. G., and Cunha, A. P., editors, *Proceedings of the 7th International Congress of the International Association of Engineering Geology (IAEG)*, pages 1031–1040. A.A. Balkema: Rotterdam, September 1994.
- [249] Medley, E. W. Systematic Characterization of Melange Bimrocks and Other Chaotic Soil/Rock Mixtures. Felsbau, 17(3):152–162, 1999.
- [250] Medley, E. W. Orderly Characterization of Chaotic Franciscan Melanges. *Felsbau*, 19(4): 20–33, 2001.
- [251] Medley, E. W. Observations on Tortuous Failure Surfaces in Bimrocks. *Felsbau*, 22(5): 35–43, 2004.
- [252] Medley, E. Tunneling Through Fault Zones and Melanges. Lecture slides of lecture 4 of the short course "Anticipating and addressing the characterization, design and construction problems of fault rocks, melanges and other bimrocks", Geological Engineering Department, Hacettepe University, Ankara, Turkey, June 2004.
- [253] Medley, E. W. Estimating Block Size Distributions of Melanges and Similar Block-in-Matrix Rocks (Bimrocks). In Hammah, R., Bawden, W., Curran, J., and Telesnicki, M., editors, Proceedings of 5th North American Rock Mechanics Symposium (NARMS), pages 599–606, Toronto, Canada, July 2002. University of Toronto Press.
- [254] Medley, E. W. and Zekkos, D. Geopractitioner approaches to working with antisocial mélanges. In Mélanges: Processes of Formation and Societal Significance, number 480, pages 261–277. The Geological Society of America, 2011.
- [255] Medley, E. W. The Engineering Characterization of Melanges and Similar Block-in-Matrix Rocks (Bimrocks). PhD thesis, University of California, Berkeley, California, USA, 1994.
- [256] Medley, E. W. and Lindquist, E. S. The engineering significance of the scale-independence of some Franciscan melanges in California, USA. In Daemen, J. J. K. and Schultz, R. A., editors, *Proceedings of the 35th U.S. Symposium on Rock Mechanics*, pages 907–914. A.A. Balkema, Rotterdam, 1995.

BIBLIOGRAPHY 304 of 498

[257] Meixner, T. Trigger Values for tunnel monitoring in SCL shallow tunnels. Master's thesis, Graz University of Technology, Graz, Austria, September 2016.

- [258] Menétrey, P. and Willam, K. J. Triaxial Failure Criterion for Concrete and its Generalization. ACI Structural Journal, 92(3):311–318, 1995.
- [259] Merriam-Webster, Inc. Dictionary: Autogenous. Electronical, 2020. URL https://www.merriam-webster.com/dictionary/autogenous. Last access: 23.06.2020.
- [260] Meschke, G. Consideration of aging of shotcrete in the context of a 3-D viscoplastic material model. *International Journal for Numerical Methods in Engineering*, 39:3123–3143, 1996.
- [261] Meschke, G., Kropik, C., and Mang, H. A. Numerical analyses of tunnel linings by means of a viscoplastic material model for shotcrete. *International Journal for Numerical Methods* in Engineering, 39:3145–3162, 1996.
- [262] Michelis, P. N. Work-softening and hardening behaviour of granular rocks. *Rock Mechanics*, 14(3):187–200, December 1981.
- [263] Mindess, S., Young, J. F., and Lawrence, F. V. Creep and drying shrinkage of calcium silicate pastes I. Specimen preparation and mechanical properties. *Cement and Concrete Research*, 8(5):591–600, 1978.
- [264] Mitchell, T. M. and Faulkner, D. R. The nature and origin of off-fault damage surrounding strike-slip fault zones with a wide range of displacements: A field study from the Atacama fault system, northern Chile. *Journal of Structural Geology*, 31(8):802–816, August 2009.
- [265] Mödlhammer, H. *Spritzbeton: In situ Versuche*. Bachelor's thesis, Montanuniversität Leoben, Leoben, Austria, April 2008.
- [266] Monsberger, C. M., Lienhart, W., Kluckner, A., Wagner, L., and Schubert, W. Continuous strain measurements in a shotcrete tunnel lining using distributed fibre optic sensing. In *Proceedings of the 9th European Workshop on Structural Health Monitoring*, pages 1–13, Manchester, United Kingdom, July 2018.
- [267] Monsberger, C. M., Lienhart, W., Kluckner, A., and Schubert, W. In-situ assessment of distributed strain and curvature characteristics in shotcrete tunnel linings based on fiber optic strain sensing. In *Proceedings of the 14th International Congress on Rock Mechanics* and Rock Engineering, pages 1–8, Foz do Iguassu, Brazil, September 2019.
- [268] Monsberger, C. M. and Lienhart, W. Distributed fiber optic shape sensing along shotcrete tunnel linings: Methodology, field applications, and monitoring results. *Journal of Civil Structural Health Monitoring*, 11(2):337–350, January 2021.
- [269] Monsberger, C. M., Bauer, P., Buchmayer, F., and Lienhart, W. Large-scale distributed fiber optic sensing network for short and long-term integrity monitoring of tunnel linings. *Journal of Civil Structural Health Monitoring*, 12(6):1317–1327, March 2022.
- [270] Moritz, B., Grossauer, K., and Schubert, W. Short Term Prediction of System Behaviour of Shallow Tunnels in Heterogeneous Ground. *Felsbau*, 22(5):44–52, 2004.
- [271] Müller, M. Kriechversuche an jungen Spritzbetonen zur Ermittlung der Parameter für Materialgesetze. mathesis, Montanuniversität Leoben, Leoben, Austria, October 2001.

BIBLIOGRAPHY 305 of 498

[272] Mutschler, T. Neufassung der Empfehlung Nr. 1 des Arbeitskreises "Versuchstechnik Fels" der Deutschen Gesellschaft für Geotechnik e. V.: Einaxiale Druckversuche an zylindrischen Gesteinsprüfkörpern. *Bautechnik*, 81(10):825–834, October 2004.

- [273] Naylor, M. A., Mandl, G., and Supesteijn, C. H. K. Fault geometries in basement-induced wrench faulting under different initial stress states. *Journal of Structural Geology*, 8(7): 737–752, January 1986.
- [274] Nefeslioglu, H. A. Evaluation of geo-mechanical properties of very weak and weak rock materials by using non-destructive techniques: Ultrasonic pulse velocity measurements and reflectance spectroscopy. *Engineering Geology*, 160:8–20, June 2013.
- [275] Neuner, M., Cordes, T., Drexel, M., and Hofstetter, G. Time-Dependent Material Properties of Shotcrete: Experimental and Numerical Study. *Materials*, 10(9):1067, September 2017.
- [276] Neuner, M., Gamnitzer, P., and Hofstetter, G. An Extended Damage Plasticity Model for Shotcrete: Formulation and Comparison with Other Shotcrete Models. *Materials*, 10(1): 1–22, January 2017.
- [277] Neuner, M., Schreter, M., Unteregger, D., and Hofstetter, G. Influence of the Constitutive Model for Shotcrete on the Predicted Structural Behavior of the Shotcrete Shell of a Deep Tunnel. *Materials*, 10(6):1–17, May 2017.
- [278] Neuner, M., Gamnitzer, P., and Hofstetter, G. Correction: An Extended Damage Plasticity Model for Shotcrete: Formulation and Comparison with Other Shotcrete Models. *Materials*, 11(1):135, January 2018.
- [279] Neville, A. M. Properties of Concrete. Prentice Hall, 4th edition, 1995.
- [280] Neville, A. M., Dilger, W. H., and Brooks, J. J. Creep of plain and structural concrete. Construction Press (Longman), Harlow, UK, 1983.
- [281] Nielsen, L. F. Composite creep analysis of concrete: A rational, incremental stress-strain approach. Byg Rapport R-178, Technical University of Denmark, Lyngby, Denmark, 2007.
- [282] Nilsson, M. Restraint Forces and Partial Coefficients for Crack Risk Analyses of Early Age Concrete Structures. PhD thesis, Luleå University of Technology, Luleå, Sweden, 2003.
- [283] Nübel, K. and Huang, W. A study of localized deformation pattern in granular media. Computer Methods in Applied Mechanics and Engineering, 193(27-29):2719–2743, July 2004.
- [284] Oberdörfer, W. Auswirkung von unterschiedlichen Betonnachbehandlungsmassnahmen auf die Qualit\u00e4t des Nassspritzbetons. Master's thesis, University of Innsbruck, Innsbruck, Austria, 1996.
- [285] Obert, L. and Duvall, W. I. Rock Mechanics and the Design of Structures in Rock. John Wiley & Sons, New York, 1967.
- [286] Obert, L., Windes, S. L., and Duvall, W. I. Standardized tests for determining the physical properties of mine rock. Report of Investigations 3891, United States Department of the Interior-Bureau of Mines, August 1946.

BIBLIOGRAPHY 306 of 498

[287] Obrzud, R. F. and Truty, A. The Hardening Soil Model-A practical guidebook (Z_Soil.PC 100701 report, revised 21.10.2018). Zace Services Ltd, October 2018.

- [288] ÖBV. Spritzbeton: Teil 1—Anwendung. Guideline, Österreichischer Betonverein (ÖBV), 1989.
- [289] ÖBV. Sprayed Concrete. Guideline, Österreichische Bautechnik Vereinigung (ÖBV), April 2013.
- [290] ÖGG. Guideline for the Geotechnical Design of Underground Structures with Conventional Excavation. Guideline, Austrian Society for Geomechanics (ÖGG), Salzburg, Austria, 2010. Translated from German version 2.1.
- [291] ÖGG. Geotechnical Monitoring in Conventional Tunnelling. Austrian Society for Geomechanics (ÖGG), Salzburg, Austria, 2014.
- [292] Oluokun, F. A., Burdette, E. G., and Deatherage, J. H. Splitting Tensile Strength and Compressive Strength Relationships at Early Ages. ACI Materials Journal, 88(2):115–121, 1991.
- [293] Ord, A. Deformation of rock: A pressure-sensitive, dilatant material. *Pure and Applied Geophysics (PAGEOPH)*, 137(4):337–366, 1991.
- [294] Oreste, P. P. A Procedure for Determining the Reaction Curve of Shotcrete Lining Considering Transient Conditions. Rock Mechanics and Rock Engineering, 36(3):209–236, June 2003.
- [295] Oreste, P., Spagnoli, G., and Ceravolo, L. A. A numerical model to assess the creep of shotcrete linings. Proceedings of the Institution of Civil Engineers - Geotechnical Engineering, 172(4):344–354, August 2019.
- [296] Palkovic, S. D., Brommer, D. B., Kupwade-Patil, K., Masic, A., Buehler, M. J., and
 Büyüköztürk, O. Roadmap across the mesoscale for durable and sustainable cement paste
 A bioinspired approach. Construction and Building Materials, 115:13-31, July 2016.
- [297] Palmström, A. and Singh, R. The deformation modulus of rock masses comparisons between in situ tests and indirect estimates. *Tunnelling and Underground Space Technology*, 16(2):115–131, April 2001.
- [298] Parent, T., Domede, N., Sellier, A., and Mouatt, L. Mechanical characterization of limestone from sound velocity measurement. *International Journal of Rock Mechanics and Mining Sciences*, 79:149–156, October 2015.
- [299] Passchier, C. W. and Trouw, R. A. J. Microtectonics. Springer Verlag, Berlin, 1996.
- [300] Paulini, P. Reaction mechanisms of concrete admixtures. Cement and Concrete Research, 20(6):910–918, November 1990.
- [301] Peacock, D. C. P., Dimmen, V., Rotevatn, A., and Sanderson, D. J. A broader classification of damage zones. *Journal of Structural Geology*, 102:179–192, 2017.
- [302] Pichler, B. and Hellmich, C. Hybrid methods for shotcrete and segmental linings tunnel shells Combining displacement and rotation measurements with computational multiscale mechanics. *Geomechanics and Tunnelling*, 11(3):226–235, June 2018.

BIBLIOGRAPHY 307 of 498

[303] Pichler, B., Hellmich, C., and Eberhardsteiner, J. Spherical and acicular representation of hydrates in a micromechanical model for cement paste: prediction of early-age elasticity and strength. *Acta Mechanica*, 203(3-4):137–162, June 2008.

- [304] Pichler, B., Hellmich, C., and Eberhardsteiner, J. Reaktionskinetik und Kriecheigenschaften des Spritzbetons, der im Zuge des Vortriebs des Koralmtunnels (Baulos KAT2) verwendet wird. Technical report (preliminary), Institute for Mechanics of Materials and Struttures, Vienna University of Technology, Vienna, Austria, December 2011.
- [305] Pilgerstorfer, T. Prediction of displacement development using closed form solutions. Diploma thesis, Graz University of Technology, Graz, Austria, May 2008.
- [306] Pilgerstorfer, T. Mechanical Characterization of Fault Zones. PhD thesis, Graz University of Technology, Graz, Austria, 2014.
- [307] Pilgerstorfer, T. Personal communication, January 2022.
- [308] Pilgerstorfer, T., Radončić, N., Moritz, B., and Goricki, A. Evaluation and interpretation of monitoring data in the test adit EKT Paierdorf. Geomechanics and Tunnelling, 4(5): 423–434, October 2011.
- [309] Pittino, G., Galler, R., Bonin, K., and Bezler, J. Experiences with polymer-modified shotcrete. In Amberg, F. and Knut, F. G., editors, *Proceedings of the 11th Conference on Shotcrete for Underground Support*, pages 1–18, Davos, Switzerland, June 2009. Engineering Conferences International (ECI).
- [310] Pötsch, M. The analysis of rotational and sliding modes of failure for slopes, foundations, and underground structures in blocky, hard rock. PhD thesis, Graz University of Technology, Graz, Austria, March 2011.
- [311] Potts, D. M. and Zdravković, L. Finite element analysis in geotechnical engineering: theory. Thomas Telford Ltd, London, 1999.
- [312] Poturovic, S., Schubert, W., and Blümel, M. Comparison of Constant Normal Load (CNL) and Constant Normal Stiffness (CNS) Direct Shear Tests. In Schubert, W. and Kluckner, A., editors, *Proceedings of the ISRM Regional Symposium EUROCK 2015 & 64th Geomechanics Colloquium—Future Development of Rock Mechanics*, pages 1–6, Salzburg, Austria, October 2015. Austrian Society for Geomechanics.
- [313] Powers, T. C. Causes and Control of Volume Change. *Journal of the PCA Research and Development Laboratories*, pages 30–39, January 1959. Portland Cement Association (PCA).
- [314] Powers, T. C. and Brownyard, T. L. Studies of the Physical Properties of Hardened Portland Cement Paste. In *Bulletin No. 22*, pages 1–342. Portland Cement Association (PCA), March 1948.
- [315] Probst, B. Entwicklung einer Langzeitdruckversuchsanlage für den Baustellenbetrieb zur Bestimmung des Materialverhaltens von jungem Spritzbeton. Diploma thesis, Montanuniversität Leoben, Leoben, Austria, 1999.
- [316] Pusch, R. Alteration of the Hydraulic Conductivity of Rock by Tunnel Excavation.

 International Journal of Rock Mechanics and Mining Sciences & Geomechanics Abstracts,
 26(1):79–83, January 1989.

BIBLIOGRAPHY 308 of 498

[317] Püstow, H. Tunnelling in a tectonic melange of high structural complexity. mathesis, Aachen University of Technology, Aachen, Germany, 2001.

- [318] R Core Team. R: A Language and Environment for Statistical Computing. R Foundation for Statistical Computing, Vienna, Austria, 2022. URL https://www.R-project.org/. Last access: 14.01.2023.
- [319] Radončić, N. Tunnel design and prediction of systembehaviour in weak ground. PhD thesis, Graz University of Technology, Graz, Austria, March 2011.
- [320] Rastrup, E. Heat of hydration in concrete. *Magazine of Concrete Research*, 6(17):79–92, September 1954.
- [321] Raymond, L. A. Classification of melanges. In Raymond, L. A., editor, *Melanges: Their Nature, Origin, and Significance*, pages 7–20. The Geological Society of America, 1984.
- [322] Reyes, O. and Einstein, H. H. Failure Mechanisms of Fractured Rock—A Fracture Coalescence Model. In Wittke, W., editor, *Proceedings of the 7th International ISRM Congress*, pages 333–339, Aachen, Germany, September 1991. A.A. Balkema.
- [323] Riedmüller, G. and Schubert, W. Tunnelling in Fault Zones Innovative Approaches. In Proceedings of the 4th North American Rock Mechanics Symposium (NARMS 2000): Rock Around The Rim, pages 1–12, Seattle, Washington, USA, July 2000. Balkema: Rotterdam. ARMA-2000-0113.
- [324] Riedmüller, G., Brosch, F. J., Klima, K., and Medley, E. W. Engineering Geological Characterization of Brittle Faults and Classification of Fault Rocks. *Felsbau*, 19(4):13–19, 2001.
- [325] Rokahr, R. B. and Lux, K. H. Einfluß des rheologischen Verhaltens des Spritzbetons auf den Ausbauwiderstand. *Felsbau*, 5(1):11–18, 1987.
- [326] Rombach, G. Spannbetonbau. Wiley-VCH Verlag GmbH, April 2010.
- [327] Roscoe, K. H. The Influence of Strains in Soil Mechanics. *Géotechnique*, 20(2):129–170, June 1970.
- [328] Rosso, R. S. A comparison of joint stiffness measurements in direct shear, triaxial compression, and In Situ. *International Journal of Rock Mechanics and Mining Sciences & Geomechanics Abstracts*, 13(6):167–172, June 1976.
- [329] Rostami, J., Kahraman, S., Yu, X., Copur, H., Balci, C., Bamford, W., and Asbury, B. The relation between uniaxial compressive and Brazilian tensile strength. In Ulusay, R., Aydan, O., Gercek, H., and Hindistan, M. A., editors, Proceedings of the 2016 Regional Symposium of the International Society for Rock Mechanics (EUROCK 2016)—Rock Mechanics and Rock Engineering: From the Past to the Future, volume 1, pages 147–152, Ürgüp, Cappadocia Region, Turkey, August 2016. Turkish National Society for Rock Mechanics, CRC Press.
- [330] Rowe, P. W. The stress-dilatancy relation for static equilibrium of an assembly of particles in contact. *Proceedings of the Royal Society of London. Series A. Mathematical and Physical Sciences*, 269(1339):500–527, October 1962.
- [331] Rowe, R. K., editor. Geotechnical and geoenvironmental engineering handbook. Springer US, 2001.

BIBLIOGRAPHY 309 of 498

[332] Ruetz, W. Das Kriechen des Zementsteins im Beton und seine Beeinflussung durch gleichzeitiges Schwinden. In *Deutscher Ausschuss für Stahlbeton*, number 183. Wilhelm Ernst & Sohn, Berlin, 1966.

- [333] Rust, W. Nichtlineare Finite-Elemente-Berechnungen. Springer Fachmedien Wiesbaden, 3rd edition, 2016.
- [334] Sadd, M. Elasticity. Academic Press, 3rd edition, 2014.
- [335] Sainsbury, B. L. and Sainsbury, D. P. Practical Use of the Ubiquitous-Joint Constitutive Model for the Simulation of Anisotropic Rock Masses. Rock Mechanics and Rock Engineering, 50(6):1507–1528, February 2017.
- [336] Salamon, M. D. G. Energy considerations in rock mechanics: fundamental results. *Journal of the South African Institute of Mining and Metallurgy*, 84:233–246, 1984.
- [337] Saldivar, G. G. and Sánchez, F. A. Tunnels and Underground Cities: Engineering and Innovation meet Archaeology, Architecture and Art, chapter Comparative study on shotcrete performance in tunnels based on different constitutive approaches, pages 1–10. CRC Press, 1st edition, April 2019.
- [338] Sammis, C. G. and Biegel, R. L. Fractals, fault-gouge, and friction. *Pure and Applied Geophysics PAGEOPH*, 131(1-2):255–271, 1989.
- [339] Sausgruber, T. and Brandner, R. The Relevance of Brittle Fault Zones in Tunnel Construction—Lower Inn Valley Feeder Line North of the Brenner Base Tunnel, Tyrol, Austria. *Mitteilungen der Österreichischen Geologischen Gesellschaft*, 94:157–172, August 2003.
- [340] Saw, H. A., Villaescusa, E., Windsor, C. R., and Thompson, A. G. Non-linear, elastic-plastic response of steel fibre reinforced shotcrete to uniaxial and triaxial compression testing. In Amberg, F. and Garshol, K. F., editors, *Shotcrete for Underground Support XI*, ECI Symposium Series, pages 1–18, June 2009.
- [341] SBT 1.1 Tunnel Gloggnitz: ARGE. Semmering Base Tunnel, construction lot SBT 1.1, tunnel Gloggnitz—Daily construction records. Project document (in german), Joint venture (ARGE): Implenia Österreich GmbH, HOCHTIEF Infrastructure GmbH, THYSSEN SCHACHTBAU GMBH, 2016.
- [342] SBT 1.1 Tunnel Gloggnitz: ARGE. Semmering Base Tunnel, construction lot SBT 1.1, tunnel Gloggnitz—Daily construction records. Project document (in german), Joint venture (ARGE): Implenia Österreich GmbH, HOCHTIEF Infrastructure GmbH, THYSSEN SCHACHTBAU GMBH, 2017.
- [343] SBT 1.1 Tunnel Gloggnitz: PGST. Semmering Base Tunnel, construction lot SBT 1.1, tunnel Gloggnitz—Tender documents: Geotechnical prognosis underground. Project document (in german), Austrian Federal Railways, 2014. Planungsgemeinschaft Semmering-Basistunnel neu Tunnelbau (PGST).
- [344] SBT 1.1 Tunnel Gloggnitz: site team. Semmering Base Tunnel, construction lot SBT 1.1, tunnel Gloggnitz—Presentation for the 13th meeting on the geotechnical conditions. Project document (in german), 2016.

BIBLIOGRAPHY 310 of 498

[345] SBT 1.1 Tunnel Gloggnitz: site team. Semmering Base Tunnel, construction lot SBT 1.1, tunnel Gloggnitz—Report on the site decisions on support. Project document (in german), 2016.

- [346] SBT 1.1 Tunnel Gloggnitz: site team. Semmering Base Tunnel, construction lot SBT 1.1, tunnel Gloggnitz—Report on the site decisions on support. Project document (in german), 2017.
- [347] Schädlich, B. and Schweiger, H. F. Shotcrete Model: Implementation, validation and application. Internal technical report, Graz University of Technology, Graz, Austria, October 2016.
- [348] Schädlich, B. and Schweiger, H. F. A new constitutive model for shotcrete. In Hicks, M. A., Brinkgreve, R. B. J., and Rohe, A., editors, Numerical Methods in Geotechnical Engineering Proceedings of the 8th European Conference on Numerical Methods in Geotechnical Engineering, NUMGE 2014, volume 1, pages 103–108, Delft, Netherlands, June 2014. Taylor & Francis Group, London, UK.
- [349] Schädlich, B., Schweiger, H. F., Marcher, T., and Saurer, E. Application of a novel constitutive shotcrete model to tunnelling. In *Rock Engineering and Rock Mechanics:* Structures in and on Rock Masses, pages 799–804. CRC Press, May 2014.
- [350] Schanz, T., Vermeer, P. A., and Bonnier, P. G. The hardening soil model: Formulation and verification. In *Proceedings of the 1st PLAXIS symposium: Beyond 2000 in Computational Geotechnics-10 Years of PLAXIS*, pages 1–16. Balkema: Rotterdam, 1999.
- [351] Scheiner, S. and Hellmich, C. Continuum Microviscoelasticity Model for Aging Basic Creep of Early-Age Concrete. *Journal of Engineering Mechanics*, 135(4):307–323, April 2009.
- [352] Scheydt, J. C. Influence of the reactive Components on Shotcrete Performance. *Tunnel*, (3):22–27, 2015.
- [353] Schlicke, D. Mindestbewehrung für zwangbeanspruchten Beton: Festlegung unter Berücksichtigung der erhärtungsbedingten Spannungsgeschichte und der Bauteilgeometrie. In Monographic Series TU Graz, Schriftenreihe des Instituts für Betonbau, volume 4. Verlag der Technischen Universität Graz, Graz, Austria, 2nd edition, 2016.
- [354] Schlicke, D. Personal communication, February 2018.
- [355] Schlicke, D. Personal communication, June 2020.
- [356] Schmid, S. M. and Handy, M. R. Controversies in Modern Geology. Evolution of Geological Theories in Sedimentology, Earth History and Tectonics., chapter 16. Towards a Genetic Classification of Fault Rocks: Geological Usage and Tectonophysical Implications, pages 339–361. Academic Press Limited, London, 1991.
- [357] Schön, J. H. Developments in Petroleum Science. In Physical Properties of Rocks-Fundamentals and Principles of Petrophysics, volume 65. Elsevier B.V., 2nd edition, December 2015.
- [358] Schubert, P. Beitrag zum rheologischen Verhalten von Spritzbeton. Felsbau, 6(3):150–153, 1988.

BIBLIOGRAPHY 311 of 498

[359] Schubert, P., Hölzl, H., Sellner, P., and Fasching, F. Geomechanical knowledge gained from the Paierdorf investigation tunnel in the section through the Lavanttal main fault zone. *Geomechanics and Tunnelling*, 3(2):163–173, April 2010.

- [360] Schubert, W. Erfahrungen bei der Durchörterung von Störzonen bei österreichischen Tunneln. In Proceedings of the "Nachdiplomkurs in angewandten Erdwissenschaften: Herausforderung Geologie im Untertagebau", pages 1–10, CSF Monte Veritá, Ascona, Switzerland, May 1996. ETH Zurich.
- [361] Schubert, W. Experience of tunnel construction in weak ground. Geomechanics and Tunnelling, 4(3):211–220, June 2011.
- [362] Schubert, W. and Riedmüller, G. Geotechnisches Gutachten zum Verbruch Galgenbergtunnel / Vortrieb Leoben Ost Sta. 1326 bis 1333,6. Technical report, The Austrian Federal Railways, Graz, Austria, April 1995. Unpublished.
- [363] Schubert, W. and Riedmüller, G. Geotechnische Nachlese eines Verbruches Erkenntnisse und Impulse. In Semprich, S., editor, *Proceedings of the 10th Christian Veder Colloquium: Innovation in der Geotechnik Entwicklungen der letzten Jahre*, number 13 in Mitteilungshefte, pages 59–68, Graz, Austria, 1995. Institute of Soil Mechanics and Foundation Engineering, Graz University of Technology.
- [364] Schubert, W. and Riedmüller, G. Tunnelling in Fault Zones State of the Art in Investigation and Construction. Felsbau, 18(2):7–15, 2000.
- [365] Schubert, W., Brandtner, M., Schweiger, H. F., Helmberger, A., Marcher, T., and Radončić, N. Proposed design strategy for tunnels. In Schubert, W. and Kluckner, A., editors, Proceedings of the ISRM Regional Symposium EUROCK 2015 & 64th Geomechanics Colloquium— Future Development of Rock Mechanics, pages 37–47, Salzburg, Austria, October 2015. Austrian Society for Geomechanics.
- [366] Schubert, W., Blümel, M., Brunnegger, S., Staudacher, R., and Sellner, P. J. Aspekte des Ausbaus. In Schubert, W. and Kluckner, A., editors, *Proceedings of the Workshop on Tunnelbau in Störungszonen—Eine Herausforderung*, pages 49–62, Graz, Austria, November 2016. Institute of Rock Mechanics and Tunnelling, Graz University of Technology.
- [367] Schubert, W., Blümel, M., Staudacher, R., and Brunnegger, S. Support aspects of tunnels in fault zones. *Geomechanics and Tunnelling*, 10(4):342–352, August 2017.
- [368] Schütz, R., Potts, D. M., and Zdravković, L. Advanced constitutive modelling of shotcrete: Model formulation and calibration. *Computers and Geotechnics*, 38(6):834–845, September 2011.
- [369] Schütz, R. Numerical Modelling of Shotcrete for Tunnelling. PhD thesis, Imperial College London, London, UK, February 2010.
- [370] Sercombe, J., Hellmich, C., Ulm, F.-J., and Mang, H. A. Modeling of early-age creep of shotcrete. I: Model and model parameters. *Journal of Engineering Mechanics*, 126(3): 284–291, 2000.
- [371] Sezaki, M., Kibe, T., Ichikawa, Y., and Kawamoto, T. An experimental study on the mechanical properties of shotcrete. *Journal of the Society of Materials Science*, 38(434): 1336–1340, 1989.

BIBLIOGRAPHY 312 of 498

[372] Sibson, R. H. Fault rocks and fault mechanisms. *Journal of the Geological Society*, 133(3): 191–213, March 1977.

- [373] Sibson, R. H. Structural permeability of fluid-driven fault-fracture meshes. *Journal of Structural Geology*, 18(8):1031–1042, August 1996.
- [374] Simo, J. C., Kennedy, J. G., and Govindjee, S. Non-smooth multisurface plasticity and viscoplasticity. Loading/unloading conditions and numerical algorithms. *International Journal for Numerical Methods in Engineering*, 26(10):2161–2185, October 1988.
- [375] Skempton, A. W. Residual strength of clays in landslides, folded strata and the laboratory. *Géotechnique*, 35(1):3–18, March 1985.
- [376] Sönmez, H., Gokceoglu, C., Tuncay, E., Medley, E. W., and Nefeslioglu, H. A. Relationships between Volumetric Block Proportions and Overall UCS of a Volcanic Bimrock. *Felsbau*, 22(5):27–34, 2004.
- [377] Sönmez, H., Tuncay, E., and Gokceoglu, C. Models to predict the uniaxial compressive strength and the modulus of elasticity for Ankara Agglomerate. *International Journal of Rock Mechanics and Mining Sciences*, 41(5):717–729, July 2004.
- [378] Sönmez, H., Gokceoglu, C., Medley, E. W., Tuncay, E., and Nefeslioglu, H. A. Estimating the uniaxial compressive strength of a volcanic bimrock. *International Journal of Rock Mechanics and Mining Sciences*, 43(4):554–561, June 2006.
- [379] Sönmez, H., Kasapoglu, K. E., Coskun, A., Tunusluoglu, C., Medley, E. W., and Zimmerman, R. W. A conceptual empirical approach for the overall strength of unwelded bimrocks. In Vrkljan, I., editor, Proceedings of the 2009 Regional Symposium of the International Society for Rock Mechanics (EUROCK 2009)—Rock Engineering in Difficult Ground Conditions Soft Rocks and Karst, pages 357–360, Dubrovnik, Croatia, October 2010. Taylor & Francis: London.
- [380] Stadlmann, T., Vanek, R., and Goricki, A. Semmering Base Tunnel, construction lot SBT 1.1, tunnel Gloggnitz—Tender documents: Rock mass types. Project document (in german), Austrian Federal Railways, 2014.
- [381] Staudacher, R. F. Anschlüsse für Arbeitsfugen bei Spritzbetonauskleidungen. Master's thesis, Graz University of Technology, Graz, Austria, November 2016.
- [382] Steindorfer, A. F. Short Term Prediction of Rock Mass Behaviour in Tunnelling by Advanced Analysis of Displacement Monitoring Data. PhD thesis, Graz University of Technology, Graz, Austria, November 1997.
- [383] Stini, J. Tunnelbaugeologie Die geologischen Grundlagen des Stollen- und Tunnelbaues. Springer Vienna, 1st edition, 1950.
- [384] Swanson, M. T. Late Paleozoic strike-slip faults and related vein arrays of Cape Elizabeth, Maine. *Journal of Structural Geology*, 28(3):456–473, March 2006.
- [385] Tazawa, E.-i., editor. Autogenous Shrinkage of Concrete: Proceedings of the International Workshop, organized by the JCI (Japan Concrete Institute), Hiroshima, Japan, June 1999. Taylor & Francis.
- [386] Terzaghi, K. Theoretical Soil Mechanics. John Wiley & Sons, Inc.: New York, 1943.

BIBLIOGRAPHY 313 of 498

[387] Thomas, A. Numerical modelling of sprayed concrete lined (SCL) tunnels. PhD thesis, University of Southampton, Southampton, United Kingdom, 2003.

- [388] Thomas, A. Sprayed Concrete Lined Tunnels—An introduction. Taylor & Francis, 2009.
- [389] Thomas, A. Sprayed Concrete Lined Tunnels—second edition. CRC Press, 2020.
- [390] Thomée, B. *Physikalisch nichtlineare Berechnung von Stahlfaserbetonkonstruktionen*. PhD thesis, Technical University Munich, Munich, Germany, 2005.
- [391] Thornton, C. Numerical simulations of deviatoric shear deformation of granular media. *Géotechnique*, 50(1):43–53, February 2000.
- [392] Thuro, K., Plinninger, R. J., Zäh, S., and Schütz, S. Scale effects in rock strength properties. Part 1: Unconfined compressive test and Brazilian test. In Särkkä and Eloranta, editors, Proceedings of the 2001 Regional Symposium of the International Society for Rock Mechanics (EUROCK 2001)—Rock Mechanics A Challenge for Society, pages 169–174. Swets & Zeitlinger Lisse, 2001.
- [393] Tigges, V. E. Die Hydratation von Hüttensanden und Möglichkeiten ihrer Beeinflussung zur Optimierung von Hochofenzementeigenschaften. PhD thesis, Clausthal University of Technology, Clausthal-Zellerfeld, Germany, 2009.
- [394] Tourenq, C. and Denis, A. La resistance a la traction des roches. Rapport de Recherches 4A, Laboratoire Central des Ponts et Chaussées, Paris, France, 1970.
- [395] Traina, L. A. Experimental stress-strain behaviour of a low strength concrete under multiaxial states of stress. Technical report AFWL-TR-82-92, Air Force Weapons Laboratory, Kirtland Air Force Base, New Mexico, USA, 1983.
- [396] Tsesarsky, M., Hazan, M., and Gal, E. Estimating the elastic moduli and isotropy of block in matrix (bim) rocks by computational homogenization. *Engineering Geology*, 200:58–65, January 2016.
- [397] Twiss, R. J. and Moores, E. M. Structural Geology. W. H. Freeman and Company, New York, USA, 2nd edition, 2007.
- [398] Tziallas, G. P., Tsiambaos, G., and Saroglou, H. Determination of Rock Strength and Deformability of Intact Rocks. *Electronic Journal of Geotechnical Engineering (EJGE)*, 14 (G):1–12, 2009.
- [399] Ulm, F.-J. Couplages thermochémomécaniques dans les bétons: Un premier bilan. Monograph LCPC OA31, Laboratoire Central des Ponts et Chaussées, Paris, France, 1998.
- [400] Ulm, F.-J. and Acker, P. Le point sur le fluage et la recouvrance des bétons. *Bulletin Liaison des Laboratoires des Ponts et Chaussées*, (XX):73–82, 1998. Special issue.
- [401] Ulm, F.-J. and Coussy, O. Modeling of Thermochemomechanical Couplings of Concrete at Early Ages. *Journal of Engineering Mechanics*, 121(7):785–794, 1995.
- [402] Ulm, F.-J. and Coussy, O. Strength Growth as Chemo-Plastic Hardening in Early Age Concrete. *Journal of Engineering Mechanics*, 122(12):1123–1132, 1996.

BIBLIOGRAPHY 314 of 498

[403] Ulusay, R., Türeli, K., and Ider, M. H. Prediction of engineering properties of a selected litharenite sandstone from its petrographic characteristics using correlation and multivariate statistical techniques. *Engineering Geology*, 38(1-2):135–157, December 1994.

- [404] U.S. Department of the Interior Bureau of Reclamation. *Engineering geology field manual*, volume I. U.S. Government Printing Office, 2nd edition, 1998.
- [405] U.S. Department of the Interior Bureau of Reclamation. Glossary of commonly used terms by the Bureau of Reclamation. Electronical, 2016. URL https://www.usbr.gov/library/glossary/index.html. Last access: 20.12.2016.
- [406] van der Pluijm, B. A. and Marshak, S. Earth structure: an introduction to structural geology and tectonics. W. W. Norton & Company, Inc.: New York, 2nd edition, 2004.
- [407] Vanek, R. and Stadlmann, T. Semmering Base Tunnel new—Legal railway approval procedure documents: Report on the construction geology. Project document (in german), Austrian Federal Railways, May 2010.
- [408] Vanek, R., Fasching, F., and Fasching, A. Ingenieurgeologische Charakterisierung von Störungszonen. In Schubert, W. and Kluckner, A., editors, *Proceedings of the Workshop on Tunnelbau in Störungszonen—Eine Herausforderung*, pages 1–11, Graz, Austria, November 2016. Institute of Rock Mechanics and Tunnelling, Graz University of Technology.
- [409] VBE. Semmering Base Tunnel, construction lot SBT 1.1, tunnel Gloggnitz—Concrete test report. Project document (in german), Verein für Baustoffprüfung und -entwicklung (VBE), 2016.
- [410] Vermeer, P. A. and de Borst, R. Non-associated plasticity for soils, concrete and rock. HERON, 29(3):1–64, 1984.
- [411] Vlachopoulos, N. and Diederichs, M. S. Improved Longitudinal Displacement Profiles for Convergence Confinement Analysis of Deep Tunnels. Rock Mechanics and Rock Engineering, 42(2):131–146, April 2009.
- [412] Volpe, R., Ahlgren, C., and Goodman, R. Selection of engineering properties for geologically variable foundations. In *Proceedings of the 17th International Congress on Large Dams*, *Vienna:Paris*, pages 1087–1101. International Commission on Large Dams, 1991.
- [413] von Rabcewicz, L. Die Ankerung im Tunnelbau ersetzt bisher gebräuchliche Einbaumethoden. Schweizerische Bauzeitung, 75(9):123–131, March 1957.
- [414] von Terzaghi, K. *Ingenieurgeologie*, chapter Tunnelgeologie, pages 365–407. Julius Springer: Vienna, 1st edition, 1929.
- [415] Wagner, L. Concept and realisation of a distributed fibre-optic sensing system for direct and continuous strain measurement in a shotcrete lining. Master's thesis, Graz University of Technology, Graz, Austria, September 2017.
- [416] Wagner, L., Kluckner, A., Monsberger, C. M., Wolf, P., Prall, K., Schubert, W., and Lienhart, W. Direct and Distributed Strain Measurements Inside a Shotcrete Lining: Concept and Realisation. *Rock Mechanics and Rock Engineering*, 53(2):641–652, August 2019.

BIBLIOGRAPHY 315 of 498

[417] Wen-jie, X., Zhong-qi, Y., and Rui-lin, H. Study on the mesostructure and mesomechanical characteristics of the soil—rock mixture using digital image processing based finite element method. *International Journal of Rock Mechanics and Mining Sciences*, 45(5):749–762, July 2008.

- [418] Wen-Jie, X., Qiang, X., and Rui-Lin, H. Study on the shear strength of soil—rock mixture by large scale direct shear test. *International Journal of Rock Mechanics and Mining Sciences*, 48(8):1235–1247, December 2011.
- [419] Wesche, K. Baustoffe für tragende Bauteile—Band 2: Beton, Mauerwerk. Bauverlag GmbH: Wiesbaden, Berlin, 3rd edition, 1993.
- [420] Wibberley, C. A. J., Yielding, G., and Toro, G. D. Recent advances in the understanding of fault zone internal structure: a review. *Geological Society, London, Special Publications*, 299(1):5–33, 2008.
- [421] Wittmann, F. Bestimmung physikalischer Eigenschaften des Zementsteins. In *Deutscher Ausschuss für Stahlbeton*, number 232. Wilhelm Ernst & Sohn, Berlin, 1974.
- [422] Wuilpart, M. Advanced Fiber Optics: Concepts and Technology, chapter Rayleigh scattering in optical fibers and applications to distributed measurements, pages 1–56. EPFL Press, Lausanne, Switzerland, 1st edition, 2011.
- [423] Wullschläger, D. Ein Verbundwerkstoffmodell für die Systemankerung im Tunnelbau. PhD thesis, Universität Karlsruhe, Karlsruhe, Germany, 1988.
- [424] Yin, J. Untersuchungen zum zeitabhängigen Tragverhalten von tiefliegenden Hohlräumen im Fels mit Spritzbetonausbau. PhD thesis, Technische Universität Clausthal, Clausthal-Zellerfeld, Germany, February 1996.
- [425] ZAMG. Zentralanstalt für Meteorologie und Geodynamik: Klimamonitoring. Electronical, 2021. URL https://www.zamg.ac.at/cms/de/klima/klima-aktuell/klimamonitoring/?view=fullscreen¶m=t&period=period-ymd-2016-11-17&ref=3. Last access: 02.12.2021.
- [426] Zhang, H.-Y., Xu, W.-J., and Yu, Y.-Z. Triaxial tests of soil—rock mixtures with different rock block distributions. *Soils and Foundations*, 56(1):44–56, February 2016.
- [427] Zhao, X. G. and Cai, M. A mobilized dilation angle model for rocks. *International Journal of Rock Mechanics and Mining Sciences*, 47(3):368–384, April 2010.
- [428] Zi, G. and Bažant, Z. P. Continuous Relaxation Spectrum for Concrete Creep and its Incorporation into Microplane Model M4. *Journal of Engineering Mechanics*, 128(12): 1331–1336, December 2002.